LOCALIZED WAVE SOLUTIONS IN OPTICAL FIBER WAVEGUIDES

by

Ashish Madhukar Vengsarkar

Dissertation submitted to the Faculty of the

Virginia Polytechnic Institute and State University

in partial fulfillment of the requirements for the degree of

DOCTOR OF PHILOSOPHY

in Electrical Engineering

APPROVED:

I. M. Besieris, Chairman

G. S. Brown

R. O. Claus

I. Jacobs

W. E. Kohler

August, 1991

Blacksburg, Virginia

LOCALIZED WAVE SOLUTIONS IN OPTICAL FIBER WAVEGUIDES

by

Ashish Madhukar Vengsarkar

I. M. Besieris, Chairman

Electrical Engineering

(ABSTRACT)

A novel bidirectional decomposition of exact solutions to the scalar wave equation has been shown to form a natural basis for synthesizing localized wave (LW) solutions that describe localized, slowly decaying transmission of energy in free space. In this work, we demonstrate the existence of LW solutions in optical fiber waveguides operated in the linear regime. In this sense, these solutions are fundamentally different from the non-linear, soliton-based communication systems. Despite the dielectric waveguiding constraints introduced by the fiber, solutions that resemble the free-space solutions can be obtained with broad bandwidth source spectra. As with the free-space case, these optical waveguide LW solutions propagate over very long distances, undergoing only local variations. Four different source modulation spectra that give rise to solutions similar to Focus Wave Modes (FWM's), splash pulses, the scalar equivalent of Hillion's spinor modes and the Modified Power Spectrum (MPS) pulses are considered. A detailed study of the MPS pulse is performed, practical issues regarding source spectra are addressed, and distances over which such LW solutions maintain their non-decaying nature are quantified. Present day state-of-the-art technology is not capable of meeting requirements that will make practical implementation of LW solution-based fiber optic systems a reality. We address futuristic technology issues and briefly describe efforts that could lead to efficient LW solution-based fiber optic systems.

Acknowledgments

This work has been made possible due to the contributions and support of several people. I wish to thank —

Prof. I. M. Besieris, my advisor and mentor, for guiding me with patience and constant words of encouragement, for keeping my enthusiasm alive and making this effort possible. Prof. R. W. Ziolkowski, University of Arizona, for his keen interest in the project, sharp eye for details and physical insight into the behavior of localized pulses which raised the level of this research immeasurably. Prof. R. O. Claus, Director of the Fiber & Electro-Optics Research Center, for presenting me with incredible opportunities and unlimited resources throughout my stay at Virginia Tech, and helping me grow professionally and as an individual. Profs. I. Jacobs, G. S. Brown and W. E. Kohler, for spurring me on with new ways of looking at my research and serving on my dissertation committee. Prof. A. Safaai-Jazi, for introducing me to the fundamentals and advanced aspects of optical waveguide theory, and Dr. A. M. Shaarawi, for discussions on LW solutions and comments on the dissertation.

Kent A. Murphy, for being a friend, and for instilling into me a sense of confidence and a positive "We can do it !" attitude toward scientific research. Brian Fogg, for his help on MATLAB programs and associated computer advice. FEORCers Mike Gunther, Ken Shaw, Russ May, Bill Miller, Jonathan Greene, Marten deVries, Linda Jones and Ann Goette, for working with me and tolerating my presence for four and a

half years. My parents, for instilling into me the value of education and for providing resources for the same.

My biggest thanks go to my wife, Mala Rao, for standing by my side through thick and thin and for being an indefatigable source of encouragement and inspiration.

Financial support on this project was provided in part by the Lawrence Livermore National Laboratory and the Virginia Center for Innovative Technology.

Table of Contents

List of Figures

1.0 INTRODUCTION

James Neil Brittingham, in his pioneering work in 1983, proposed Focus Wave Mode (FWM) solutions to Maxwell's equations in free space [1]. These solutions were real, nonsingular, continuous functions that remained focussed for all time with only local variations and traveled with the velocity of light. Wu and King subsequently showed that Brittingham's three-region-formulation to obtain finite energy solutions was incorrect and proved that although FWM solutions had a finite energy density, they possessed infinite energy [2]. Wu and Lehmann further proved that any finite-energy solution to Maxwell's equations without sources would eventually spread and the amplitude would decay to zero as time approached infinity [3]. However, a lack of finite energy content, which physically precludes practical feasibility, did not deter researchers from exploring the mathematical and physical richness that was inherent in Brittingham's formalism. Belanger [4, 5], Sezginer [6] and Ziolkowski [7] showed that the FWM solutions were related to exact solutions of the scalar wave equation. Belanger [4] and Sezginer [6] rewrote the FWM solutions in terms of Gauss-Laguerre and Gauss-Hermite packet-like solutions and Ziolkowski [7] proved that complex

sources could give rise to such FWM's.

Brittingham's work, therefore, inspired several researchers to explore the existence of non-dispersive, packet-like solutions to the wave equation that could propagate through free space without any decay. While the infinite energy content remained an unresolved issue, Ziolkowski made the significant observation that plane waves share the property of infinite energy with the FWM's [7, 8]. He argued that although the FWM solutions have an infinite total energy content, a superposition of FWM's might have an advantage over the standard plane wave superposition when it comes to describing the transfer of directed pulses in free space. Such pulses, characterized by high directionality and slow energy decay, were termed localized waves (LW's).

Experimental investigations of launching acoustical LW's showed considerable success [9]. It was established that a LW pulse launched from a linear synthetic array maintained its shape and did not spread out for distances up to twice the Rayleigh length. Subsequent results showed that a ten-fold improvement over continuous wave excitations was possible [10]. Another area of research based on similar underlying principles was Durnin's diffraction-free "Bessel beam" [11]. Experimental verification of the larger depth of such a beam, as compared to a Gaussian beam, was provided by Durnin, Miceli and Eberly [12].

In order to uniformize these attempts toward synthesizing highly directional pulses and beams, Besieris, Shaarawi and Ziolkowski proposed a novel approach to

the synthesis of wave signals [13]. Within the framework of this new approach, exact solutions were decomposed into bidirectional, backward and forward, plane waves traveling along a preferred direction z, viz., exp $[-i\alpha(z-ct)]$ exp$[i\beta(z+ct)]$. These bilinear expressions were elementary solutions to the Fourier-transformed (with respect to x and y) three-dimensional wave equation provided that a constraint relationship involving α, β and the Fourier variables dual to x and y was satisfied. Such elementary blocks were shown to constitute a natural basis for synthesizing Brittingham-like solutions, such as Ziolkowski's splash pulses, Hillion's spinor modes [14] and the Ziolkowski-Belanger-Sezginer scalar FWM's. An application of this technique to infinitely long, cylindrical, metallic waveguides was discussed by Shaarawi, Besieris and Ziolkowski [15]. By varying the free parameters of specific source modulation spectra, localized, non-decaying pulses that moved predominantly in the positive direction could be synthesized within the waveguide.

The various attempts to synthesize focussed beams in free-space and in waveguiding structures leads one to speculate about the possibility of generating and maintaining a LW within the most efficient and popular waveguiding structure in communications systems today - an optical fiber. It is the intent of this work to demonstrate the theoretical existence of LW solutions in optical fibers, to outline practical requirements that lead to such solutions and to prognosticate technology movements that would make future LW-based fiber systems a reality.

With the above goal in mind, we apply the method of bidirectional decomposition to optical fiber waveguides and investigate the possibility of

synthesizing pulsed solutions that can propagate along such guides with only local variations. The analysis is similar to that of the infinite waveguide described by Shaarawi *et al.* [15], with the exception of the boundary conditions that the fields must satisfy at the core-cladding interface. For simplicity, the core and cladding materials are assumed to be both nondispersive and nonabsorptive. The only dispersive characteristics are due solely to the core-cladding interface (waveguide dispersion). The general solution to the scalar wave equation in an optical fiber is analyzed for four source modulation spectra and the approximations that need to be made in order to generate solutions similar to Focus Wave Modes (FWM's), splash pulses, the scalar equivalent of Hillion's spinor modes and the Modified Power Spectrum (MPS) pulses are considered.

The motivation for this research is based on recent developments in optical fiber communications and sensing. Current research efforts in the area of high-speed, long-distance fiber-optic communications are concentrated on the development of new methods that will counter the pulse dispersion effects introduced during information transmission. The transmission of stationary, non-linear optical pulses, termed solitons, in dispersive optical fibers was first proposed by Hasegawa and Tappert in 1973 [16] and demonstrated in practice by Mollenauer *et al.* in 1980 [17]. Solitons are localized pulses that propagate through an optical fiber operated in its anomalous dispersion regime where a delicate interplay between the dispersion (material and waveguide) and nonlinearities results in a cancellation of distortive effects. While soliton-based communications systems are on the verge of becoming a practical reality, limitations imposed on system performance by fiber loss, frequency chirp and the interaction

(collision) of neighboring pulses are currently being studied. The novel method of wave synthesis proposed in our work does not invoke the need for non-linear effects in optical fibers and leads to solutions that are capable of countering the dispersive effects introduced by the waveguide. Although only a theoretical discussion is presented here, we are optimistic that this technique will lead to the emergence of a competing technology in the area of high-capacity, fiber-optic communications. Other areas that would benefit from the availability of LW solutions are those of remote sensing, novel scattering and diffraction phenomena, and the use of fibers as carriers of photon torpedoes, a la Star Trek!

In Chapter 2, we first provide the background for the analysis of optical fiber waveguides and describe the methods used to obtain elementary, monochromatic, plane-wave-type solutions. The classical Fourier synthesis method for generating solutions for generic source spectra is outlined. The optical waveguide is then analyzed by assuming a solution of the bidirectional-type and we arrive at a generic elementary solution to the scalar equation in terms of the newly defined parameters. We take recourse to the classical waveguide analysis in order to further simplify the solution. A one-to-one correspondence is established between the two methods and conditions for the core and cladding regions are established. This leads to an elimination of practically unrealizable solutions and simplifies the mathematical analysis that follows. We briefly review linearly polarized (LP) modes in optical fibers and use properties derived in the literature to specify the boundary conditions. The superposition of elementary solutions after the boundary conditions have been invoked is also developed. In summary, a complete development of optical waveguide theory in terms of the bidirectional

parameters is undertaken in this chapter.

In Chapter 3, we consider four different spectra that have given rise to LW solutions in the free-space case: the singular source spectrum, the splash pulse spectrum, the zero-order Bessel spectrum and the MPS spectrum. We derive expressions for pulse-like solutions resulting from the aforementioned spectra in optical fibers and show that merely picking established source spectra that have led to LW solutions in free space will not result in LW solutions in dielectric waveguiding structures. The synthesis, therefore, needs to be performed with caution and we consider reasons why some of the solutions may be practically unstable.

In Chapter 4, the non-decaying nature of the MPS pulse shape is evaluated and the free parameters are related to physically meaningful quantities. The similarity of the MPS pulse in the fiber to its free-space counterpart is presented and we quantify the distance for which no decay will be observed. A graphical description provides a clearer picture of the pulse behavior at different distances along the fiber as well as for different choices of the source spectrum parameters.

Feasibility of practical implementation of the spectra considered in Chapter 4 as well as future theoretical directions are considered in Chapter 5. Issues relating to material dispersion in the fiber are addressed; we show by analogy that the presence of material dispersion does not significantly affect the localization of solutions by considering the case of a plasma-filled metallic cylindrical waveguide. Absorption effects are commented upon and we briefly describe the resulting changes that need to

be incorporated in the analysis to include the lossy nature of the waveguide. Practical issues regarding sources and technology improvements are addressed. Finally, we summarize and conclude our findings in Chapter 6.

2.0 OPTICAL WAVEGUIDE THEORY

The analysis of electromagnetic wave propagation in optical fiber waveguides dates back to 1961 when Snitzer investigated the modal content of a multimode fiber and observed the different modal patterns of the lower order modes[18, 19]. Until 1971, the investigations were performed using a vector mode analysis which accounted for all polarizations and all the true modes of the waveguide [20]. Gloge [21] first proposed his weakly guiding theory based on the assumption that in a practical fiber the core and the cladding indices were very close to each other; this assumption is valid in both multimode and single mode fibers for different reasons. In a multimode fiber, the intermodal dispersion is directly dependent on the difference in the refractive indices and since a reduction in dispersion results in efficient data transmission at high bit-rates, it is necessary to fabricate the core and cladding indices such that the weak-guidance condition is met. On the other hand, for a single mode fiber, the core and cladding indices should be close to each other in order to have manageable and manufacturable fiber core diameters. To elaborate, a typical practical single mode fiber has a core size of about eight micrometers and a fractional index difference between

core and cladding of less than one percent. If the difference in the core and the cladding were large, the fiber core diameter would have to be significantly reduced in order to maintain single-mode operation. The weakly guiding theory, which was thus based on practically sound reasons, introduced the concept of linearly polarized (LP) modes, significantly simplified the analysis and provided a basis for the development of modern-day optical fiber theory.

In this chapter we will use the weakly guiding assumptions and develop the optical waveguide theory in terms of the bidirectional representation. A concise summary of the one-to-one correspondence between the classical analysis and the bidirectional synthesis will be available as a result of this effort.

2.1 Classical Analysis

2. 1. 1 Monochromatic Plane-Wave Solutions

The scalar wave equation for an idealized optical fiber made of a nondispersive and nonabsorptive material can be written as

$$(\nabla^2 - \frac{n_i^2}{c^2} \partial_t^2) \psi_i = 0 ; \quad i = 1 \Rightarrow \text{Core} ; i = 2 \Rightarrow \text{Cladding} , \tag{2.1}$$

where ∇^2 is the 3D Laplacian, n is the refractive index ($n_1 > n_2$; n_1, n_2 assumed to be constant), and c is the velocity of light *in vacuo*. In Eq. (2.1), ψ_i represents either of the transverse fields (E_x, H_y, E_y, H_x) or any of the longitudinal fields (E_z, H_z) in the fiber. A more detailed exposition of this behavior of the transverse as well as the longitudinal components of the modes will be given in the next section.

In the classical analysis, we consider solutions of the form

$$\psi(\rho,\phi,z,t) = \Phi (\rho,\phi) \ \exp \{\pm i\beta_{cl} z\} \ \exp \{+ i\omega_{cl} t \}, \tag{2.2}$$

where β_{cl} is the propagation constant, ω_{cl} is the angular frequency given by $2\pi c/\lambda$ in terms of the free space wavelength λ, and the subscript cl is used to denote the classical approach.

Equation (2.1) then becomes

$$(\nabla_t^2 + \kappa_i^2) \Phi = 0, \tag{2.3a}$$

where

$$\kappa_i^2 = k_0^2 n_i^2 - \beta_{cl}^2; k_0 = \omega_{cl}/c. \tag{2.3b}$$

In cylindrical coordinates, ∇_t^2 is given by

$$\nabla_t^2 = \partial^2/\partial\rho^2 + \rho^{-1}\,\partial/\partial\rho + \rho^{-2}\,\partial^2/\partial\phi^2 . \tag{2.4}$$

Substituting (2.4) into (2.3) and assuming separability with respect to the variables ρ and ϕ, viz., $\Phi(\rho,\phi) = R(\rho)\ F(\phi)$, we get a set of ordinary differential equations; specifically,

$$d^2R/d\rho^2 + \rho^{-1}\ dR/d\rho + (\kappa_i^2 - \nu^2/\rho^2)\,R = 0\,, \tag{2.5a}$$

$$d^2F/d\phi^2 + \nu^2 F = 0, \tag{2.5b}$$

where ν is an integer. Eq. (2.5a) is the Bessel differential equation and Eq. (2.5b) is the second-order, ordinary, harmonic differential equation. Solving (2.5a) and (2.5b) and recombining variables, a general solution to the Helmholtz equation (2.3) can now be written as

$$\Phi(\rho,\phi) = \begin{cases} A\,J_\nu(\kappa_i\rho) + B\,Y_\nu(\kappa_i\rho) \\ C\,I_\nu(\bar{\kappa}_i\rho) + D\,K_\nu(\bar{\kappa}_i\rho) \end{cases} \cos\nu\phi\,, \qquad \begin{matrix} \kappa_i^2 > 0 \\ \kappa_i^2 < 0 \end{matrix} \tag{2.6a}$$

where A, B, C, and D are constants; J_ν, Y_ν, I_ν, and K_ν are the ordinary and the modified Bessel functions, and

$$\bar{\kappa}_i = \pm j\,\kappa_i\,. \tag{2.6b}$$

In the classical analysis of a waveguide solution, one would determine which of these

constants need to be zero so as to acquire practically realizable solutions. In order to do that, we will first determine the respective regions of the waveguide in which $\kappa_i^2 > 0$ and $\kappa_i^2 < 0$.

The waveguiding condition for the propagation constant β_{cl} is given by

$$n_2\ \omega_{cl} < \beta_{cl}\ c < n_1\ \omega_{cl}\,. \tag{2.7}$$

When the condition (2.7) is not met, evanescent or leaky modes are generated since it is not possible to have real values of β_{cl} satisfy the eigenvalue equation. The eigenvalue (or, dispersion) equation governs the behavior of β_{cl} with respect to the angular frequency ω of operation and we will derive it later. Condition (2.7) implies that $\kappa_i^2 > 0$ in the core and $\kappa_i^2 < 0$ in the cladding region.

Elementary solutions for the Helmholtz equation (2.3) in the two regions of interest, the core and the cladding, are thus given by Eqs. (2.6), with the top expression in the brackets corresponding to the core region and the bottom expression being valid in the cladding. Since $Y_\nu(\kappa_1\rho) \to \infty$ for $\rho = 0$ and $I_\nu(\kappa_2\rho) \to \infty$ as $\rho \to \infty$, the constants B and C are taken to be zero so that physically realizable solutions are obtained. Further, for simplicity of analysis, we assume that there is no azimuthal dependence of the field ($\nu = 0$). Hence, the solution simplifies to

$$\Phi(\rho) = \begin{cases} A\,J_0(\kappa_1\rho) \\ D\,K_0(\bar{\kappa}_2\rho) \end{cases}, \qquad \begin{matrix} \rho < a \\ \rho > a \end{matrix}\ . \tag{2.8}$$

The constants A and D can be determined by imposing the boundary conditions, as shown below.

2. 1. 2 Weakly Guiding Fibers & Linearly Polarized Modes

In most practical optical fibers, the refractive indices of the core and the cladding are nearly equal. If the parameter Δ is defined as

$$\Delta = \frac{n_1^2 - n_2^2}{2n_1^2} \cong \frac{n_1 - n_2}{n_1} , \qquad (2.9)$$

then the condition $\Delta << 1$ is called the weak-guidance condition and an optical fiber with this property is called a weakly-guiding fiber. Using this weakly-guiding condition, the exact solutions of Maxwell's equations can be simplified to give an insight into the properties of certain combinations of modes, termed linearly polarized (LP) modes. Apart from the simplification in the analysis and the ease in understanding the mode phenomena, the concept of LP modes has other useful properties. Gloge has shown that it is possible to calculate the fields in the fiber and the characteristic equations of LP modes directly from Maxwell's equations [21]. The solutions so obtained are based on the scalar wave equation and for this reason, the LP modes are sometimes referred to as "scalar modes".

At this point in the analysis, it is interesting to note the use of Eq. (2.1) to describe the transverse fields in the fiber. Typically, in the exact analysis of an optical fiber waveguide, the vector mode solutions for all transverse components can be explicitly expressed in terms of the longitudinal components which can be derived from an equivalent scalar wave equation. It is a property of the Laplacian in the Cartesian

coordinate system that enables us to express each of the six components (E_x, H_y, E_y, H_x, E_z, H_z) as a solution to the scalar wave equation. Note that the fields E_ρ, E_ϕ, H_ρ, H_ϕ do not satisfy the scalar wave equation. Another point of importance, and often of confusion, is that although we postulate a set of LP mode components in the Cartesian system [either (E_x, H_y) or (E_y, H_x)] to constitute the fields in the fiber, we express their behavior in the cylindrical coordinate system (ρ, ϕ, z).

These properties of LP modes imply that the solution $\Phi(\rho)$ in Eq. (2.8) can be considered as a representation of the LP_{01} mode of a fiber, the first subscript denoting that $\nu = 0$. In order to find a relation between the constants A and D in Equation (2.8), we use the property of LP modes that to meet all boundary conditions, it is sufficient that Φ and $d\Phi/d\rho$ be continuous at $\rho = a$, where a is the radius of the fiber. This leads us to our final expression for the elementary solution for the Helmholtz equation (2.3), viz.,

$$\Phi(\rho) = \begin{cases} A\, J_0(\kappa_1 \rho) & \rho < a \\ \dfrac{A\, K_0(\bar{\kappa}_2 \rho)}{K_0(\bar{\kappa}_2 a)} J_0(\kappa_1 a) & \rho > a \end{cases}, \qquad (2.10)$$

as well as to the characteristic equation of the fiber

$$\frac{\kappa_1 J_1(\kappa_1 a)}{J_0(\kappa_1 a)} = \frac{\bar{\kappa}_2 K_1(\bar{\kappa}_2 a)}{K_0(\bar{\kappa}_2 a)}, \qquad (2.11)$$

where we have used the property of the Bessel functions, $J_0'(\kappa_1 a) = -J_1(\kappa_1 a)$ and $K_0'(\kappa_2 a) = -K_1(\kappa_2 a)$, and the primes indicate derivatives with respect to the arguments

of the Bessel functions. The dispersion relationship (2.11) along with the relation

$$V^2 = a^2 (\kappa_1^2 + \bar{\kappa}_2^2) \tag{2.12}$$

forms a set of equations which can be evaluated numerically to generate a graph of β versus ω. In Eq. (2.12), V is the normalized frequency given by

$$V = \frac{2\pi a}{\lambda} \sqrt{n_1^2 - n_2^2} = \frac{\omega a}{c} \sqrt{n_1^2 - n_2^2} \; . \tag{2.13}$$

Instead of plotting the graph of β versus ω, one conventionally plots a normalized version of the same, namely, the variation of the normalized propagation constant b versus the normalized frequency V, where b is defined as [21]

$$b = \frac{\frac{\beta^2}{k_0^2} - n_2^2}{n_1^2 - n_2^2} \; . \tag{2.14}$$

The dispersion relationship for the fundamental LP_{01} mode, plotted in Figure 2.1, defines the allowed propagation constant value for a given frequency of operation. This relationship is a direct upshot of the waveguiding constraints imposed by the cylindrical wall (cladding) and introduces the major difference in this analysis as compared to the free-space case. The other criterion that will be different in this analysis is the inclusion of material dispersion which we will consider in Chapter 5.

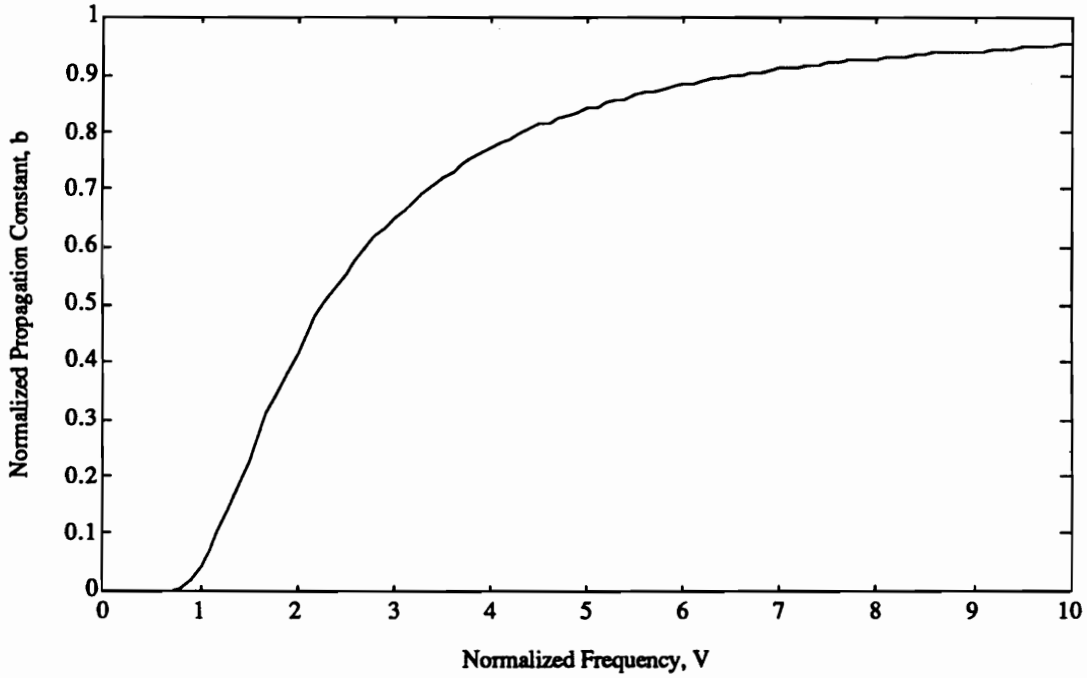

Figure 2.1. Dependence of the normalized propagation constant on normalized frequency. Below V values of 0.4 numerical evaluation gives insignificant values. In theory, the fundamental mode has a zero cutoff value.

2. 1. 3 Temporal Fourier Synthesis

Solutions obtained in the previous section are valid only for a single operational frequency, ω. Practical solutions can be obtained for any source spectrum $A(\omega)$ by using the temporal Fourier synthesis, namely,

$$\psi(\rho,z,t) = \frac{1}{2\pi} \int d\omega \int d\beta \; A(\omega) J_0(\kappa_1 \rho) \exp(i\omega t) \times \exp(-i\beta z) \, \delta(\beta - f(\omega)), \tag{2.15}$$

where the plane wave defined by $\exp[i\omega t - i\beta z]$ is used as the basis function and $f(\omega)$ is defined by the plot in Fig. 2.2, where we show the explicit dependence of β on ω.

All previous analyses of complicated source spectra have been performed using the classical Fourier approach where modal solutions have been obtained for a monochromatic plane-wave variation in the longitudinal direction of propagation. Our aim in this thesis is to construct different source spectra that will give rise to nondispersive packet-like solutions. Shaarawi [22] has shown that in the classical Fourier method of synthesis, it is very difficult to conjure up, or design, apposite source spectra because of their complicated mathematical nature. We will show in the following sections how a transformation to the bidirectional representation will solve this complexity and lead to simpler expressions for source spectra that will lead to LW solutions.

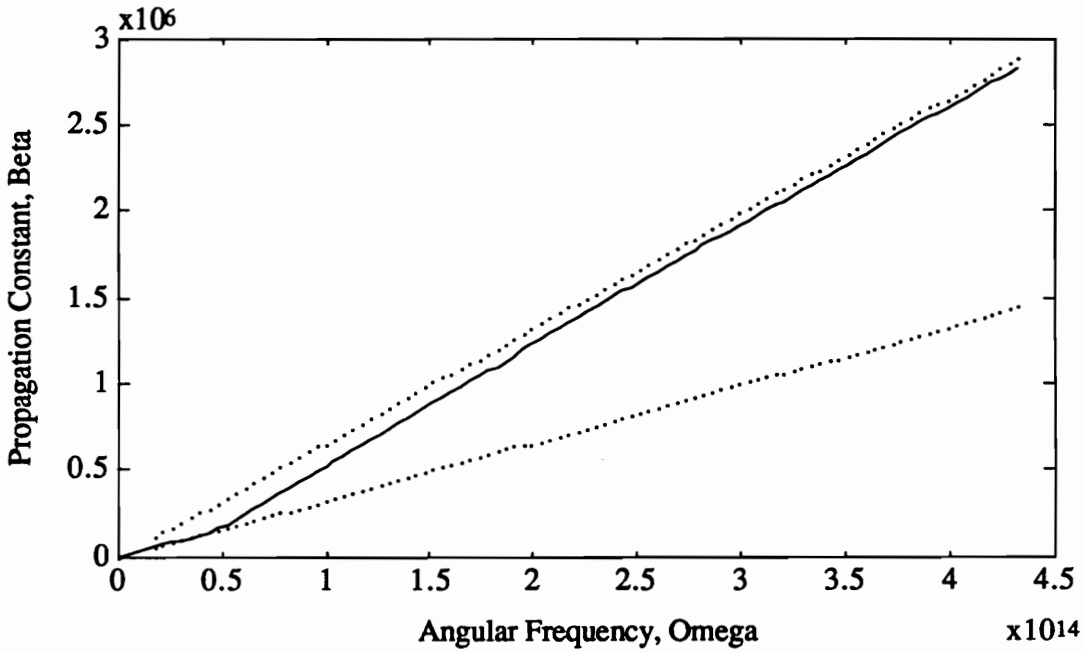

Figure 2.2. Dependence of the propagation constant, β, on angular frequency, ω. Values used: $n_1 = 2.0$, $n_2 = 1.0$, $a = 4\ \mu m$. Note that the graph lies between two straight lines with slopes n_1/c and n_2/c shown by dotted lines. The specific values of n_1 and n_2 were chosen only to highlight the behavior of the plot. Note that at low frequency, the propagation constant is essentially given by that corresponding to the cladding; at high frequency, it approaches that of the core.

2.2 Bidirectional Representation

2. 2. 1 Background

According to the bidirectional decomposition [13], we use basis functions that comprise a product of two counterpropagating plane waves. As described by Shaarawi [22], this method of superposition leads to several simplifications. Specifically, some of the branch-cut singularities that one encounters in the Fourier synthesis are now converted into tame algebraic singularities; this leads to the elimination of the multivaluedness that typically accompanies branch-cut singularities and for numerical evaluation of solutions, large oscillations that are present due to the branch-cut singularities are now removed. As mentioned before, it is now easier to consider different spectra that can give rise to LW solutions.

We therefore assume a solution of the type

$$\psi(\rho,\phi,z,t) = \Phi(\rho,\phi)\ \exp\{i\beta(z+ct)\}\ \exp\{-i\alpha(z-ct)\}$$

$$= \Phi(\rho,\phi)\ \exp\{i\beta\eta\}\ \exp\{-i\alpha\zeta\}, \qquad (2.16)$$

where $\eta = z + ct$ and $\zeta = z - ct$. Note that we have not made any changes in the transverse variation of the field and the expressions derived earlier will still be valid, with a few substitutions. In Eq. (2.16), α and β correspond to the propagation constants of the multiplicatively forward and backward propagating plane waves, respectively, that form the basis function. Breaking up the Laplacian into its transverse

component ∇_t^2 and a longitudinal component ∂_z^2, we can write the following:

$$\partial_z^2\psi = -(\beta-\alpha)^2\psi, \tag{2.17}$$

$$\partial_t^2\psi = -c^2(\beta+\alpha)^2\psi. \tag{2.18}$$

We seek to establish a one-to-one correspondence between the parameters in the bidirectional approach and in the classical analysis. Since the waveguiding conditions that the mode propagation constant β_{cl} should satisfy are known in the classical analysis, the one-to-one correspondence will determine the constraints on the parameters α and β, as well as help in establishing the regions denoted by $\kappa_i^2 > 0$ and $\kappa_i^2 < 0$, respectively. This is a valid means of obtaining some of the desired conditions because the bidirectional decomposition is an alternate method for the synthesis of pulse-like solutions and not a replacement for the classical Fourier synthesis. There exists a parallel between the two methods, and it is most advantageous to extract maximum information from each of these approaches.

Comparing Eqs. (2.2) and (2.16), we can show the correspondence:

$$\beta_{cl} \leftrightarrow (\beta-\alpha) \text{ and } \omega_{cl} \leftrightarrow -(\alpha+\beta)c\,, \tag{2.19}$$

or

$$\beta_{cl} \leftrightarrow (\alpha-\beta) \text{ and } \omega_{cl} \leftrightarrow (\alpha+\beta)c\,. \tag{2.20}$$

The constraint on the range of β_{cl} given by Eq. (2.7) can also be expressed as the set of equations

$$(n_1\,\omega_{cl})^2 - (\beta_{cl}\,c)^2 > 0, \tag{2.21}$$

$$(\beta_{cl}\,c)^2 - (n_2\,\omega_{cl})^2 > 0\,. \tag{2.22}$$

The corresponding equations for the bidirectional approach give us

$$n_1^2 (\alpha+\beta)^2 - (\alpha-\beta)^2 > 0, \tag{2.23}$$

$$n_2^2 (\alpha+\beta)^2 - (\alpha-\beta)^2 < 0, \tag{2.24}$$

thereby implying, as in the classical analysis, that $\kappa_1^2 > 0$ and $\kappa_2^2 < 0$.

We now proceed to develop the generalized solution to the scalar wave equation by using the bidirectional representation. In the analysis that follows, the constraint on α and β, given by the equation $\kappa_i^2 = n_i^2 (\alpha+\beta)^2 - (\alpha-\beta)^2$, is difficult to handle. For this reason, we model the waveguide as one with a core of refractive index $n_1 = 1$ and a cladding of effective refractive index $n_2 = n_e$ ($n_e < 1$). It is fairly simple to calculate this effective index n_e, as shown below.

2. 2. 2 Equivalent Waveguide with $n_1 = 1$

A method to calculate the effective refractive index, n_e, of the cladding for a unity core refractive index is now given. The analysis will be carried out in the classical notation. The underlying principle is that the expressions for the fields in the core and the cladding, as well as the eigenvalue equation, should remain unchanged by this transformation. The fields in the core and the cladding can be described completely in terms of κ_1 and κ_2. The eigenvalue equation given by (2.11) can be expressed in the form $f(\kappa_1, \kappa_2) = 0$. This implies that, if by a simple transformation, we can express κ_1 and κ_2 in terms of $n_1 = 1$ and $n_2 = n_e$, we will have an equivalent waveguide.

Consider the transformation, $k_0' = k_0 n_1$. κ_1 and κ_2 can then be defined by

$$\kappa_1^2 = k_0'^2 - \beta^2 \tag{2.25a}$$

and

$$\kappa_2^2 = k_0'^2 \left(\frac{n_2}{n_1}\right)^2 - \beta^2, \tag{2.25b}$$

respectively. Comparing Eqs. (2.25) with (2.3b) we see that for $n_1 = 1$ and $n_e = n_2/n_1$, we now have an equivalent waveguide in a frequency-scaled system which maintains the eigenvalue equation of the fiber as well as the expressions for the fields in the core and the cladding regions. All results obtained in the sequel are in the frequency-scaled system.

2. 2. 3 Generalized Solution

The change in notations for the refractive indices alters the relation between κ_i and (α, β) to

$$\kappa_1^2 = 4\alpha\beta \tag{2.26a}$$

and

$$\kappa_2^2 = n_e^2 (\alpha+\beta)^2 - (\alpha-\beta)^2. \tag{2.26b}$$

Before we arrive at the generalized solution that corresponds to the Fourier synthesis described by Eq. (2.15) we will consider the constraint imposed by the eigenvalue equation (2.11) and its implications in the (α, β) domain or, equivalently, in the (κ_1, κ_2) domain where κ_1 and κ_2 are defined by Eqs. (2.26). There are two distinct ways of understanding these implications and these two distinct interpretations will lead to

different methods of solving for explicit expressions for LW solutions.

2.2.3.1 Approach # 1.

In the first approach, we assume that the eigenvalue equation is a form of the expression

$$f(\alpha, \beta) = 0 \ . \tag{2.27}$$

A numerical evaluation of (2.11) gives us the constraint on the choice of β's given a value for α. This dependence is shown in Figure 2.3. The solution is plotted for various values of the effective refractive index n_e. We notice that as n_e approaches unity, the dependence of β on α becomes weaker as expected.

We can then write the generalized solution as

$$\psi(\rho,\zeta,\eta) = \frac{1}{(2\pi)^2} \int d\kappa_1 \int d\alpha \int d\beta \ A(\alpha,\beta,\kappa_1)\, \kappa_1 J_0(\kappa_1\rho)\, e^{-i\alpha\zeta}\, e^{i\beta\eta} \times \delta(4\alpha\beta - \kappa_1^2)\, \delta\big(\beta - g(\alpha)\big), \tag{2.28}$$

for $\rho \leq a$, where the constraint (2.26a) has been incorporated within the integral by the delta function and $g(\alpha)$ is the dependence of β on α defined in Figure 2.3. Similarly, for the region $\rho \geq a$, we have

$$\psi(\rho,\zeta,\eta) = \frac{1}{(2\pi)^2} \int d\kappa_1 \int d\bar{\kappa}_2 \int d\alpha \int d\beta \; A(\alpha,\beta,\kappa_1)\, \kappa_1 \; K_0(\bar{\kappa}_2\rho)$$

$$\times \frac{J_0(\kappa_1 a)}{K_0(\bar{\kappa}_2 a)} \; e^{-i\alpha\zeta}\, e^{i\beta\eta}\, \delta\left(\kappa_1^2 - 4\alpha\beta\right) \tag{2.29}$$

$$\times \; \delta\left(\bar{\kappa}_2^{\,2} + n_e^2 (\alpha+\beta)^2 - (\alpha - \beta)^2\right) \quad \delta\left(\beta - g(\alpha)\right),$$

where we have included all the conditions imposed on the choice of κ_1, κ_2, α and β with the help of delta functions.

In the analysis that follows, we will be concerned mainly with the evaluation of the core solutions and hence we need to further investigate the limits on the integrals in (2.28). The constraints on α and β are given by the bidirectional equivalent of (2.7). This condition was implicit in the acquisition of Figure 2.3; that is, in order to obtain real-valued solutions for α and β to the eigenvalue equation, we had already taken the waveguiding constraint into account. Hence, if we perform the κ_1 integral first and the β integral next, the integral over β needs to be carried out only in the α range in which $g(\alpha)$ is valid and real. Hence, in this approach we require the use of numerical techniques to evaluate the final LW solutions to any given spectrum $A(\alpha, \beta)$.

2.2.3.2 Approach # 2.

In the second approach, we consider the eigenvalue equation (2.11) to be expressible in the form

$$f(\kappa_1, \kappa_2) = 0 \; . \tag{2.30}$$

This relation gives the dependence of κ_1, an equivalent propagation constant related to α and β, on another equivalent propagation constant, κ_2, that is directly dependent on α, β and n_e. This variation of κ_1 with κ_2 is shown in Figure 2.4.

A general solution to the scalar wave equation can now be written in terms of the superposition

$$\psi(\rho,\zeta,\eta) = \frac{1}{(2\pi)^2} \int d\kappa_1 \int d\alpha \int d\beta \; A(\alpha,\beta,\kappa_1)\, \kappa_1 J_0(\kappa_1\rho) \times e^{-i\alpha\zeta} e^{i\beta\eta} \delta(4\alpha\beta - \kappa_1^2), \tag{2.31}$$

for $\rho \leq a$, where only the constraint (2.26a) has been incorporated within the integral. Similarly, for the region $\rho \geq a$, we have

$$\psi(\rho,\zeta,\eta) = \frac{1}{(2\pi)^2} \int d\kappa_1 \int d\bar{\kappa}_2 \int d\alpha \int d\beta \; A(\alpha,\beta,\kappa_1)\, \kappa_1 \; K_0(\bar{\kappa}_2\rho) \times \frac{J_0(\kappa_1 a)}{K_0(\bar{\kappa}_2 a)} e^{-i\alpha\zeta} e^{i\beta\eta} \delta\left(\bar{\kappa}_2 - h(\kappa_1)\right) \times \delta\left(4\alpha\beta - \kappa_1^2\right) \; \delta\left(\bar{\kappa}_2^2 + n_e^2(\alpha+\beta)^2 - (\alpha-\beta)^2\right), \tag{2.32}$$

which includes all the boundary conditions that ψ should satisfy at $\rho = a$ as well as the constraints (2.26) and (2.30). In Eq. (2.32), $h(\kappa_1)$ denotes the constraint imposed on the choice of κ_2 once a value is chosen for κ_1 and is shown in Fig. 2.4. In this approach, therefore, we have transferred all responsibility of accounting for the waveguide dispersion to the cladding solution evaluation. The simplifying beauty resulting from this mathematical sleight of hand is evident from the ease of evaluating

the core solutions without invoking the need for numerical techniques. The only complication that goes into the evaluation of ψ in the core is the determining of the limits on the integrals, which we shall address next.

The limits on the integrals in the Equations (2.31) and (2.32) will be dependent on the constraints given by the expressions (2.23) and (2.24) along with the two choices for the one-to-one correspondence between the classical analysis and the bidirectional approach, (2.19) and (2.20).

Choice 1: Equation (2.19) reduces the constraint (2.23) to

$$- n_2 (\alpha + \beta) < (\beta - \alpha) < - n_1 (\alpha + \beta), \tag{2.33}$$

which, for $n_1 = 1$ and $n_2 = n_e$ gives us the two conditions

$$\alpha/\beta < s \text{ and } \alpha\beta < 0, \tag{2.34}$$

where $s = [(1+n_e) / (1-n_e)]$. As a consequence, the limits of the integrals in Equations (2.31) and (2.32) can be written as

$$\int_0^{\infty} d\kappa_i \int_{-\infty}^{0} d\beta \int_0^{\beta s} d\alpha \, I \ , \tag{2.35}$$

or

$$\int_0^{\infty} d\kappa_i \int_{-\infty}^{0} d\alpha \int_0^{\alpha/s} d\beta \, I \ , \tag{2.36}$$

where I represents the integrand in each of the integrals. The order in which the integrations are carried out (first over the variable α and then over β, or vice versa)

determines which of the above two equations is applicable. In Eq. (2.35) we note, however, that since β is always negative, the integration over α is from zero to a negative number, β's ($s > 0$). But α should always be positive to satisfy the condition, $\alpha\beta < 0$. Hence, Eq. (2.35) gives us a contradiction in terms and leads to a trivial solution that is always equal to zero. Similarly, we can show that changing the order of integration [cf. Equation (2.36)] will also lead to a situation where both the conditions in (2.34) cannot be satisfied.

Choice 2: Equation (2.20) reduces the constraint (2.24) to

$$n_2 (\alpha + \beta) < (\alpha - \beta) < n_1 (\alpha + \beta), \tag{2.37}$$

which, for $n_1 = 1$ and $n_2 = n_e$ gives us the two conditions

$$\alpha/\beta > s \text{ and } \alpha\beta > 0. \tag{2.38}$$

As a result, the limits of the integrals in Equations (2.31) and (2.32) can be written, for the case when both α and β are greater than zero, as

$$\int_0^{\infty} d\kappa_i \int_0^{\infty} d\beta \int_{\beta s}^{\infty} d\alpha \, I \ , \tag{2.39}$$

or

$$\int_0^{\infty} d\kappa_i \int_0^{\infty} d\alpha \int_0^{\alpha/s} d\beta \, I \ , \tag{2.40}$$

where I represents the integrand in each of the integrals. With this choice of the one-to-one correspondence, it is possible to satisfy both conditions in the expression (2.38). Also, in the limit $n_e \rightarrow 1$, we would expect that the solution should vanish since the

waveguiding constraint is no longer met. This is evident from the limits, since $s \rightarrow \infty$, and the integrals (2.39) and (2.40) go to zero for any integrand.

The generalized solutions (2.31) and (2.32) have been obtained under the assumption that the constraints (2.23) and (2.24) are satisfied in all regions. Hence, the limits in (2.39) and (2.40) are applicable to the evaluation of the generalized solutions in the core as well as the cladding regions in this approach. Analogous to our argument in Approach # 1 that the limits are no longer necessary when the dispersion relation is incorporated as a delta function into the integral, one would tend to believe that this reasoning would be true for the cladding solution in this approach. However, this is not the case since the only conclusion that can be drawn from the analysis in the classical scheme is that the constraints imply that real values of β_{cl} will result; this statement can be extended to imply in the first approach that real values of α and β will be obtained. However, for the expressions for κ_1 and κ_2 there are no such guarantees because of the squared terms that appear in their respective defining relations (2.26).

In summary, the two approaches presented above lead to different methods of analysis. We will choose the latter since closed-form solutions can be obtained through this method and it provides a physical picture of the LW solutions. The first approach necessitates the use of numerical methods and we will consider this approach only briefly in this work. We will show later, in Chapter 5, how this approach may be better suited when we consider material dispersion.

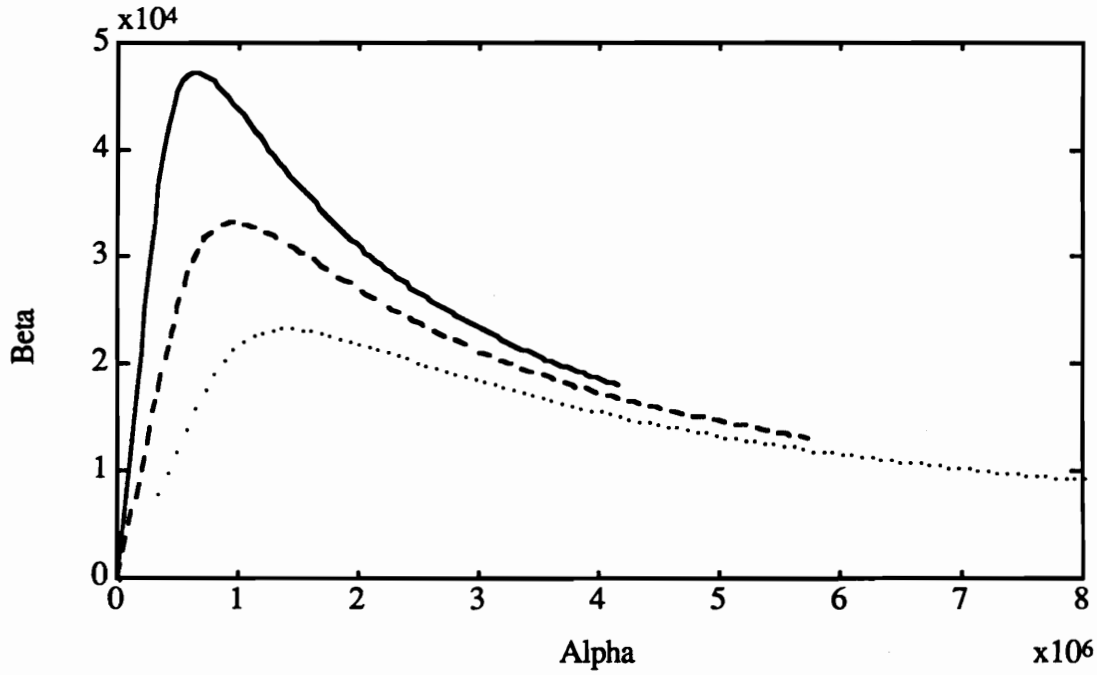

Figure 2.3. Relationship between the forward and backward propagation constants, α and β, respectively, for different values of effective refractive index. The graph shows the condition imposed on the choice of α and β due to waveguide dispersion. Solid Line: $n_e = 0.80$. Dashed line: $n_e = 0.9$. Dotted Line: $n_e = 0.95$.

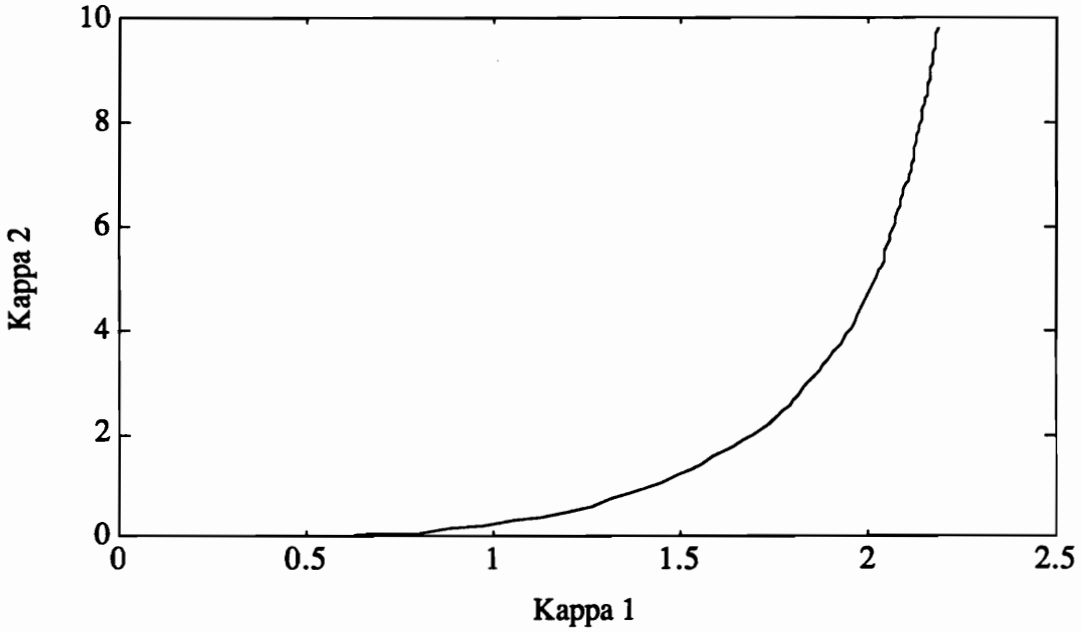

Figure 2.4. Constraint imposed on the choice of κ_2 once a value of κ_1 is selected.

3.0 PACKET-LIKE SOLUTIONS IN FIBERS

Different choices of the modulation spectrum $A(\alpha,\beta,\kappa)$ entering into the bidirectional representations (2.31) and (2.32) can now lead to the desired packet-like solutions. In this section, we consider four specific spectra and derive solutions which resemble the ideal FWM, the scalar analog to Hillion's spinor modes, the ideal splash pulse, and the ideal modified power spectrum pulse. It is interesting to note in the analysis that follows that the simplicity of the final expressions for the localized solutions depends on the order in which the integrations in Equation (2.31) are carried out. For instance, the integration, first over α and then over β, described by Equation (2.35), would very likely lead to a compact solution in the form of an integral which might need numerical evaluation. On the other hand, if the order of integration were reversed, as described by Equation (2.36), we might be able to extract information about the ideal free space solution which the pulse would resemble. In such cases, the solution ψ is broken up into two parts, viz., $\psi = \psi_u + \psi_w$, where the subscript u indicates the unperturbed packet-like solution and the subscript w stands for the additional wall term introduced by the waveguiding constraint.

3.1 Examples of Source Spectra

In the following subsections, we summarize results obtained from the synthesis of four different spectra. All spectra are chosen based on their track record, namely, their ability to generate packet-like solutions in free space. Only an evaluation of the integrals is presented in this section. Detailed numerical results are given in Section 3.2.

3.1.1 Focus Wave Modes

We first consider the singular spectrum

$$A(\alpha,\beta,\kappa_1) = (8\pi^2 a_1)\ \delta\ (\beta-\beta')\ \exp\ (-\alpha a_1), \tag{3.1}$$

which, in free space, has given rise to FWM's, as introduced by Belanger, Sezginer and Ziolkowski. The constants a_1 and β' are free parameters in the source modulation spectrum which will be useful in adjusting the synthesized solutions to give directed energy transfer in the waveguide.

We first substitute the singular spectrum (3.1) into the bidirectional representation (2.31). After integrating over κ_1 and using the sifting property of the delta function, ψ_u is found to be

$$\psi_u\ (\rho,\zeta,\eta) = a_1 \int_0^\infty d\alpha\quad J_0\ (\sqrt{4\alpha\beta'}\ \rho)\ \exp\left(-i\alpha\zeta - \alpha a_1\right) \exp\left(+i\beta'\eta\right)\ , \tag{3.2}$$

and ψ_w is expressed as

$$\psi_w(\rho,\zeta,\eta) = -a_1 \int_0^{\alpha'} d\alpha \quad J_0(\sqrt{4\alpha\beta'}\,\rho) \exp(-i\alpha\zeta - \alpha a_1) \exp(+i\beta'\eta) \quad , \quad (3.3)$$

where $\alpha' = \beta's$.

We first obtain a closed-form solution for ψ_u. Using the identity (6.614.1) from Gradshteyn and Ryzhik [23], viz.,

$$\int_0^{\infty} d\beta \quad J_0(\sqrt{\beta}\,b)\; e^{-\beta a} \quad = \frac{b}{4}\sqrt{\frac{\pi}{a^3}} \exp\left[-\frac{b^2}{8a}\right] \left(I_{-1/2}\left(\frac{b^2}{8a}\right) - I_{1/2}\left(\frac{b^2}{8a}\right) \right) \quad (3.4)$$

and the Bessel function relation

$$\left[I_{-1/2}(z) - I_{1/2}(z) \right] = \sqrt{\frac{2}{\pi z}} \exp(-z), \quad (3.5)$$

we obtain the relation

$$\int_0^{\infty} d\beta \;\; J_0(b\sqrt{\beta})\, e^{-\beta a} \;\; = \frac{1}{a} \exp\left(-\frac{b^2}{4a}\right) . \quad (3.6)$$

From Eqs. (3.2) and (3.6), we then obtain the FWM solution

$$\psi_u(\rho,\zeta,\eta) = a_1 \frac{\exp(i\beta'\eta)}{(a_1 + i\zeta)} \exp\left[-\frac{\beta'\rho^2}{(a_1 + i\zeta)}\right]. \quad (3.7)$$

We can rewrite the expression for ψ_w, (3.3), as

$$\psi_w(\rho,\zeta,\eta) = -2\, a_1\, e^{+i\beta'\eta} \int_0^{\sqrt{\alpha'}} w\, dw \quad J_0(\sqrt{4\beta'}\,\rho w)\, e^{-w^2(a_1 + i\zeta)} \quad , \quad (3.8)$$

where we have made the substitution $w^2 = \alpha$. Using the identity (1.8.2.4) from Prudnikov *et al.* [24], namely,

$$\int_0^x x^{\nu+1} e^{ax^2} J_\nu(bx)\, dx = \frac{b^\nu e^{ax^2}}{(2ia)^{\nu+1}} \left[U_{\nu+1}(2iax^2, bx) + i\, U_{\nu+2}(2iax^2, bx)\right], \quad (3.9)$$

where

$$U_n(z,\zeta) = \sum_{k=0}^{\infty} (-1)^k \left(\frac{z}{\zeta}\right)^{2k+\nu} J_{2k+\nu}(\zeta) \quad (3.10)$$

is the Lommel function of two variables, we obtain

$$\psi_w = \frac{i\, a_1\, e^{-\beta'(a+i\zeta)s}}{(a+i\zeta)} \times \left(U_1\left[-2i\beta'(a_1+i\xi)s,\, 2\rho\beta'\sqrt{s}\right] + iU_2\left[-2i\beta'(a_1+i\xi)s,\, 2\rho\beta'\sqrt{s}\right]\right), \quad (3.11)$$

which gives us the final closed-form solution for the wall term. In Eq. (3.10), s, as defined earlier, is given by $[(1+n_e)/(1-n_e)]$.

A similar analysis can now be extended to the scalar field solution in the cladding. The constraints imposed by the delta functions in Eq. (2.32), however, necessi the use of a numerical integration and we will not address this issue in this section

3. 1. 2 sh Pulses

We co der next the spectrum

$$A(\alpha,\beta,\kappa_1) = 8\pi^2 a_1 a_2 \delta(\kappa_1 - \gamma) \exp\left[-(\alpha a_1 + \beta a_2)\right], \tag{3.12}$$

which, without the delta function, yields Ziolkowski's splash pulse in free space. Substituting the splash pulse spectrum (3.12) in the expression for the generalized solution of the scalar wave equation [cf. Eq. (2.31)] and integrating over β and κ_1, we get

$$\psi(\rho,\zeta,\eta) = 2\gamma a_1 a_2 J_0(\gamma\rho) \times \int_{\gamma\sqrt{s}/2}^{\infty} \frac{d\alpha}{4\alpha} \exp\left(-\alpha(a_1 + i\zeta)\right) \exp\left(-\frac{\gamma^2}{4\alpha}(a_2 - i\eta)\right). \tag{3.13}$$

Breaking up the solution into ψ_u and ψ_w, and using the identity (2.3.16.1) from Prudnikov *et al.* [24], namely,

$$\int_0^{\infty} \frac{dx}{x} \exp(-xa) \exp\left(-\frac{b}{x}\right) = 2K_0(2\sqrt{ab}), \tag{3.14}$$

we can arrive at the expressions

$$\psi_u = a_1 a_2 \gamma J_0(\gamma\rho) K_0\left(\gamma\sqrt{(a_1 + i\zeta)(a_2 - i\eta)}\right) \tag{3.15}$$

and

$$\psi_w = -\frac{a_1 a_2 \gamma}{2} \int_0^{\gamma\sqrt{s}/2} \frac{d\alpha}{\alpha} \exp\left[-\alpha(a_1 + i\zeta)\right] \exp\left[-\frac{\gamma^2}{4\alpha}(a_2 - i\eta)\right] \tag{3.16}$$

in the fiber core. Expressions for the cladding region can be obtained using numerical methods.

3.1.3 Scalar Analog to Hillion's Spinor Modes

We consider next the Bessel spectrum of order zero

$$A(\alpha,\beta,\kappa_1) = 8\pi^2 a_1 b J_0(\beta b) \exp(-\alpha a_1), \tag{3.17}$$

which, in free space, yields the scalar analog to Hillion's spinor modes. This spectrum presents a good example of arriving at different forms of expressions depending on the order of integration, as mentioned earlier. We will consider both cases here.

3.1.3.1 Integrate over β first.

Substituting the Bessel spectrum (3.17) into Equation (2.31) and integrating over κ_1, we obtain

$$\psi(\rho,\zeta,\eta) = a_1 b \int_0^{\infty} d\alpha \; e^{-\alpha(a_1 + i\zeta)} \int_0^{\alpha'} d\beta \; J_0(\sqrt{4\alpha\beta}\rho) \; J_0(\beta b) \, e^{i\beta\eta}, \tag{3.18}$$

where $\alpha' = \alpha / s$. Substituting $\beta = r\cos\theta$, $\alpha = r\sin\theta$ and $d\alpha \, d\beta = r \, dr \, d\theta$, Eq. (3.18) becomes

$$\psi(\rho,\zeta,\eta) = a_1 b \int_0^{\theta'} d\theta \int_0^{\infty} r \, dr \; J_0(\sqrt{4\sin\theta\cos\theta}\rho r) \; J_0(br\sin\theta) \times \exp\left(-r\left[\cos\theta\,(a_1 + i\xi) - i\eta\sin\theta\right]\right), \tag{3.19}$$

where $\tan\theta' = 1/s$. Using the identity (2.12.38.2) from Prudnikov *et al.* [24], namely,

$$\int_0^\infty dx \; x \; J_0(bx) \; J_0(cx) \, e^{-px} = A_{0,0}^2 \; , \tag{3.20}$$

where

$$A_{0,0}^2 = \frac{-p\,k^2\,(qd)^{-3/2}}{2\pi\sqrt{1-k^2}} \; Q_{-1/2}^1 \left(\frac{2-k^2}{k^2}\right), \tag{3.21}$$

we obtain

$$\psi = a_1 \, b \int_0^{\theta'} d\theta \, \frac{p}{\sqrt{qd} \; \left[(p^2+q^2+d^2) - 4\,q^2\,d^2\right]^{1/2}} Q_{-1/2}^1 \left(\frac{p^2+q^2+d^2}{2qd}\right) . \tag{3.22}$$

Here $k^2 = 4qc / [p^2 + (b+d)^2]$, $p = (a_1 + i\zeta)\cos\theta - i\eta \sin\theta$, $q = 2\rho\,(\sin\theta\,\cos\theta)^{1/2}$, $d = b\sin\theta$, and θ' is as defined earlier. $Q_n^m(z)$, an associated Legendre function, is a solution of the differential equation

$$\left(1-z^2\right)\frac{d^2Q_n^m}{dz^2} - 2z\frac{dQ_n^m}{dz} + \left[n(n+1) - \frac{m^2}{1-z^2}\right] Q_n^m = 0 . \tag{3.23}$$

3.1.3.2 Integrate over α first.

Substituting the Bessel spectrum (3.17) into Equation (2.31), integrating over κ_1, and breaking the solution into two parts, ψ_u and ψ_w, we obtain

$$\psi(\zeta,\eta) = b\,a_1 \int_0^\infty d\beta \int_0^\infty d\alpha \;\; e^{-\alpha(a_1 + i\zeta)} \; J_0\left(\sqrt{4\alpha\beta}\rho\right) \; J_0(\beta b) \, e^{i\beta\eta} . \tag{3.24}$$

Using the identities (2.12.39.10) and (2.12.8.3) from Prudnikov *et al.* [24], namely,

$$\int_0^{\infty} e^{-ipx}\, J_0\,(c\sqrt{x})\, J_0\,(bx)\, dx \;=\; \frac{1}{\sqrt{b^2 - p^2}}\; \exp\left(-\frac{ic^2 p}{4(b^2 - p^2)}\right) J_0\left(\frac{c^2 b}{4(b^2 - p^2)}\right), \quad (3.25)$$

and

$$\int_0^{\infty} e^{-ipx}\, J_0\,(cx)\, dx \;=\; \frac{1}{\sqrt{c^2 - p^2}}\,, \quad (3.26)$$

respectively, we obtain the following expression for the unperturbed pulse:

$$\psi_u = \frac{b\, a_1}{(a_1 + i\zeta)} \left[\left(\frac{\rho^2}{(a_1 + i\zeta)} - i\eta\right)^2 + b^2\right]^{-1/2}. \quad (3.27)$$

The contribution from the wall term, ψ_w, can be written as

$$\psi_w\,(\rho,\zeta,\eta) = -\, a_1 b \int_0^{\infty} d\beta\, J_0\,(\beta b)\, e^{i\beta\eta} \int_0^{\beta s} d\alpha \quad e^{-\alpha(a_1 + i\zeta)}\, J_0\,(\sqrt{4\alpha\beta}\rho). \quad (3.28)$$

The integral over α is of the same form as (3.3). Using an approach similar to that adopted for solving (3.3), we obtain

$$\psi_w = \frac{i\, a_1\, b}{(a + i\zeta)} \int_0^{\infty} d\beta\, \exp\left(-\beta\, \left[(a + i\zeta)s - i\eta\right]\right)$$
$$\times\; \left(U_1\,[-2i\beta(a_1+i\xi)s.\, 2\rho\beta\sqrt{s}\,] + iU_2[-2i\beta(a_1+i\xi)s.\, 2\rho\beta\sqrt{s}\,]\right). \quad (3.29)$$

3. 1. 4 Modified Power Spectrum (MPS) Pulse

We now consider the MPS pulse spectrum

$$A(\alpha, \beta, \kappa) = \left\{ \begin{array}{ll} \dfrac{\pi p}{2} \exp\left[-\alpha a_1 - (p\beta - b)\, a_2\right], & \beta > b/p \\ 0, & b/p > \beta > 0 \end{array} \right\}, \qquad (3.30)$$

which leads to localized, slowly decaying solutions in free space. We substitute the MPS pulse spectrum (3.30) into (2.31) and separate the integral into two parts, viz.,

$$\psi = \psi_u + \psi_w = \int_0^\infty d\kappa_1 \int_0^\infty d\alpha \int_0^\infty d\beta\, I \; - \int_0^\infty d\kappa_1 \int_0^\infty d\alpha \int_{\alpha/s}^\infty d\beta\, I\,, \qquad (3.31)$$

where ψ_u and ψ_w correspond to the first and second terms, respectively. We first evaluate ψ_u. Integrating over α first, ψ_u can be written as

$$\psi_u = \frac{p}{8\pi} \int_{b/p}^\infty \frac{d\beta}{\beta} \exp\left[(-\beta p + b)\, a_2 + i\eta\right] \times \int_0^\infty d\kappa_1\, \kappa_1\, J_0(\kappa_1 \rho) \exp\left(-\frac{\kappa_1^2 (a_1 + i\zeta)}{4\beta}\right). \qquad (3.32)$$

Using the identity (3.6), and integrating over κ_1 and β, we obtain

$$\psi_u(\rho, \zeta, \eta) = \frac{\exp\left[-\dfrac{b\chi}{p}\right]}{4\pi (a_1 + i\zeta)(a_2 + \chi/p)}\,, \qquad (3.33)$$

which is identical to the MPS pulse derived by Besieris *et al.* [13].

To evaluate ψ_w we switch the order of integration of α and β, and use the identity (3.9) to obtain

$$\psi_w = \frac{i\,p\,\exp(ba_2)}{2\pi\,(a+i\zeta)} \int_{b/p}^{\infty} d\beta\ \left\{ U_1\,[2i\beta(a_1+i\xi)s,\, 2\rho\beta\sqrt{s}\,] + iU_2[2i\beta(a_1+i\xi)s,\, 2\rho\beta\sqrt{s}\,] \right\} \times \exp\left(-\beta\Omega\right), \tag{3.34}$$

where $\Omega = (pa_2 - i\eta) + s\,(a_1 + i\zeta)$. By expressing the Lommel functions U_1 and U_2 in terms of a series of Bessel functions [cf. Eq. (3.10)], and switching the summation and integral evaluation one can show that the integrand is bounded and an end-point evaluation of the form

$$\int_a^{\infty} \exp\left[-\mu\, f(x)\right] g(x)\ dx \approx \frac{\exp\left[-\mu\, f(a)\right]\ g(a)}{\mu\left[\frac{df}{dx}(a)\right]} + O\left(\mu^{-2}\right) \tag{3.35}$$

is justified. Using the result from such an end-point evaluation, we arrive at the final expression for ψ_w, viz.,

$$\psi_w \approx \frac{i\,p\ \exp\left(ba_2 - b\Omega/p\right)}{2\pi\,(a+i\zeta)} \times \left\{ U_1\,[2i\frac{b}{p}(a_1+i\xi)s,\, 2\rho\frac{b}{p}\sqrt{s}\,] + iU_2[2i\frac{b}{p}(a_1+i\xi)s,\, 2\rho\frac{b}{p}\sqrt{s}\,] \right\}. \tag{3.36}$$

3. 1. 5 Splash Pulse Spectrum Without the Delta Function

The splash pulse spectrum described in 3.1.2 can be changed slightly by

removing the delta function $\delta(\kappa_1 - \gamma)$. The reason for considering this variation will become evident when we evaluate the distances over which such solutions remain localized. The spectrum, given by

$$A(\alpha,\beta,\kappa_1) = 8\pi^2 a_1 a_2 \exp\left[-(\alpha a_1 + \beta a_2)\right], \tag{3.37}$$

can now be substituted into Eq. (2.31) to obtain LW solutions. Integrating over κ_1, we obtain

$$\begin{aligned}\psi(\rho,\zeta,\eta) = 2 a_1 a_2 \int_0^\infty d\alpha \exp\left[-\alpha(a + i\zeta)\right] \\ \times \int_0^{\alpha_1} m\,dm \quad J_0(\sqrt{4\alpha}\,\rho m) \exp\left[-m^2(a_2 - i\eta)\right],\end{aligned} \tag{3.38}$$

where we have substituted $\beta = m^2$ and $\alpha_1 = (\alpha/s)^{1/2}$. Using the identity (3.9), we can write (3.38) as

$$\psi(\rho,\zeta,\eta) = \frac{a_1 a_2}{(a_2 - i\eta)} [I_1 + I_2], \tag{3.39}$$

where

$$\begin{aligned}I_1 = i \int_0^\infty d\alpha \exp\left[-\alpha(a_1 + i\zeta) - \alpha\frac{(a_2 - i\eta)}{s}\right] \\ \times U_1\left[-2i\frac{(a_2 - i\eta)\alpha}{s}, \frac{2\rho\alpha}{\sqrt{s}}\right],\end{aligned} \tag{3.40a}$$

$$\begin{aligned}I_2 = -\int_0^\infty d\alpha \exp\left[-\alpha(a_1 + i\zeta) - \alpha\frac{(a_2 - i\eta)}{s}\right] \\ \times U_2\left[-2i\frac{(a_2 - i\eta)\alpha}{s}, \frac{2\rho\alpha}{\sqrt{s}}\right],\end{aligned} \tag{3.40b}$$

and U_n is the Lommel function of two variables. Using the expansion of the Lommel function in terms of Bessel functions, defined by Eq. (3.10), interchanging the summation and integration operations, and using the expression (6.611.1) from Gradhsteyn ad Ryzhik [23], namely,

$$\int_0^\infty dx\ e^{-qx} J_\nu(px) = \frac{p^{-\nu}\left[\sqrt{p^2+q^2} - q\right]^\nu}{\sqrt{p^2+q^2}}, \tag{3.41}$$

we can arrive at

$$I_n = i\left(\sqrt{p^2+q^2}\right)^{-1} \sum_{k=0}^{\infty} (-1)^k (\ell)^{2k+n}, \tag{3.42}$$

where

$$\ell = -i\frac{(a_2 + i\eta)}{\rho\sqrt{s}} \times \frac{\left[\sqrt{p^2+q^2} - q\right]}{p}, \tag{3.43a}$$

$$p = \frac{2\rho}{\sqrt{s}}, \tag{3.43b}$$

and

$$q = (a_2 + i\zeta) + \frac{(a_1 - i\eta)}{s}. \tag{3.43c}$$

Assuming $q^2 >> 4\rho^2/s$, and going through a simple but lengthy algebraic evaluation, we obtain the final closed-form expression for ψ, given by

$$\psi = \frac{a_1 a_2}{(a_1 + i\zeta)} \left\{4\rho^2 s + \left[(a_1 + i\zeta)s + (a_2 - i\eta)\right]^2\right\}^{-1/2}. \tag{3.44}$$

3.2 *Evaluation of Localization Distances*

In this section we will evaluate distances up to which the solutions derived in the previous section remain localized. A typical trade-off observed during the analysis is the following. The pulse energy needs to be localized to the fiber core dimensions as well as in the longitudinal direction of propagation. In order to achieve both these qualities we need to pick values for the free parameters that will not contradict the two requirements. Our analysis therefore is limited to looking at the solution at $z = 0$ and analyzing the behavior with respect to ρ, and to observing the amplitude of the pulse as a function of z, the longitudinal direction of propagation. We define a decay parameter $\Gamma(z)$ as the ratio of the amplitude of the pulse after it has traveled some distance z to the initial amplitude at $z = 0$, to aid our analysis. We also define $|\psi|^0$ as the initial pulse amplitude, $|\psi|^+$ as the amplitude of the pulse propagating in the positive z–direction and $|\psi|^-$ as the amplitude of the pulse propagating in the negative z–direction.

3.2.1 *FWM Solution*

The initial pulse amplitude of the ideal FWM solution is given by

$$|\psi_u|^0 = \exp\left[-\frac{\beta' \rho^2}{a_1}\right]. \tag{3.45}$$

The variation of the field amplitude in the radial direction is dictated by the magnitude of the ratio β'/a_1 and is shown in Figure 3.1. A pulse propagating in the positive z direction has a pulse peak given by

$$|\psi_u|^+ = \exp\left[-\frac{\beta' \rho^2}{a_1}\right], \tag{3.46}$$

which is identical to the initial pulse amplitude. The distance over which this pulse can be utilized for communications purposes depends on the losses and the material dispersion of the waveguide. Transmission of energy in the positive direction seems possible with very little constraint on the free parameters of the source spectra. The wall term comprising the Lommel functions can be expected to impose further constraints on the pulse parameters. The behavior of Lommel functions will be more clearly seen for the MPS pulse in the next chapter.

3.2.2 Splash Pulse Solution

The amplitude of the unperturbed splash pulse solution, ψ_u, evaluated at $z = t = 0$ can be expressed as

$$\psi_u = a_1 a_2 \gamma J_0(\gamma\rho) K_0\left(\gamma \sqrt{a_1 a_2}\right). \tag{3.47}$$

The radial dependence of the field is governed by the magnitude of γ and is a simple Bessel function of order zero. The parameter γ is thus fixed to a value on the order of 10^{-6} m^{-1}. We need to ensure during synthesis that we do not impose any further constraints on the free parameter γ when considering the distances over which this pulse can remain nondecaying. At $z = t = 0$, $|\psi_u|^0$ is given at the center of the fiber ($\rho = 0$) by the equation

$$\left(|\psi_u|^0\right)^4 = a_1^3 a_2^3 \gamma^2 \frac{\pi^2}{4} \exp\left(-4\gamma \sqrt{a_1 a_2}\right), \tag{3.48}$$

where we have used the large argument expansion of the Bessel function and the fourth

power of the amplitude is taken only for convenience in deriving the results that follow. At z=ct, the amplitude of the pulse traveling in the positive direction, $|\psi_u|^+$, can be written as

$$(|\psi_u|^+)^4 = a_1^3 a_2^4 \gamma^2 \frac{\pi^2}{4\sqrt{a_2^2 + 4z^2}} \exp\left(-4\gamma\sqrt{a_1}\left[a_2^2 + 4z^2\right]^{1/4} \cos\phi\right), \quad (3.49)$$

where ϕ is given by the relation $\tan 2\phi = 2z/a_2$. Expressing $\cos\phi$ in terms of z and a_2, using the approximation $a_2 >> z$ of interest, and defining a decay factor Γ_u^4 as $|\psi_u^+|^4 / |\psi_u^0|^4$, we obtain an estimate for the nondecaying pulse distances. The decay factor Γ_u^4 can be written as

$$(\Gamma_u)^4 = \left(1 + \frac{4z^2}{a_2^2}\right)^{-1/2} \exp\left(-2\gamma\sqrt{a_1 a_2}\,\frac{z^2}{a_2^2}\right), \quad (3.50)$$

which shows that for the decay factor to remain ≈ 1, the value of the free parameter a_2 should be a few orders of magnitude greater than the distance, z, of interest. The decay parameter is plotted in Figure 3.2. Note also that the nondecaying nature of the solution can be controlled irrespective of the choice of values for the parameter γ, which defined the confinement of the field in the fiber core.

3. 2. 3 Scalar Analog to Hillion's Spinor Modes

The amplitude of the unperturbed pulse expression for the Bessel spectrum can be written, at $z = t = 0$, as

$$\psi_u = \left[1 + \left(\frac{\rho^2}{a_1 b}\right)^2\right]^{-1/2}. \quad (3.51)$$

This behavior is plotted in Figure 3.3. The corresponding expressions for

$|\psi_u|^0$ and $|\psi_u|^+$ are

$$|\psi_u|^0 = 1 \tag{3.52}$$

and

$$|\psi_u|^+ = \left[1 - \frac{4z^2}{b^2}\right]^{-1/2}. \tag{3.53}$$

The decay factor Γ has the same expression as $|\psi_u|^+$, given by (3.53), and we note that the pulse in the positive direction is singular at $\rho = 0$ and $z = b/2$. This behavior of the unperturbed, ideal pulse is physically unrealizable. If the wall term ψ_w cancels this singularity, the sensitivity to variations in initial distribution may make this pulse extremely difficult to realize in a practical sense.

3. 2. 4 Splash Pulse Spectrum Without the Delta Function

In all the previous examples in this section, we have considered the effect of the free parameters on the ideal pulse shapes. The only total pulse, $(\psi_u + \psi_w)$, that we will consider is the MPS pulse in Chapter 4. We will now investigate a pulse where the free parameters cannot be tweaked in order to generate a pulse that will propagate for long distances and at the same time be confined to the fiber core. Consider the splash pulse spectrum without the delta function $\delta(\kappa_1 - \gamma)$.

The initial pulse amplitude is given by

$$|\psi|^0 = a_2 \left\{4\rho^2 s + [a_1 s + a_2]^2\right\}^{-1/2}. \tag{3.54}$$

At the center of the fiber core, the amplitude of the pulse traveling in the positive direction can be written as

$$|\psi|^{+} = a_2 \left\{ 4z^2 s + [a_1 s + a_2]^2 \right\}^{-1/2} . \tag{3.55}$$

As a result, the decay factor, Γ, can be expressed in the form

$$\Gamma = \frac{|\psi|^{+}}{|\psi|^{0}} = \left\{ 1 + \frac{4z^2 s}{[a_1 s + a_2]^2} \right\}^{-1/2} . \tag{3.56}$$

From (3.54), the variation of the initial field amplitude in the core can be plotted versus the radius ρ as shown in Figure 3.4. The variation of the decay factor, Γ, is given in Figure 3.5, where we have made the assumption that $a_1 s << a_2$. Figure 3.4 shows that in order to confine the field to the core, the free parameter values should be on the order of 10^{-4} to 10^{-5}. At the same time, Figure 3.5 shows the decay factor will remain close to 1 for a_2 values on the order of 10^7 if nondecaying solutions over 1000 km distances are desired. This shows that the free parameter a_2 dictates both the variation of the field within the core and the distance over which the field remains non-decaying, and cannot meet the necessary requirements.

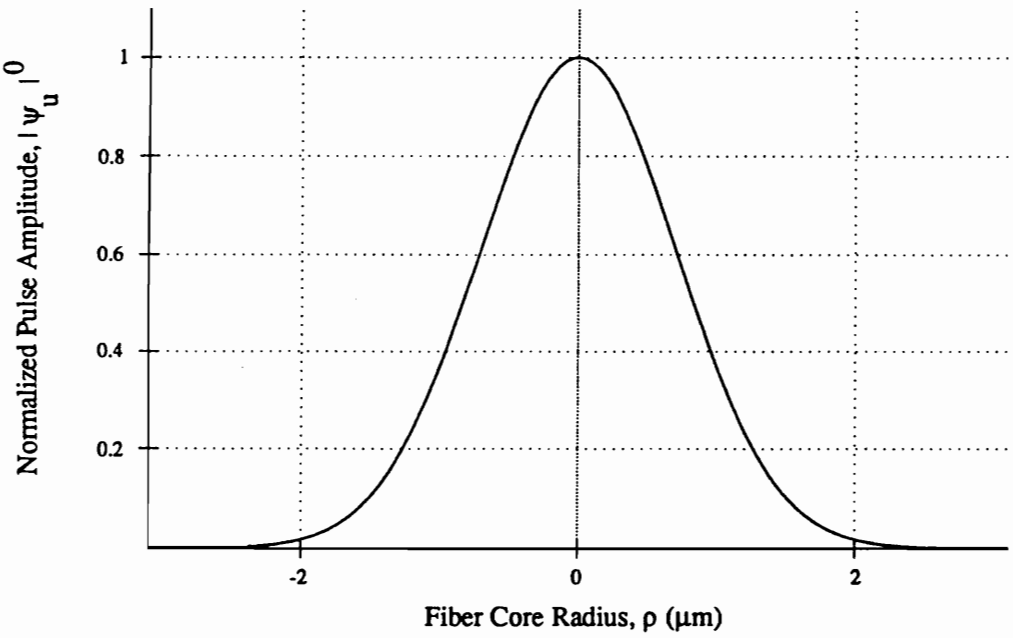

Figure 3.1. Variation of the ideal FWM solution in the fiber core. Parametric values used: $\beta' = 10^{-14}\ m^{-1}$, $a_1 = 0.10$ m.

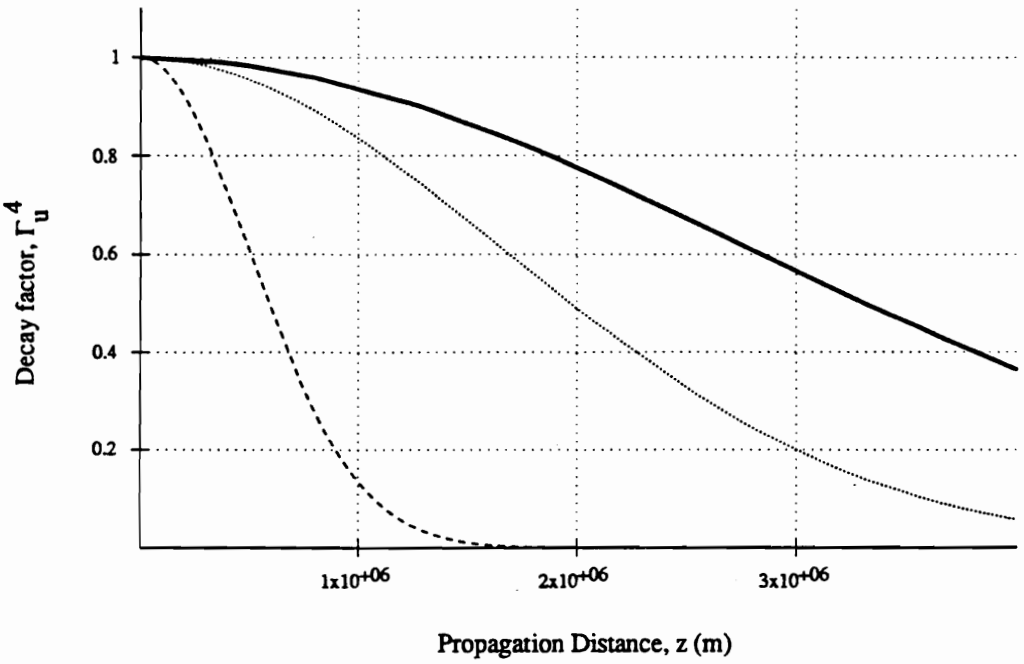

Figure 3.2. Variation of the decay factor for the splash pulse. Parametric values used: $a_1 = 1$ m, $\gamma = 10^6$ m^{-1}. Solid Line: $a_2 = 10^{13}$ m. Dashed Line: $a_2 = 5 \times 10^{12}$ m. Dotted Line: $a_2 = 10^{12}$ m.

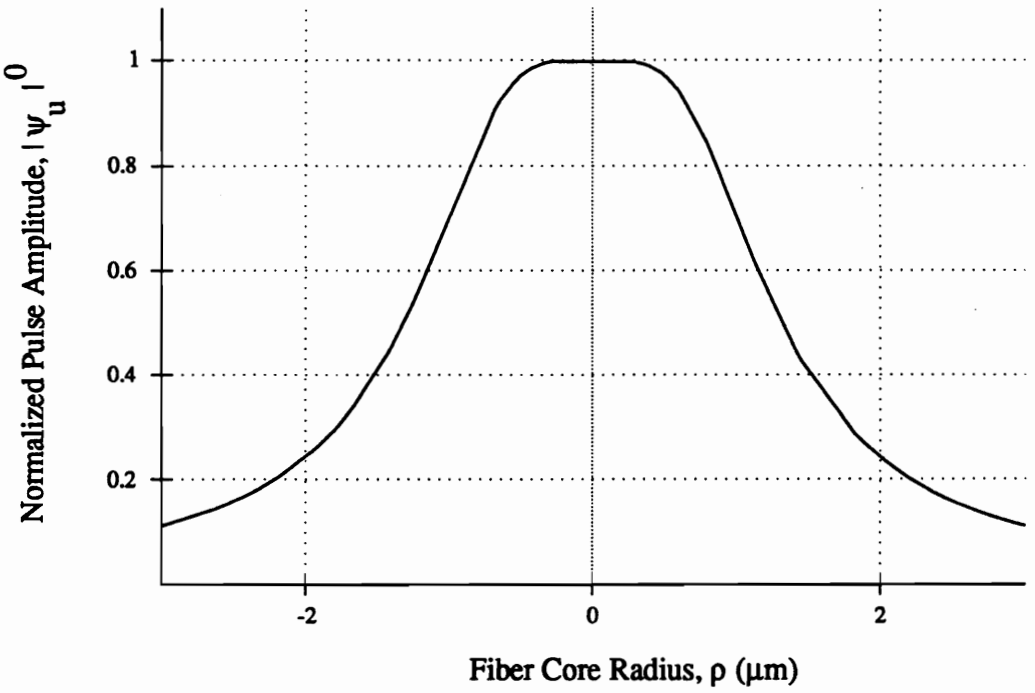

Figure 3.3. Variation of the ideal solution resulting from the Bessel spectrum in the fiber core. Parametric values used: $b = 10^{12}$ m, $a_1 = 1$ m.

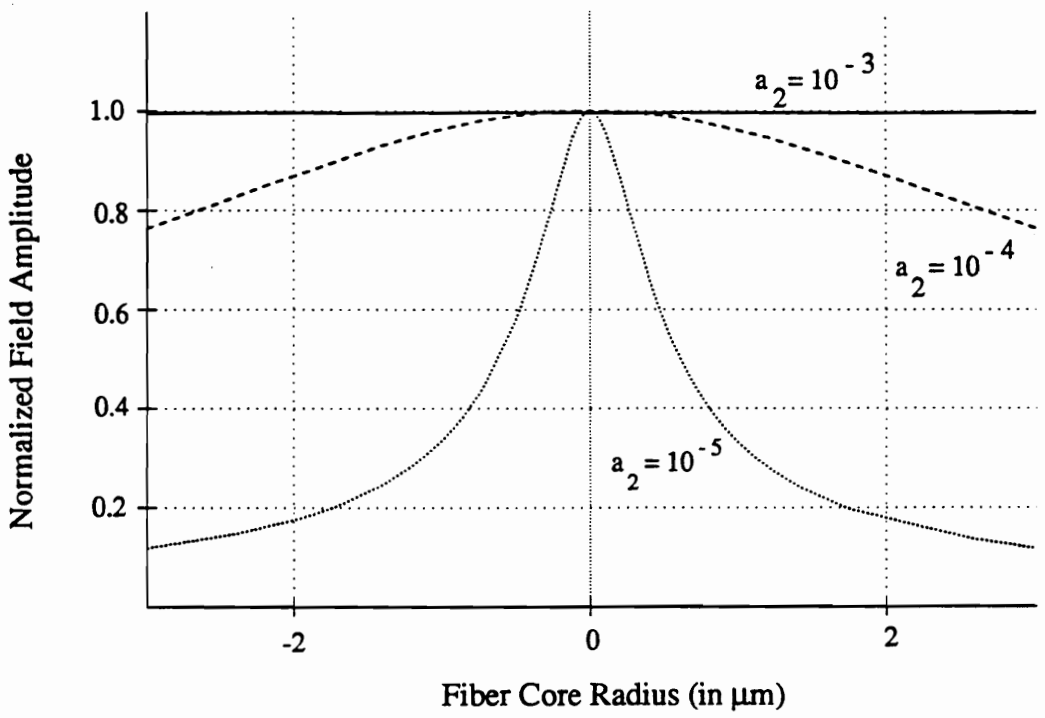

Figure 3.4. Dependence of the field confinement in the fiber on the free parameter a_2 for the splash pulse. For guided confinement of the field power, a_2 values on the order of 10^{-5} will be preferred.

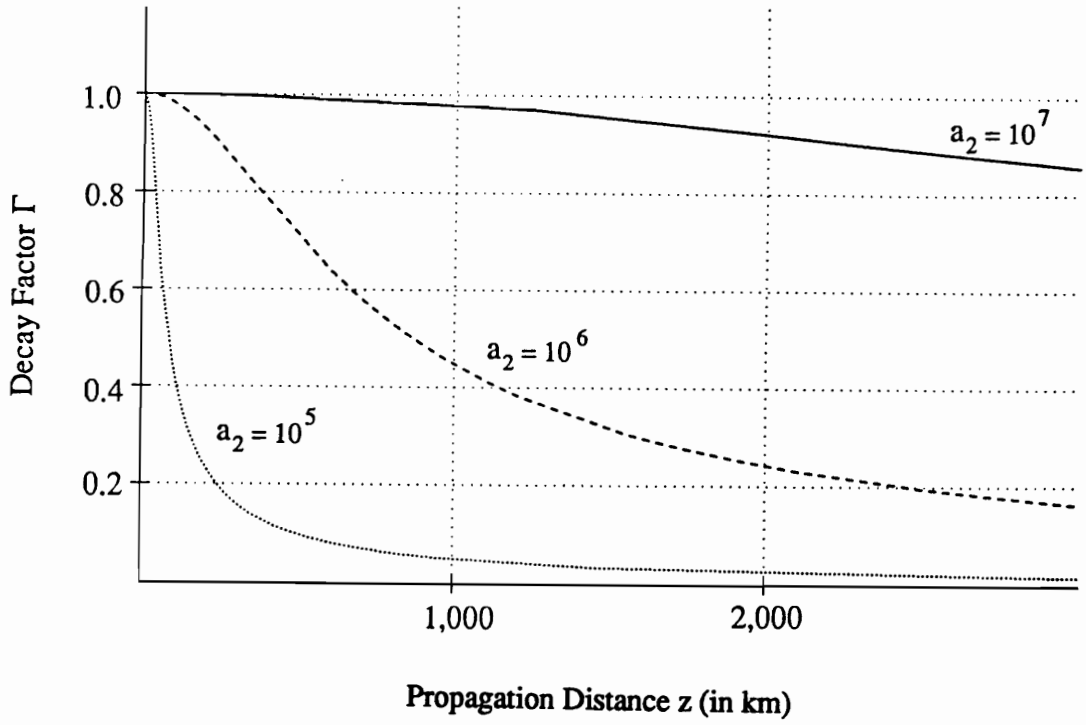

Figure 3.5. Variation of the decay factor Γ as a function of the free parameter a_2 for the splash pulse. Note that for nondecaying transmission of energy the values of a_2 should be on the order of 10^7, which contradicts the requirement imposed on the field confinement as seen from Figure 3.4.

4.0 DETAILED STUDY OF THE MPS PULSE

Expressions (3.7), (3.15), (3.27) and (3.33) for ψ_u represent the non-decaying, ideal, LW solutions in the core for the FWM's, splash pulses, the scalar equivalent of Hillion's spinor modes and the Modified Power Spectrum pulses, respectively, while equations (3.11), (3.16), (3.29) and (3.36) for ψ_w describe the deviations in those free-space solutions because of the waveguiding constraint. The behavior of these solutions is sensitive to the values of the free parameters. In order to understand the properties of these solutions, we analyzed the ideal pulses as they propagated through the waveguide and quantified the distances over which they maintained their non-decaying nature in the last chapter.

In this chapter, we will restrict ourselves to a detailed analysis and quantification of the MPS pulse for which a tractable, closed-form solution is available. Substituting values of the free parameters in the source modulation spectra into the equations, we will be able to determine the amount of localization of the initial pulse, and the behavior of the pulses traveling in the positive and the negative directions. By doing so, we will relate the free parameters in the spectra to physically

meaningful quantities, such as the minimum and maximum wavelengths in the source spectrum range, the width of the initial pulse and the pulse amplitude.

4.1 Similarity with the Free-Space MPS Pulse

It is known that the unperturbed MPS pulse is localized in free-space and can propagate without decay for thousands of kilometers (for an appropriate choice of the free parameters). The total solution for the MPS pulse in a fiber comprises the unperturbed term as well as a contribution from the wall term. The relative significance of each of these terms in the total solution provides an indication of the localized nature of the MPS pulse in the fiber. In this analysis, therefore, we compare the relative amplitudes of the unperturbed and the wall terms for a specific case, namely, at $\rho = 0$ and $z = 0$. A ratio of the unperturbed and the wall terms will be obtained and we will strive to make this ratio as large as possible by tuning the values of the free parameters in order to maintain localization. This analysis will therefore give us a first indication of the magnitudes of the free parameters.

We use the Bessel function expansion of Lommel functions [cf. Eq. (3.10)] in order to evaluate the wall term at $\rho = 0$. We are thus interested in finding the limit of $[U_1 + iU_2]$ as $\rho \to 0$. Using L'Hopital's rule and the recursive relations for Bessel functions we can show that

$$\lim_{z \to 0} \frac{J_m(\alpha z)}{z^m} = \frac{\alpha^m}{m!\, 2^m} . \tag{4.1}$$

The wall term ψ_w can be expressed at $\rho = 0$, from Eqs. (3.36) and (4.1), as

$$\psi_w \approx \frac{p \exp(ib\eta/p)}{2\pi (a_1 + i\zeta)} \frac{1}{\left[s(a_1 + i\zeta) + (pa_2 - i\eta)\right]}$$

$$\times \sum_{k=0}^{\infty} \frac{(-1)^k \left[i(a_1 + i\zeta)\sqrt{s}\right]^{2k+1}}{(2k+1)!\ 2^{2k+1}} \left(\frac{2b\sqrt{s}}{p}\right)^{2k+1} \tag{4.2}$$

$$+ i \sum_{k=0}^{\infty} \frac{(-1)^k \left[i(a_1 + i\zeta)\sqrt{s}\right]^{2k+2}}{(2k+2)!\ 2^{2k+2}} \left(\frac{2b\sqrt{s}}{p}\right)^{2k+2} .$$

Grouping the summation terms together, and using the series definition of the exponential function, we obtain the final expression for the wall term at $\rho = 0$, namely,

$$\psi_w \approx \frac{p \exp(ib\eta/p)}{2\pi (a_1 + i\zeta)} \times \frac{\left(1 - \exp\left[-\frac{sb(a_1 + i\zeta)}{p}\right]\right)}{\left[s(a_1 + i\zeta) + (pa_2 - i\eta)\right]} . \tag{4.3}$$

At $z = ct$, $z = 0$, the amplitude of the wall term is then given by

$$|\psi_w(\rho = 0, z = 0)| = \frac{1}{2\pi a_1 a_2} \left[1 - \exp\left(-\frac{a_1 sb}{p}\right)\right] , \tag{4.4}$$

where we have assumed that $pa_2 >> sa_1$. Since the amplitude of the unperturbed term at $\rho = 0$, $z = 0$ is given by $|\psi_u| = [4\pi a_1 a_2]^{-1}$, the ratio of the unperturbed term to the wall term then becomes

$$\frac{|\psi_u|}{|\psi_w|} = \frac{1}{2[1 - \exp(-x)]} , \tag{4.5}$$

where $x = sba_1/p$. For very small values of x, this ratio becomes

$$\frac{|\psi_u|}{|\psi_w|} \approx \frac{1}{2x} , \tag{4.6}$$

which implies that for a more pronounced localization of the total solution, one should choose the factor x to be very small. The first indication obtained from this comparison to the free-space pulse is that s should be chosen as small as possible, and given a value for s, the ratio ba_1/p should be made as small as possible. We will look at the practical implications of this statement next. The various pulse solutions for different combinations of the x parameter are easily visualized graphically and are shown in Section 4.3.

4.2 Practical Implications of Free Parameters

Using our knowledge from the analysis of the free-space MPS pulse, the behavior of the guided localized wave solution can now be connected directly to the values of its defining constants. We intentionally fix the constant $a_2 = 1.0$ m (without loss of generality) ; the other constants control the following properties.

Normalizing the magnitude of the solution ψ at $\rho = 0, z = ct$, to its initial value $4\pi a_1 a_2$ we obtain

$$|\psi(\rho = 0, z = ct)| = \frac{3}{\sqrt{1 + \left[\frac{2z}{pa_2}\right]^2}} \quad . \tag{4.7}$$

This means the amplitude of the solution is maintained out to the distance $L \approx pa_2$. Since we desire to maintain the initial amplitude over distances $L \sim 40,000$ km, we take p to be very large, i.e., $p = 10^8$. We will ensure in the following analysis that this

choice of p does not violate any other physical constraint.

One of the features that remains hidden in the bidirectional analysis is the natural angular frequency, ω. Although often considered a disadvantage in comprehending the physical significance of spectra, this problem can be easily solved by using the one-to-one correspondence between the Fourier method and the bidirectional synthesis. The solution to the ideal MPS pulse, given by Eq. (3.33), although written in the form $f(\rho, \zeta, \eta)$, can be recast in the form $f(\rho, z, t)$. A Fourier transform, given by

$$\mathcal{F}(\rho, z, \omega) = \int_{-\infty}^{\infty} dt \ \exp(i\,\omega\, t) \ f(\rho, z, t) \tag{4.8}$$

can then lead us to the spectrum of the MPS pulse in the ω domain. However, the expression for the MPS pulse solution is very complicated and, as a consequence, only plots of the spectra resulting from numerical calculations can be obtained. To gain a physical handle on the behavior of the spectrum, we will adopt another approach described by Ziolkowski [25] and derive closed form expressions for the spectrum; this method will lead to a practical understanding of each individual free parameter.

In our analysis of the MPS pulse solution, we used the bidirectional representation given by Eq. (3.30). The method we use to determine the spectrum considers the MPS pulse solution as a superposition of Gaussian pulses emanating from complex source points. The general localized wave solution is written as

$$f(\rho, z, t) = \int_0^{\infty} d\beta \, \frac{F(\beta) \exp\left[-\beta \, s(\rho, z, t)\right]}{\left[a_1 + i(z - ct)\right]}, \tag{4.9}$$

where

$$s(\rho, z, t) = \frac{\rho^2}{a + i(z - ct)} - i(z + ct) \tag{4.10}$$

and $F(\beta)$ denotes the MPS pulse spectrum, given by [25]

$$F(\beta) = a_1 \, a_2 \, p \, H(\beta - b/p) \, \exp\left[-a_2 (p\beta - b)\right], \tag{4.11}$$

where H(x) is Heaviside's function. Normalizing the value of a_2 ($a_2 = 1$), and using the definition for the Fourier transform given by (4.8) we can evaluate the spectrum for a specific case, namely, $z = 0$. Assuming $pa_2 >> 1$, the Fourier transform for the MPS pulse is written as

$$\mathcal{F}(\rho, z = 0, \omega) = \int_0^{\infty} d\beta \, F(\beta) \int_{-\infty}^{\infty} dt \, \frac{\exp\left[-i(\omega - \beta ct)\right]}{\left[a_1 - i ct\right]} \times \exp\left[-\frac{k\rho^2}{a_1 - i ct}\right]. \tag{4.12}$$

Using the series expansion of the exponential function, Eq. (4.12) can be rewritten as

$$\mathcal{F}(\rho, z=0, \omega) = \int_0^{\infty} d\beta\, F(\beta) \sum_{n=0}^{\infty} \frac{(-k\rho^2)^n}{n!} \times \int_{-\infty}^{\infty} dt\, \frac{\exp[-i(\omega-\beta ct)]}{[a_1 - ict]^{n+1}}. \tag{4.13}$$

Using the identity (3.382.7) from Gradhsteyn and Ryzhik [23], namely,

$$\int_{-\infty}^{\infty} dx\, (\beta - ix)^{-n} \exp[-ipx] = H(p) \frac{2\pi p^{n-1}}{\Gamma(n)} \exp(-\beta p), \tag{4.14}$$

and the series definition of the Bessel function given by

$$J_0(2x) = \sum_{n=0}^{\infty} \frac{(-1)^n x^{2n}}{n!\, n!}, \tag{4.15}$$

the generic Fourier transform for any LW solution becomes

$$\mathcal{F}(\rho, z=0, \omega) = \frac{2\pi}{c} \int_0^{\infty} d\beta\, F(\beta)\; H\left(\frac{\omega}{c} - \beta\right) \exp\left[-a_1\left(\frac{\omega}{c} - \beta\right)\right] \times J_0\left(2\rho\sqrt{\beta\left(\frac{\omega}{c} - \beta\right)}\right). \tag{4.16}$$

Substituting the MPS pulse spectrum (4.11) into (4.16) and accounting for the Heaviside functions, Eq. (4.16) is reduced to the form

$$\mathcal{F}(\rho, z=0, \omega) = \frac{2\pi\, p\, a_1}{c}\, H\left(\frac{\omega}{c} - \frac{b}{p}\right)\, \exp\left[-p\left(\frac{\omega}{c} - \frac{b}{p}\right)\right] \tag{4.17}$$

$$\times \int_0^{\frac{\omega}{c} - \frac{b}{p}} du\ \exp\left[-u\,(p - a_1)\right]\, J_0\left(2\rho\sqrt{u\left(\frac{\omega}{c} - u\right)}\ \right),$$

where u is a dummy variable. Using the series expansion of the Bessel function (4.15), and rearranging terms within the integral, we obtain

$$\mathcal{F}(\rho, z=0, \omega) = \frac{2\pi\, p\, a_1}{c}\, H\left(\frac{\omega}{c} - \frac{b}{p}\right)\, \exp\left[-p\left(\frac{\omega}{c} - \frac{b}{p}\right)\right] \tag{4.18}$$

$$\times \sum_{n=0}^{\infty} \frac{(-1)^n\,(2\rho)^{2n}}{n!\ n!} \int_0^{\frac{\omega}{c} - \frac{b}{p}} du\ \exp\left[-u\,(p - a_1)\right]\, u^n \left(\frac{\omega}{c} - u\right)^n .$$

The identity (2.321.2) from Gradhsteyn and Ryzhik [23], namely,

$$\int x^n\, e^{ax}\, dx = e^{ax}\left(\frac{x^n}{a} + \sum_{k=1}^{n} (-1)\, \frac{n!}{k!}\, \frac{x^{n-k}}{a^{k+1}}\right) \tag{4.19}$$

gives us a series form of the Fourier transform

$$\mathcal{F}(\rho, z=0, \omega) = \frac{2\pi\, p\, a_1}{c}\, H\left(\frac{\omega}{c} - \frac{b}{p}\right)\, \exp\left[-p\left(\frac{\omega}{c} - \frac{b}{p}\right)\right]$$

$$\times \sum_{n=0}^{\infty} \frac{(-1)^n\,(2\rho)^{2n}}{n!\ n!\,(p - a_1)} \exp\left[-\left(\frac{\omega}{c} - \frac{b}{p}\right)(p - a_1)\right] \tag{4.20}$$

$$\times \left[\left(\frac{b}{p}\right)^n \left(\frac{\omega}{c} - \frac{b}{p}\right)^n + O\left[(p - a_1)^{-2}\right]\right] .$$

Assuming $p >> a_1$ and reverting to the compact Bessel function form, we obtain the approximate MPS pulse spectrum in the ω domain, viz.,

$$\mathcal{F}(\rho, z = 0, \omega) \approx \frac{2\pi a_1}{c} H\left(\frac{\omega}{c} - \frac{b}{p}\right) \exp\left[-a_1\left(\frac{\omega}{c} - \frac{b}{p}\right)\right] \times J_0\left(2\rho \sqrt{\frac{b}{p}\left(\frac{\omega}{c} - \frac{b}{p}\right)}\right). \tag{4.21}$$

This expression can be recast in the physically appealing form

$$\mathcal{F}(\rho, z = 0, \omega) \approx \frac{2\pi}{\omega_{max}} H\left(\omega - \omega_{min}\right) \exp\left[-\frac{\left(\omega - \omega_{min}\right)}{\omega_{max}}\right] \times J_0\left(\frac{2\rho}{c}\sqrt{\omega_{min}\left(\omega - \omega_{min}\right)}\right), \tag{4.22}$$

where

$$\omega_{max} = c/a_1 \tag{4.23}$$

and

$$\omega_{min} = cb/p. \tag{4.24}$$

The maximum angular frequency of interest ω_{max} is thus fixed by a_1 and the minimum angular frequency ω_{min} by the ratio b/p. Before proceeding with a more detailed exposition of the practical significance of the free parameters, a few comments about the MPS pulse spectrum are in order. First, the approximate expression for the spectrum seems to indicate a discontinuity at ω

$= \omega_{min}$. However, an exact evaluation shows that this is not the case. Second, to test if the approximation is close to the exact expression we consider the case, $\rho = 0$. The exact Fourier transform expression leads to

$$\mathcal{F}(\rho = 0, z = 0, \omega) = \frac{2\pi a_1}{c} \frac{p}{p - a_1} H\left(\frac{\omega}{c} - \frac{b}{p}\right) \times \left[\exp\left\{-a_1\left(\frac{\omega}{c} - \frac{b}{p}\right)\right\} - \exp\left\{-p\left(\frac{\omega}{c} - \frac{b}{p}\right)\right\}\right]. \tag{4.25}$$

For $p >> a_1$, Eq. (4.25) reduces to the approximation (4.21) for $\rho = 0$. Ziolkowski [25] has also shown that exact and approximate expressions for the spectrum at $z \neq 0$ are very similar to those for $z = 0$ except for some z-dependent phase terms that typically play no role in practical calculations. We plot the approximate Fourier transform given by (4.22) in Figure 4.1, where $\omega_{min} = 3\pi \times 10^{14}$ rad/s and $\omega_{max} = 12\pi \times 10^{14}$ rad/s . The amplitude of the transform has been normalized and the equivalent optical wavelengths corresponding to ω_{min} and ω_{max} are 2 μm and 0.5 μm, respectively. The plot shows that the frequency spectrum is dependent on the radius under consideration. This observation will play a role in our consideration of source requirements for the practical feasibility of such a system and will be discussed in Chapter 5.

The transverse localization of the unperturbed MPS pulse is given by its initial waist

$$w_0^2 = \frac{pa_1}{b} = \frac{\lambda_{min}}{2\pi} \times \frac{\lambda_{max}}{2\pi}, \tag{4.26}$$

where $\lambda_{max} = 2\pi c/\omega_{min}$ and $\lambda_{min} = 2\pi c/\omega_{max}$. Hence the waist is fixed if the minimum and the maximum wavelengths are specified. On the other hand,

$$\frac{b}{p} = \frac{a_1}{w_0^2} = \frac{2\pi}{\lambda_{max}} \quad . \tag{4.27}$$

Eqs. (4.26) and (4.27) imply that the maximum and minimum wavelengths λ_{min} and λ_{max} are fixed if a_1 and w_0 are specified. Since in practice the available frequencies in the fiber are limited, we have chosen, for the sake of demonstration, $\lambda_{min} = 0.3$ μm and $\lambda_{max} = 30$ μm. The fiber dimensions limit the allowed choices for the waists. Since our wavelength selection gives $w_0 = 0.50$ μm, the initial waist is smaller than the chosen fiber radius ($r \approx 2$ - 5 μm). Then the ratio $b/p = 2.1 \times 10^5$ finally fixes the remaining constant b to be very large: $b = 2.1 \times 10^{13}$. Therefore the assumption that $a_1 << p/a_2$, or since

$$x = \frac{s\, b\, a_1}{p} = s\left(\frac{a_1}{w_0}\right)^2 << 1 \quad , \tag{4.28}$$

that $x << b/a_2$, which was used to obtain (4.5), is valid. In this small x limit, Eq.(4.4) reduces to the form

$$\frac{|\psi_u|}{|\psi_w|} \approx \frac{1}{2x} = \frac{1}{2s}\frac{w_0^2}{a_1^2} = \frac{1}{2s}\frac{\lambda_{max}}{\lambda_{min}} = \frac{1}{2s}\frac{\omega_{max}}{\omega_{min}} \quad . \tag{4.29}$$

This result indicates that an increase in the bandwidth or equivalently an increase in the number of minimum wavelengths in the waist will increase the difference between the unperturbed MPS core term and the wall term, thus making the

guided localized wave solution more like its free-space counterpart. The requirement, $x << 1$, sets a practical limitation on the fiber structure: Either the fiber material should be highly transparent to a broad window of wavelengths or the fiber should be strongly guiding. One would therefore have to explore materials with large transparent windows of transmission, or, reevaluate the entire analysis without using the LP mode formulation. The latter approach would necessitate the use of smaller core fibers in order to remain close to single-mode operation and would, in turn, imply added complexity of source design. Eq. (4.29) also underscores the contribution of the wall term as a function of the weak-guidance condition of the fiber. For example, if the index of refraction of the fiber cladding were made closer to the core refractive index, the fiber would guide the modes in a weaker fashion and we would expect the contribution from the wall term to increase. This physical insight is confirmed by Eq. (4.29) since as $n_e \rightarrow 1$, s increases and the ratio $|\psi_u| / |\psi_w|$ decreases, implying a growing influence of the wall term.

Returning to the explicit representation of the wall term (3.36) one finds that its transverse variations are controlled by the Lommel function terms. Since

$$\sqrt{s}\ \frac{b}{p}\ \rho = 4\pi x \frac{\rho\sqrt{s}}{\lambda_{min}} \tag{4.30}$$

except when $\rho < \lambda_{min}$, an explicit numerical evaluation of those terms is necessary. These terms yield an oscillatory, rapidly damped function of ρ. The decay rate can be obtained since as $z \rightarrow \infty$, the function

$$\frac{J_n(\alpha z)}{z^n} \rightarrow (\alpha z^{2n+1})^{-1/2} \tag{4.31}$$

so that only the n = 1 term survives and it goes to zero like $(\rho / \lambda_{min})^{-3/2}$. In contrast, the perturbed core term decays transversely as $\exp[-(\rho^2 / w_0^2)]$ except in the (forward and backward) tail regions of the MPS pulse where $| z - ct | >> a_1$ so that it decays more gradually like its axial decay:

$$\frac{\exp\left[-\frac{\rho^2}{w_0^2\left(1+\frac{(z-ct)^2}{a_1^2}\right)}\right]}{1+\frac{(z-ct)^2}{a_1^2}} \sim \frac{\exp\left[-\frac{\rho^2 a_1^2}{w_0^2 (z-ct)^2}\right]}{1+\frac{(z-ct)^2}{a_1^2}} \sim \left[1+\frac{(z-ct)^2}{a_1^2}\right]^{-1} . \tag{4.32}$$

Thus if the waist is many wavelengths in size, the wall term will be much smaller than the core term everywhere except near the wall where its decay rate becomes slightly less than the core's. This comparison illustrates that the wall term in the forward tail region of the core MPS component will lead the central peak. This means one can visualize the wall component of the guided localized wave solution as a a low-level background field propagating in the fiber with little significant contribution except near the wall where it provides a guiding and renovating mechanism for the central, core component. Heuristically, it appears that the core component surfs along in the fiber on the background wall field.

4.3 Graphical Description

A graphical description will provide a physical picture of the MPS pulse and

confirm our heuristic feel for the surfing solution. The variation of the square of the amplitude of the unperturbed solution, $|\psi_u|^2$, for $\lambda_{max} / \lambda_{min} = 100$ is shown in Figure 4.2. The parametric values used are: $a_1 = 5 \times 10^{-8}$ m, $a_2 = 1$ m, $b = 2.1 \times 10^{13}$ m^{-1}, $p = 10^8$, $s = 10$. The wall term for the same is shown in Figure 4.3. Figure 4.4 shows the total launched pulse at the input end of the fiber ($z = 0$); for a fiber core diameter on the order of a few micrometers, the pulse is considerably confined to the core. The total pulse looks exactly like the unperturbed solution indicating that the effect of the wall term is negligible for this choice of free parameters. Local variations in the pulse shape are seen as a function of the parameter ζ. At distances of propagation on the order of several thousands of kilometers, there is no variation in the amplitude of the pulse. At $z = 40{,}000$ km [shown in Figure 4.5], the localized nature of the solution starts collapsing, the pulse shape changes and the peak amplitude drops to less than half its original amplitude. Plots in Figures 4.2 - 4.5 were obtained for an x value of 0.2 and hence the contribution due to the wall term is not noticeable for a ratio $|\psi_u| / |\psi_w| = 5.0$. To emphasize the heuristic surfing nature of the unperturbed core term along the wall term, we plot the different components of the MPS pulse for $\lambda_{max} / \lambda_{min} = 25$, or equivalently, for $|\psi_u| / |\psi_w| = 1.25$. These plots are shown in Figures 4.6 - 4.8. Once again, the normalized unperturbed and wall terms behave like their counterparts in Figures 4.2 - 4.5; however, the total pulse now appears to possess a noticeable contribution form the wall term. Note that in Figures 4.2 - 4.8 the squares of the amplitudes are normalized; as a result, the total pulse solution should not be considered to be a mere sum of the the individual contributions from the ψ_u and ψ_w terms.

In order to ensure propagation of electromagnetic energy in the positive

direction, it is instructive to analyze the behavior of the pulse traveling in the negative direction. We have evaluated the behavior of the MPS pulse in the negative direction and found that the solution in the negative direction decays rapidly over distances on the order of 10^{-18} meter and is on the order of 10^{-19} times the original pulse amplitude after propagating a distance of one meter. This result, plotted in Figure 4.9, further confirms that the choice of the free parameter values can lead to positive pulse propagation without any negative component being supported by the waveguide.

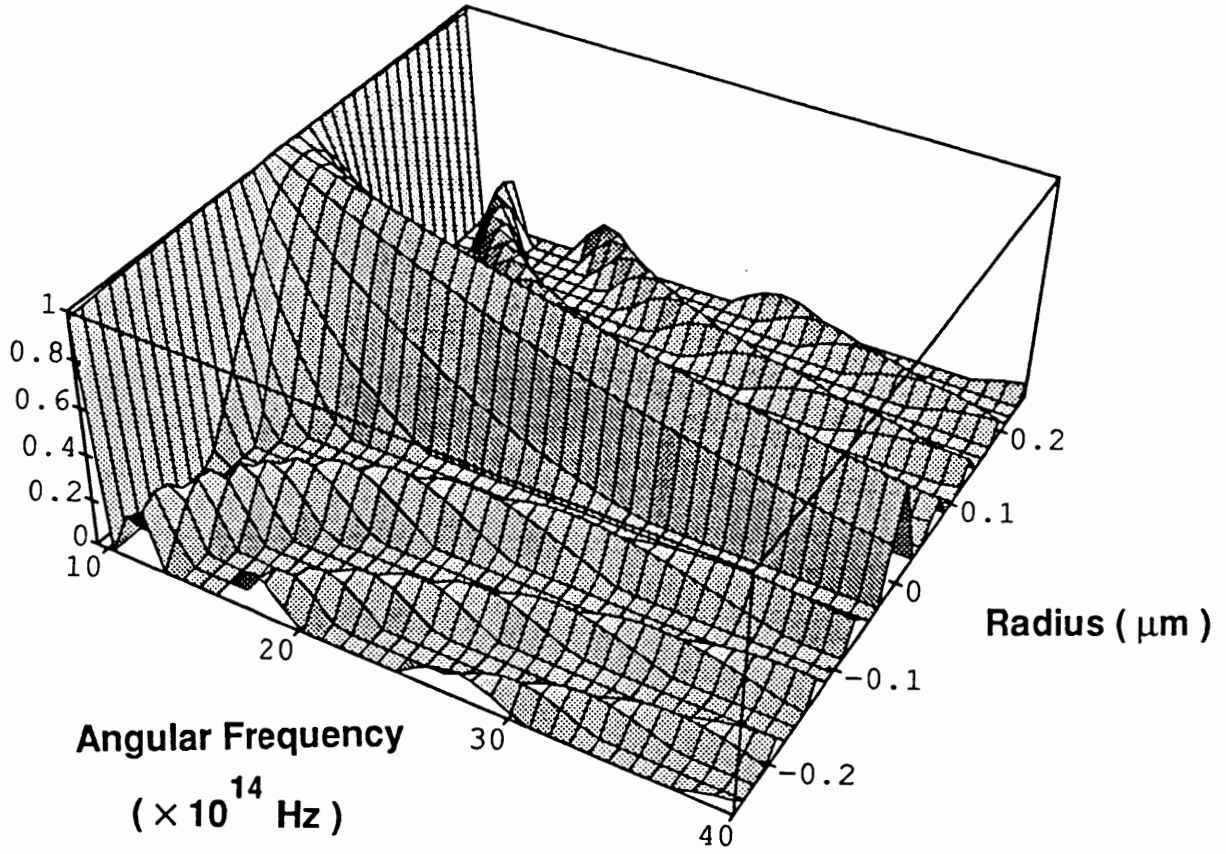

Figure 4.1. Approximate Fourier domain spectrum of the MPS pulse plotted from Equation (4.22).

Parametric values used: $\omega_{min} = 3\pi \times 10^{14}$ Hz and $\omega_{max} = 12\pi \times 10^{14}$ Hz.

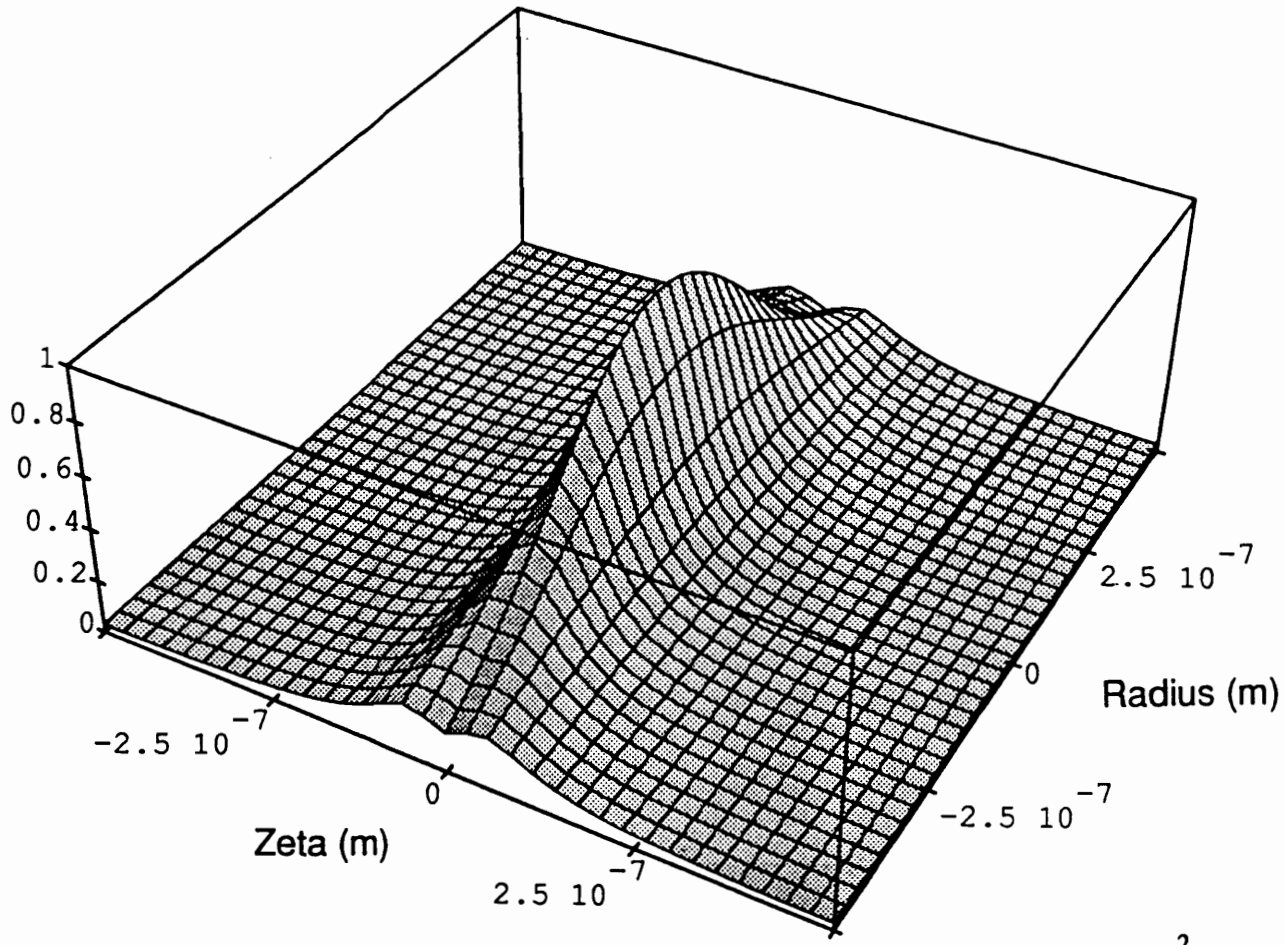

Figure 4.2. Evolution of the normalized unperturbed free-space equivalent, $|\psi_u|^2$ for the MPS pulse as it propagates through the fiber. Plot is shown at z = 0.

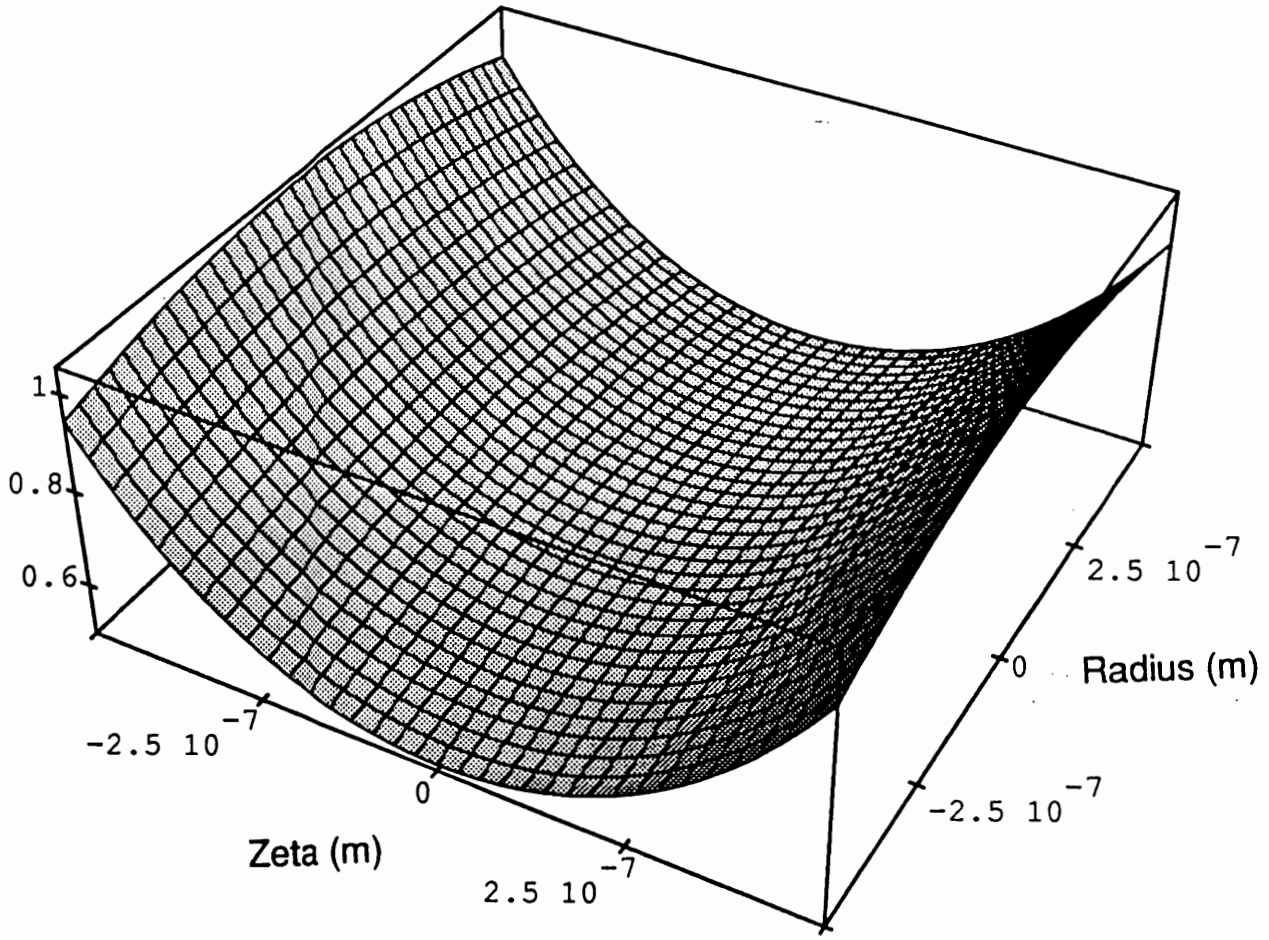

Figure 4.3. Evolution of the normalized wall term, $|\psi_w|^2$ for the MPS pulse as it propagates through the fiber. Plot is shown at z = 0.

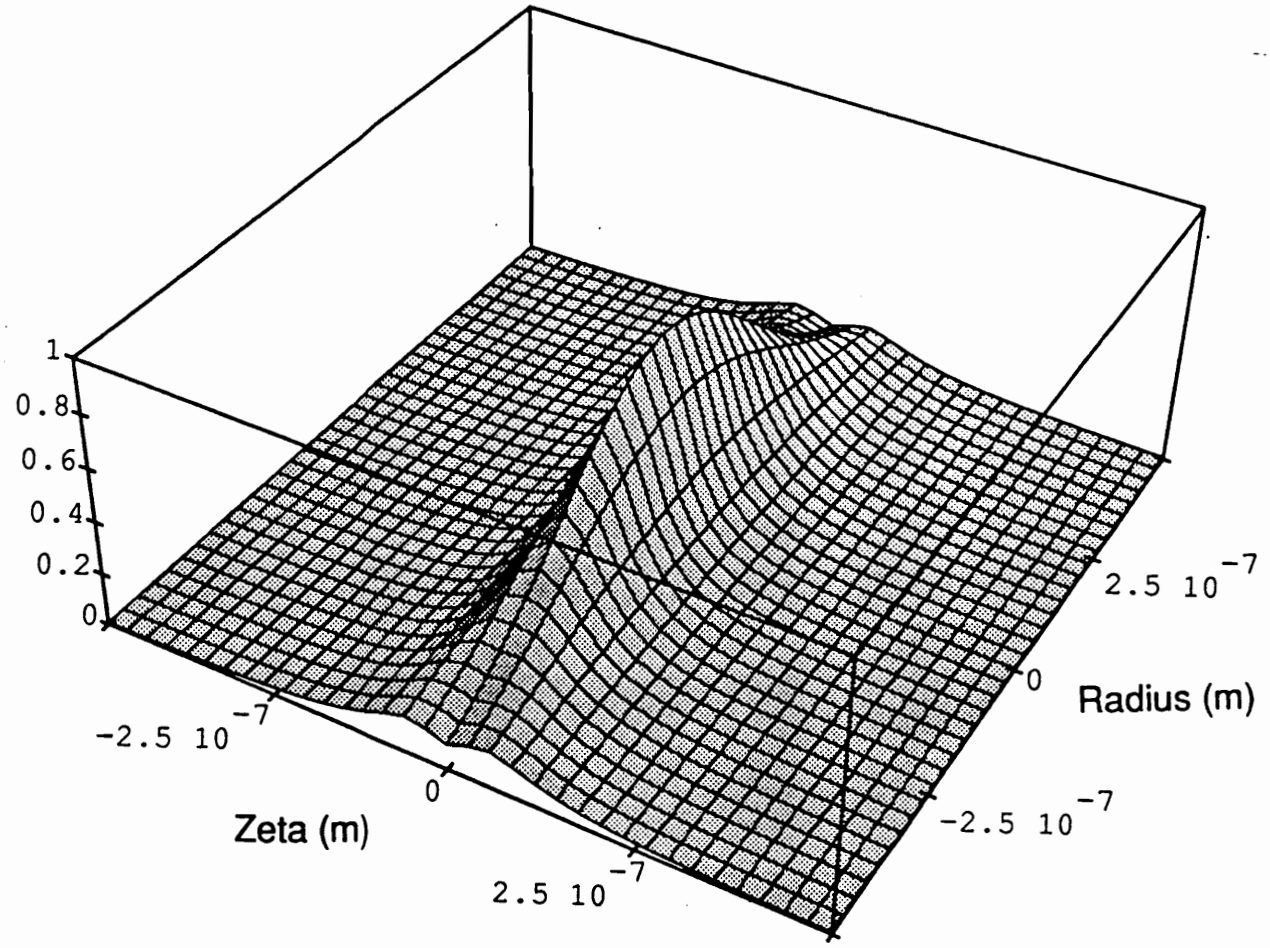

Figure 4.4. Evolution of the normalized total solution, $|\psi_u + \psi_w|^2$ for the MPS pulse as it propagates through the fiber. Plot is shown at z = 0.

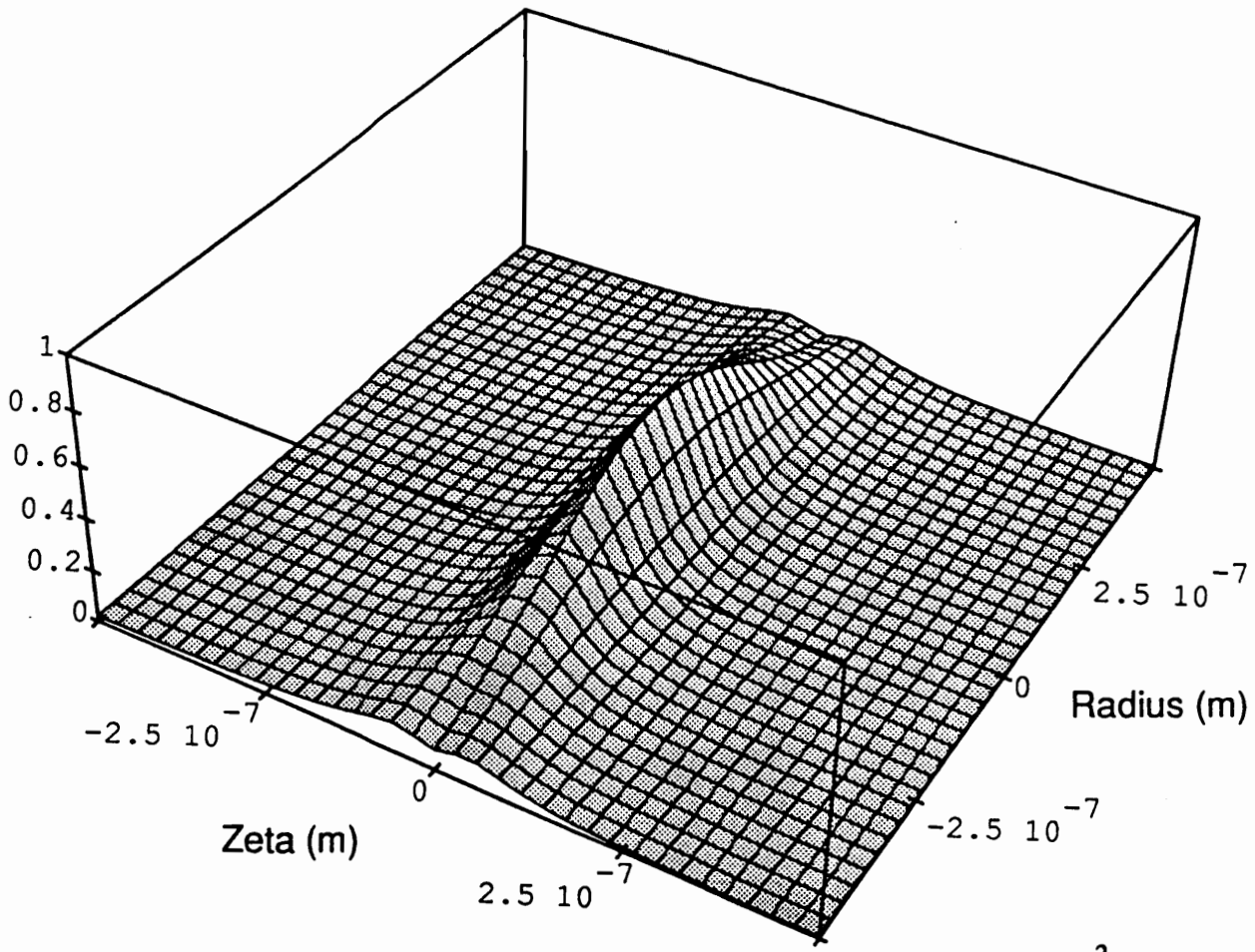

Figure 4.5. Evolution of the normalized total solution, $|\psi_u + \psi_w|^2$ for the MPS pulse as it propagates through the fiber. Plot is shown at z = 40,000 km.

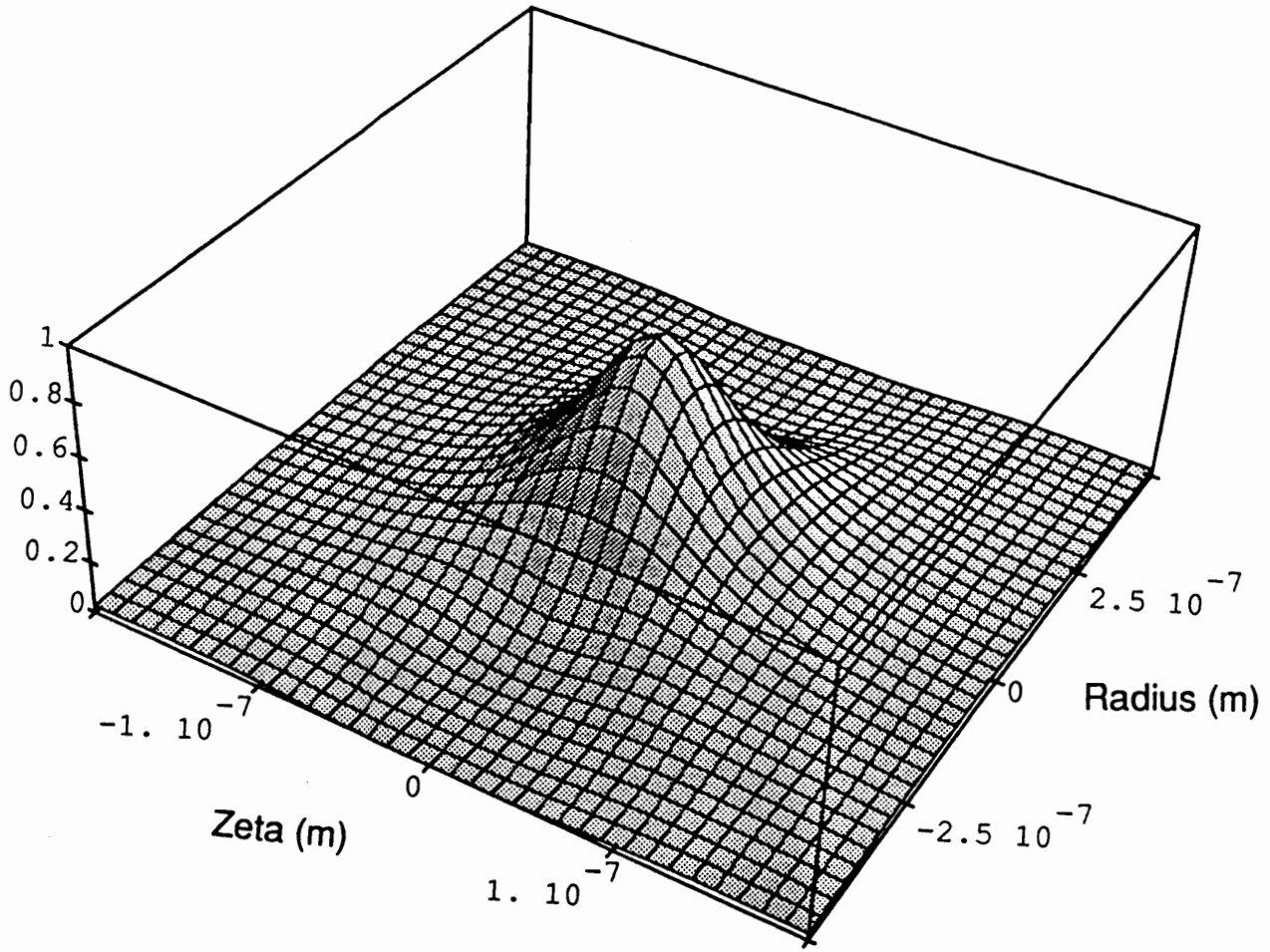

Figure 4.6 Normalized unperturbed free-space equivalent, $|\psi_u|^2$ for the MPS pulse for $\lambda_{max}/\lambda_{min} = 25$; $z = 0$.

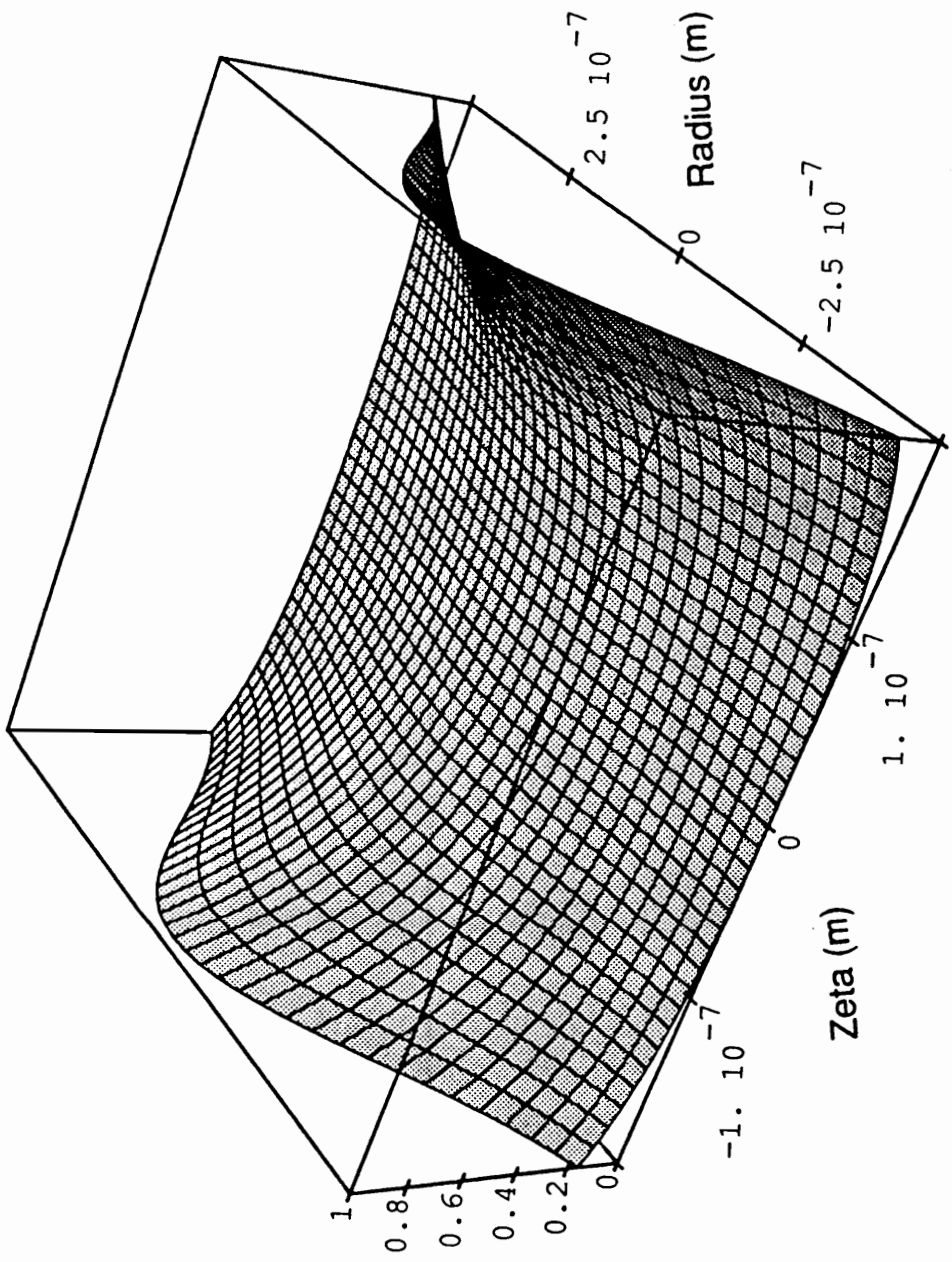

Figure 4.7. Normalized wall term, $|\psi_w|^2$ for the MPS pulse for $\lambda_{max}/\lambda_{min} = 25$; $z = 0$.

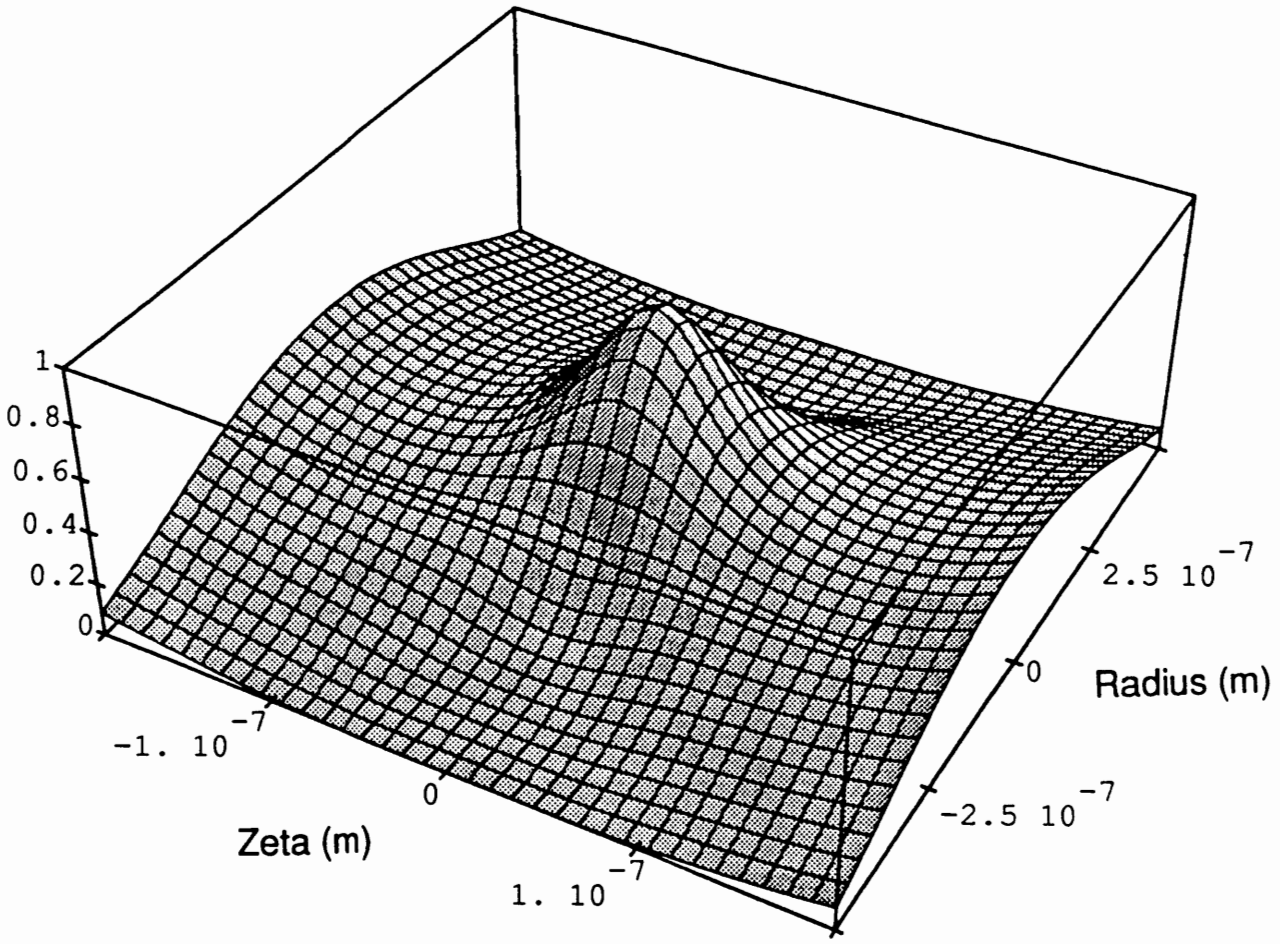

Figure 4.8. Normalized total solution, $|\psi_u + \psi_w|^2$ for the MPS pulse composition for $\lambda_{max} / \lambda_{min} = 25$; $z = 0$.

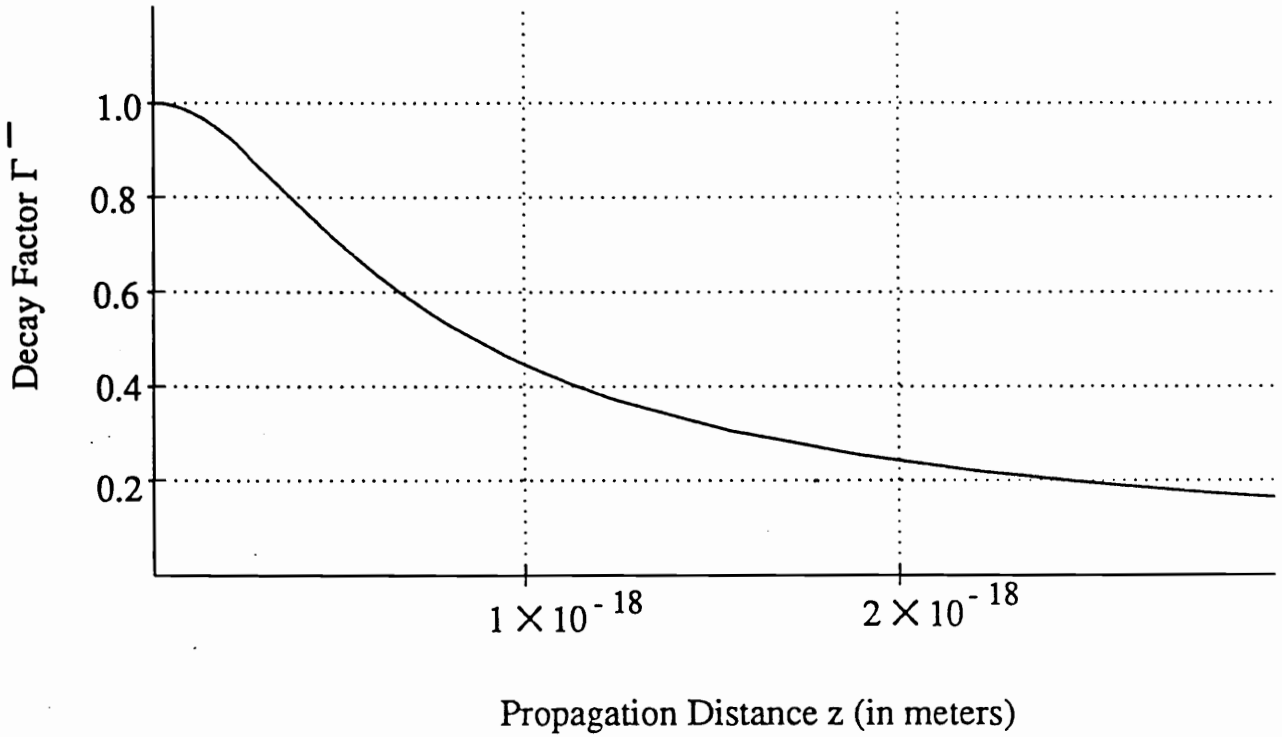

Figure 4.9. MPS pulse propagation in the negative z direction. The decay factor Γ^{-}, defined by $|\psi|^{-}/|\psi|^{0}$, is plotted.

5.0 PRACTICAL ISSUES

The synthesis of pulses resulting from source spectra considered in the preceding chapters led to localized packet-like solutions that could propagate through an optical fiber by effectively neutralizing the dispersive effects introduced by the walls of the waveguide. The waveguide structure used for the synthesis can be considered ideal in the sense that we did not incorporate the effects of losses in the medium as well as the dispersive nature of silica-based glasses. Practical demonstration of LW solutions will depend critically upon these effects and we will present approaches to analyzing these effects in this chapter.

One of the notable features of all spectra that give rise to LW solutions is that they are broadband in the optical sense; this factor causes a major deviation in understanding the resulting modes in an optical fiber. One such effect is the potential of generating the higher order LP_{11} mode, which will act as a noise source in the system. We will evaluate the behavior of the LP_{11} mode in the fiber for the MPS pulse.

Having discussed the negative effects of an absorptive, dispersive medium, we will revert our attention to the problem of sources - the requirements imposed on them by the spectra, the need for arrays for effective LW pulse transmission and the robustness of the source spectra to minor deviations in implementation.

5.1 Lossy Dispersive Media

5. 1. 1 Material Dispersion

The refractive index of the optical fiber material is dependent on the wavelength of the source being used. This dependence, termed material dispersion, has a significant effect on an optical pulse propagating in the fiber. Since the group velocity is directly related to the refractive index of the medium, a pulse tends to spread out at the receiving end due to the different frequency (or wavelength) components of the pulse propagating at different velocities. An extensive analysis of this effect has been performed by several researchers and we will summarize the method of using part of that analysis as applicable to the bidirectional representation.

Assuming a harmonic oscillator model for the dielectric material, the index of refraction can be written as

$$n^2(\omega) = 1 + \sum_{j=1}^{M} \frac{A_j}{\omega_j^2 - \omega^2}, \tag{5.1}$$

where ω_j's are the multiple resonance frequencies within the structure. Expressed in terms of wavelengths, Eq. (5. 1) reduces to the Sellmeier equation,

$$n^2(\lambda) = 1 + \sum_{j=1}^{M} \frac{B_j \lambda^2}{\lambda^2 - \lambda_j^2}, \tag{5.2}$$

where each $\lambda_j = 2\pi c/\omega_j$. The constants A_j's and B_j's can be obtained empirically by

interpolating between data-points where exact refractive indices are known. The first two resonances for pure fused–silica glass are found to be at $\lambda_1 = 0.1\ \mu m$ and $\lambda_2 = 9\ \mu m$, and the corresponding coefficients have been derived empirically to be $B_1 = 1.0955$ and $B_2 = 0.9$. The truncation of the Sellmeier equation, (5.2), to two terms is sufficient for understanding the behavior of the refractive index, and more importantly, the dispersion as a function of wavelength. Defining dispersion as

$$D = \frac{1}{L}\,\frac{\Delta\tau}{\Delta\lambda}\ , \tag{5.3}$$

(with L = total length of the fiber and $\Delta\tau$ = the pulse spread) we plot the behavior of n and D as a function of λ in Figure 5.1. The dispersion curve crosses zero at a wavelength of approximately 1.3 μm using the specified values of B_1 and B_2, which is in close agreement to experimental observed values.

Using the approximation (5.2) along with the best-fit values for B_j's (or A_j's), one can express the refractive index as a function of wavelength (or frequency). A substitution of this relation in the synthesis of LW solutions can then lead to an understanding of the effects of material dispersion on the degree of localization. A closer look however indicates a need for intensive numerical computation as a result of the complication of the constraint (2.3b), which now becomes

$$\delta\left[\ \kappa_1^2 - 4\alpha\beta - \frac{A_1}{\left(\dfrac{\omega_1^2}{(\alpha+\beta)^2} - c^2\right)} - \frac{A_2}{\left(\dfrac{\omega_2^2}{(\alpha+\beta)^2} - c^2\right)}\ \right]. \tag{5.4}$$

While numerical calculations can result in plots of LW solutions, these tend to be complex and difficult (if not impossible) to perform. A major drawback, which is an upshot of the numerical computation process, is a loss of physical insight; it would be very useful in the preliminary stages of research to possess the useful tool of analytical tractability. In an effort to maintain a physical handle over the proceedings, we first investigate the effect of material dispersion in another waveguiding structure that can be easily modeled to obtain closed-form solutions.

Our choice of waveguide for this segment of research is a hollow, cylindrical metallic-waveguide filled with plasma, an ionized gas within which positively charged ions and negatively charged electrons are free to move. The structure, shown in Figure 5.2, provides two important properties that facilitate ease of mathematical handling: i) The metallic cylinder imposes the boundary condition that tangential components of the electric field should be zero at $\rho = R$; ii) for the case of an isotropic and low-density plasma, one can ignore the effect of collisions so that one can assume that the magnetic permeability μ_p is equal to that of the neutral un-ionized gas, can consider the conductivity σ_p to be small, and can obtain a simple algebraic formula that describes the permittivity ε_p, as shown below.

We use a simplified analysis for modeling the plasma. When a time-harmonic electric field, **E**, is applied to the plasma, an electron experiences a force

$$\mathbf{F} = -e\,\mathbf{E}, \tag{5.5}$$

where $e = 1.6 \times 10^{-19}$ Coulomb. The charged particles in a plasma are assumed to

move according to Newton's law, viz., the force exerted on the electron due to a nearby proton can be expressed as

$$F = m \frac{d^2 \chi}{dt^2} = - m \omega^2 \chi , \tag{5.6}$$

where $m = 9.1 \times 10^{-31}$ kg is the mass of the electron, ω is the angular frequency of the **E** field and χ is the displacement of the electron away from the positive ion. The charged particle pair constitutes a dipole and the total dipole moment density **P** in the plasma is given by

$$\mathbf{P} = - N e \chi , \tag{5.7}$$

where N is the number of electrons in the plasma per unit volume. The electric flux density, **D**, can then be expressed from Eqs. (5.5) - (5.7) as

$$\mathbf{D} = \varepsilon_0 \mathbf{E} + \mathbf{P} = \varepsilon_0 \left[1 - \left(\frac{\omega_p}{\omega} \right)^2 \right] \mathbf{E} = \varepsilon_p \mathbf{E} , \tag{5.8}$$

where ω_p is the plasma frequency given by

$$\omega_p = \sqrt{\frac{N e}{m \varepsilon_0}} . \tag{5.9}$$

We now evaluate the constraint (2.3b) in terms of the bidirectional representation. Using the one-to-one correspondence, $\omega_{cl}^2 \leftrightarrow c^2(\alpha + \beta)^2$ and $\beta_{cl}^2 \leftrightarrow (\alpha - \beta)^2$, we can rewrite (2.3b) for the waveguide under consideration as

$$\kappa_p^2 = n_p^2 (\alpha, \beta) \left(\alpha + \beta \right)^2 - \left(\alpha - \beta \right)^2 . \tag{5.10}$$

Substituting the expression for n_p in the (α, β) domain, namely,

$$n_p^2(\alpha,\beta) = \frac{\varepsilon_p(\alpha,\beta)}{\varepsilon_0} = \left[1 - \frac{\omega_p^2}{c^2(\alpha+\beta)^2}\right], \tag{5.11}$$

in Eq. (5.10) and assuming a system where ε_0 is normalized to unity, the bidirectional superposition (2.31) is given by

$$\psi(\rho,\zeta,\eta) = \frac{1}{(2\pi)^2}\sum_{m=1}^{M}\int_0^\infty d\alpha \int_0^\infty d\beta\ A(\alpha,\beta,\kappa_{0m})\ J_0\left(\frac{\kappa_{0m}\rho}{R}\right) \times\ e^{-i\alpha\zeta}\, e^{i\beta\eta}\ \delta\left(4\alpha\beta - \frac{\omega_p^2}{c^2} - \frac{\kappa_{0m}^2}{R^2}\right), \tag{5.12}$$

where we have replaced the integral over κ by a summation sign in order to satisfy the boundary condition $\psi(R, z, t) = 0$ for any mode of order m. In Eq. (5.12), κ_{om} is the mth zero of the zeroth order Bessel function. Substitution of different pulse spectra described in Chapter 3 into Eq. (5.12) will now lead to an evaluation of final expressions for the pulse shapes. We will first consider the splash pulse spectrum without the delta function given by (3.37).

Substituting (3.37) into Eq. (5.12) and integrating over β, we obtain

$$\psi(\rho,\zeta,\eta) = a_1 a_2 J_0\left(\frac{\kappa_{01}\rho}{R}\right)\int_0^\infty \frac{d\alpha}{2\alpha}\ \exp\left[-\alpha(a_1 + i\zeta)\right] \times \exp\left[-\frac{1}{4\alpha}\left(\frac{\omega_p^2}{c^2} + \frac{\kappa_{01}^2}{R^2}\right)(a_2 - i\eta)\right], \tag{5.13}$$

where we have limited our analysis to a mode with the characteristic modal number m =

1. Using the identity (3.14), we obtain a closed form expression for the LW solution, viz.,

$$\psi(\rho,\zeta,\eta) = \frac{a_1 a_2}{2} J_0\left(\frac{\kappa_{01}\rho}{R}\right) K_0\left(\sqrt{\left[\frac{\omega_p^2}{c^2} + \frac{\kappa_{01}^2}{R^2}\right]\left[a_1 + i\zeta\right]\left[a_2 - i\eta\right]}\right). \quad (5.14)$$

We can now evaluate the magnitudes of the pulse at the launching point, $z = t = 0$, to be

$$|\psi(\rho, z = t = 0)|^0 = \frac{J_0\left(\frac{\kappa_{01}\rho}{R}\right)}{\left(\frac{a_1 a_2}{2}\right)^{-1}} K_0\left(\sqrt{\left[\frac{\omega_p^2}{c^2} + \frac{\kappa_{01}^2}{R^2}\right] a_1 a_2}\right). \quad (5.15)$$

Similarly, the amplitude of the pulse propagating in the positive z-direction, with $z = ct$, $\zeta = 0$, $\eta = 2z$, is given by

$$|\psi(\rho, 0, 2z/c)|^+ = \frac{J_0\left(\frac{\kappa_{01}\rho}{R}\right)}{\left(\frac{a_1 a_2}{2}\right)^{-1}} \left| K_0\left(\sqrt{\left[\frac{\omega_p^2}{c^2} + \frac{\kappa_{01}^2}{R^2}\right] a_1 \left[a_2 - i\,2z\right]}\right)\right|. \quad (5.16)$$

Assuming that the values of a_1, a_2, ω_p and R are such that the large argument expansion of the Bessel function, namely,

$$K_0(z) \approx \sqrt{\frac{\pi}{2z}}\ \exp(-z), \quad (5.17)$$

is valid, we obtain an expression for the amplitude decay factor Γ, viz.,

$$\Gamma = \frac{|\psi|^+}{|\psi|^0} \approx \left(1 - \frac{z^2}{2a_2^2}\right) \exp\left\{-\frac{z^2}{2a_2^2}\sqrt{\left[\frac{\omega_p^2}{c^2} + \frac{\kappa_{01}^2}{R^2}\right] a_1 a_2}\right\}, \quad (5.18)$$

where we have assumed that $z << a_2$. A careful observation of the role of ω_p and R in (5.18) provides a physical insight into the effect of material dispersion. As ω_p

increases (which may be due to an increase in the number of electrons per unit volume for a denser plasma), the decay factor is seen to fall faster as a function of z. This implies that as the plasma becomes denser, the localization of the splash pulse becomes weaker. This result is to be expected intuitively. Also, Eq. (5.18) shows that as R decreases, the effect of the plasma in the cylindrical waveguide becomes more pronounced, as expected. To quantify this behavior we plot the decay factor, Γ, as a function of z for two values of R in Figure 5.3. For a fixed radius, R = 50 cm, the dependence of Γ on ω_p is shown in Figure 5.4. A similar plot for a smaller radius, R = 10 cm, is given in Figure 5.5.

If there were no plasma in the hollow cylindrical waveguide ($\omega_p = 0$), the decay factor would vary as

$$\Gamma = \frac{|\psi|^+}{|\psi|^0} \approx \left(1 - \frac{z^2}{2a_2^2}\right) \exp\left[-\frac{z^2}{2a_2} \frac{\kappa_{01}}{R} \sqrt{\frac{a_1}{a_2}} \right]. \qquad (5.19)$$

The effect of the plasma is therefore dependent on the relative magnitudes of ω_p/c and κ_{01}/R. As long as $\omega_p / c < \kappa_{01} /R$, the LW solution remains fairly localized and the effect of material dispersion is to reduce the longitudinal localization distance from its free-space value by a factor < 10. However, for $\omega_p /c >> \kappa_{01} /R$, the effect of material dispersion becomes predominant and the localization of the pulses is no longer guaranteed. An intuitive extrapolation to the fiber optic case would lead one to believe that as long as the fiber sizes are picked to be the largest possible (while maintaining single-mode operation) and as long as the operational band of wavelengths are chosen to be away from the resonance wavelengths ($\lambda_1 = 0.1$ μm and $\lambda_2 = 9$ μm), the effect

of material dispersion seems to be defeatable and LW propagation seems possible, albeit with localization distances smaller than those in the ideal case; however, this intuitive leap of faith needs to be confirmed numerically.

Two other examples where the effect of the plasma is not noticeable are now presented. Consider first the FWM spectrum given by Eq. (3.1). Substitution of the spectrum into the bidirectional superposition given by (5.12) and considering, once again, only the case m = 1, we obtain

$$\psi(\rho,\zeta,\eta) = J_0\left(\frac{\kappa_{01}\rho}{R}\right)\frac{\exp(i\beta'\eta)}{\beta'}\exp\left\{-\frac{a_1}{4\beta'}\left[\frac{\omega_p^2}{c^2}+\frac{\kappa_{01}{}^2}{R^2}\right]\right\} \times \exp\left\{-\frac{i\zeta}{4\beta'}\left[\frac{\omega_p^2}{c^2}+\frac{\kappa_{01}{}^2}{R^2}\right]\right\} \tag{5.20}$$

after integration over β and α. The FWM decay factor Γ is given by

$$\Gamma = J_0\left(\frac{\kappa_{01}\rho}{R}\right), \tag{5.21}$$

which is independent of both z and ω_p. The expression for the pulse given in Eq. (5.20) is fundamentally different from the one in Eq.(5.16) where the ω_p and z terms were coupled together. In Eq. (5.20) we notice that ω_p is not coupled to any of the η or ζ terms in the real part of the solution. More specifically, if we take the real values of the solution at z = 0 and for any z in the positive direction, we find that the pulses are identical to one another irrespective of the material dispersion represented by ω_p.

Another such example is the MPS pulse spectrum given by Eq. (3.30).

Substituting the spectrum into the bidirectional superposition (5.12) and integrating over α, we obtain

$$\psi(\rho,\zeta,\eta) = \frac{p}{(2\pi)} J_0\left(\frac{\kappa_{01}\rho}{R}\right) \int_{b/p}^{\infty} d\beta \exp\left(-\frac{u}{\beta}\right) \frac{\exp(-v\beta)}{\beta}, \qquad (5.22a)$$

where

$$v = pa_2 - i\eta \qquad (5.22b)$$

and

$$u = \frac{(a_1 + i\zeta)}{4}\left[\frac{\omega_p^2}{c^2} + \frac{\kappa_{01}^2}{R^2}\right]. \qquad (5.22c)$$

Since the integrand is bounded within the range of integration and at infinity, we can use the end-point evaluation described by Eq. (3.35) and arrive at an approximate expression for the LW solution, namely,

$$\psi(\rho,\zeta,\eta) \approx \frac{b\,p^2}{(2\pi)(pa_2 - i\eta)} J_0\left(\frac{\kappa_{01}\rho}{R}\right) \exp\left(i\frac{b}{p}\eta\right) \exp\left(-u\frac{p}{b}\right), \qquad (5.23a)$$

where u is as defined earlier. The MPS pulse decay factor can be written as

$$\Gamma = [\, p^2 a_2^2 + 4z^2 \,]^{-1/2} J_0\left(\frac{\kappa_{01}\rho}{R}\right), \qquad (5.23b)$$

which is again independent of ω_p. We note that the plasma frequency ω_p is coupled with ζ and not with η; hence, it does not enter into the evaluation of the decay factor. Consequently, the MPS pulse propagating in the forward direction is not affected by the material dispersion within the cylindrical metallic waveguide. It begins to decay

after the distance $z = pa_2$ has been surpassed, just as it does in the free-space case.

5. 1. 2 Dissipative Scalar Wave Equation

The dissipative scalar wave equation for an optical fiber waveguide can be written as

$$\left(\nabla^2 - \frac{n_i^2}{c^2} \left[\partial_t^2 + (c_1 + c_2)\, \partial_t + c_1\, c_2 \right] \right) \psi = 0, \tag{5.24}$$

where the constants c_1 and c_2 ($c_1 \neq c_2$) represent the losses in the waveguide. Note that this equation bears a resemblance to the classical telegraph equation. An exponential transformation of the form

$$\psi(\bar{r}, t) = \exp\left[-\frac{1}{2}(c_1 + c_2)\, t \right] \tilde{\psi}(\bar{r}, t) \tag{5.25}$$

leads to the expression

$$\left(\nabla^2 - \frac{n_i^2}{c^2} \partial_t^2 + \frac{n_i^2}{4c^2} (c_1 - c_2)^2 \right) \tilde{\psi} = 0. \tag{5.26}$$

The lossless case therefore corresponds to the condition $c_1 = c_2$. Assuming a solution of the form described by Eq. (2.16), which we repeat here for easy readability, viz.,

$$\begin{aligned} \tilde{\psi}(\rho,\phi,\zeta,t) &= \Phi(\rho, \phi)\ \exp\{i\beta(z+ct)\}\ \exp\{-i\alpha(z-ct) \\ &= \Phi(\rho, \phi)\ \exp\{i\beta\eta\}\ \exp\{-i\alpha\zeta\}, \end{aligned} \tag{2.16}$$

with $\eta = z + ct$ and $\zeta = z - ct$, and substituting the expressions describing ∂_z^2 and ∂_t^2 from Eqs. (2.17) and (2.18), namely,

$$\partial_z^2 \tilde{\psi} = -(\beta - \alpha)^2 \tilde{\psi}, \tag{2.17}$$

$$\partial_t^2 \tilde{\psi} = - c^2(\beta+\alpha)^2\tilde{\psi}. \tag{2.18}$$

into (5.22), we obtain

$$(\nabla_t^2 + \kappa_i^2)\,\Phi = 0, \tag{5.27}$$

where

$$\kappa_i^2 = n_i^2\,(\alpha+\beta)^2 - (\alpha-\beta)^2 + \frac{n_i^2}{4}(c_1 - c_2)^2\,. \tag{5.28}$$

In Eq. (5.28), we have assumed that the term c^2 has been absorbed by the constants c_1 and c_2. Substituting the corresponding values for the refractive indices in the expression for κ_i^2 in the two regions, we get the general solution for the dissipative waveguide in terms of the bidirectional superposition, viz.,

$$\tilde{\psi}(\rho,\zeta,\eta) = \frac{1}{(2\pi)^2}\int d\kappa_1 \int d\alpha \int d\beta\; A(\alpha,\beta,\kappa_1)\,\kappa_1\,J_0(\kappa_1\rho) \times e^{-i\alpha\zeta}\,e^{i\beta\eta}\;\delta\left[\frac{(c_1 - c_2)^2}{4} + 4\alpha\beta - \kappa_1^2\right] \tag{5.29}$$

in the core and

$$\tilde{\psi}(\rho,\zeta,\eta) = \frac{1}{(2\pi)^2}\int d\kappa_1 \int d\kappa_2 \int d\alpha \int d\beta\; A(\alpha,\beta,\kappa_1)\,\kappa_1\;\; K_0(\kappa_2\rho) \times \frac{J_0(\kappa_1 a)}{K_0(\kappa_2 a)}\;\; e^{-i\alpha\zeta}\,e^{i\beta\eta}\;\delta\big(\kappa_2 - f(\kappa_1)\big) \tag{5.30}$$

$$\times\;\delta\left[\frac{(c_1 - c_2)^2}{4} + 4\alpha\beta - \kappa_1^2\right]\;\;\delta\left[\kappa_2^2 - n_e^2\,(\alpha+\beta)^2 + (\alpha-\beta)^2 - \frac{n_i^2(c_1 - c_2)^2}{4}\right]$$

in the cladding.

The limits on the integrals in Eqs. (5.29) and (5.30) are now given by the

waveguiding conditions, namely, $\kappa_1^2 > 0$ and $\kappa_2^2 < 0$. Since the delta function in (5.29) implies the relation

$$4\alpha\beta = \kappa_1^2 - \frac{(c_1 - c_2)^2}{4}, \tag{5.31}$$

we see that the integration in the α - β plane can lie in the first or third quadrants for $4\kappa_1^2 > (c_1 - c_2)^2$, or, in the second or fourth quadrants for $4\kappa_1^2 < (c_1 - c_2)^2$. The relative values of the loss coefficients and the choice of κ_1 thus define the quadrants of operation. Another requirement on κ_1^2, namely, $k_1^2 > 0$, implies that

$$16\alpha\beta > -(c_1 - c_2)^2. \tag{5.32}$$

The requirement that κ_2^2 should be less than zero leads to the expression

$$4\, n_e^2\, (\alpha+\beta)^2 - 4\,(\alpha - \beta)^2 + n_i^2 (c_1 - c_2)^2 < 0 \tag{5.33}$$

which can be expressed in another manner, viz.,

$$\frac{(\alpha+\beta)^2}{\gamma^2} - \frac{(\alpha - \beta)^2}{n_e^2\, \gamma^2} < 1, \tag{5.34}$$

where $4\gamma^2 = (c_1 - c_2)^2$. The relation (5.34) describes the interior of a hyperbola in the $(\alpha-\beta)$ vs. $(\alpha+\beta)$ plane, as shown in Figure 5.6. The shaded region in Figure 5.6 describes the valid region for integration. The asymptotes of the hyperbola are given by the equations $(\alpha - \beta) = \pm n_e (\alpha + \beta)$, and the curves intersect the $(\alpha + \beta)$ axis at $\pm\gamma$. The shaded region can be further transformed into the α vs. β plane to obtain the limits on the integrals. The figure shows that the limits on the integrals go asymptotically towards the lossless waveguide when $c_1 \rightarrow c_2$ and $\gamma \rightarrow 0$. As an aside, it is worth noting that the condition $c_1 = c_2$ corresponds to Lord Kelvin's celebrated solution for

the transmission line equation.

Eqs. (5.31) - (5.34) are the defining relations for the limits on the integrals in the bidirectional superposition of solutions in the lossy case. A delicate balance between all these constraints needs to be achieved as a starting step prior to performing a numerical analysis to evaluate the localization of solutions. In a nutshell, we have described in this subsection an approach toward the analysis of a lossy waveguide and the effect of the losses on the constraints on κ_1 and κ_2 in the integrals as well as their influence on the limits of the integration. With the guidelines mentioned in this section, it still seems feasible to obtain novel, exact solutions using the bidirectional approach. We will leave the numerical derivation of these results for future research and investigations.

5. 1. 3 Asymptotic and Numerical Methods

Having described the complications resulting from incorporating material dispersion and losses in our problem formulation, it is instructive to describe some of the efforts that have been undertaken by researchers in the past for the evaluation of pulse propagation in lossy dispersive media. As a result of this essay, we will also gain an idea about possible approaches to solving the complex problem of synthesizing LW solutions in lossy dispersive waveguides.

Connor and Felsen [26] first proposed a method based on the use of complex space-time rays for understanding the behavior of pulse propagation in lossy dispersive

media. Their approach involves the use of solutions of the form A (r, t) exp [iS (r, t)], where S is a rapidly varying function of space and time, whereas A is a slowly varying function of the same variables. The solutions are analyzed in terms of wave packets that travel with central frequency $\omega = -\partial S/\partial t$ and central wave number $k = -\nabla S$. When the medium is lossy, the wave packets are shown to propagate along trajectories in the complex (r, t) domain. While complex space-time rays have obscure physical significance, their intersections with the real (r, t) space describe physical fields. Using this approach, Connor and Felsen were able to describe the propagation of a Gaussian pulse in a cold dissipative plasma. We are currently investigating the adaptation of this method for analyzing the synthesis of LW solutions in waveguide structures. Preliminary explorations indicate that this technique may be applied to multimode waveguides where wave propagation may be adequately described in terms of a geometric ray approach. For single-mode fibers, however, the applicability of this formulation is not clear.

One of the reasons Connor and Felsen chose the complex space-time ray approach was to sidestep the complexities arising from the alternate conventional approach where analytical techniques would involve the evaluation of complex saddle points within integrals. As described earlier, in conventional Fourier methods of synthesis, plane wave eigenfunctions are used in conjunction with a given spectrum and an integration is performed with respect to the temporal frequency ω and a transverse propagation constant. The integral may be evaluated asymptotically using saddle point techniques when the observation times are sufficiently large to be able to call the dispersion mature [27, 28]. In this method of analysis, the saddle points are real

for lossless media; however, when the medium becomes absorptive, the saddle points become complex and a very complicated evaluation of their behavior is required; information about the evolution of the branch points and branch cuts is also needed for an accurate analysis. Oughstun, Sherman and coworkers, in a series of papers [29 – 34], have developed a comprehensive theory for the analysis of pulse propagation in Lorentz-like, lossy, dispersive media. The analysis starts with the substitution of the refractive index in a Lorentz - like medium, described by

$$n(\omega) = \left(1 - \frac{b^2}{\omega^2 - \omega_0^2 + 2i\delta\omega} \right)^{1/2} \tag{5.35}$$

in the phase function $\phi(\omega, \theta) = i\omega[n(\omega) - \theta]$, which appears in the Fourier representation of a pulse at (z, t), namely,

$$\psi(z, t) = \int_C \mathcal{F}(\omega) \exp\left[\frac{z}{c} \phi(\omega, \theta) \right] d\omega, \tag{5.36}$$

where $\theta = ct/z$ characterizes a space-time point in the field, $\mathcal{F}(\omega)$ is the temporal Fourier spectrum of the initial pulse $f(t) = \psi(0, t)$, $b^2 = 4\pi Ne^2/m$ is the square of the plasma frequency of the medium, N is the number density of electrons of charge e and mass m, ω_0 is the undamped resonance frequency and δ is the associated phenomenological damping constant. In order to evaluate the pulse evolution at large distances z, the topography of the real part of the phase function, $\phi(\omega, \theta)$, needs to be understood. Specifically, an evaluation of the saddle points of $\phi(\omega, \theta)$ and the values of the phase function at these points are needed. The saddle points of the complex phase function are given by solutions of the equation $\phi'(\omega, \theta) = 0$, which can be written as

$$n(\omega) + \omega n'(\omega) - \theta = 0. \tag{5.37}$$

Using approximations for various regimes of operation (namely, when ω is very large, very small, and comparable to the undamped resonance frequencies) Oughstun *et al.* have shown that it is possible to obtain a complete, uniformly valid description of the entire dynamical field evolution in the mature dispersion limit. For a Lorentz-medium with two resonances, with the refractive index being expressed as

$$n(\omega) = \left(1 - \frac{b_0^2}{\omega^2 - \omega_0^2 + 2i\delta_0\omega} - \frac{b_2^2}{\omega^2 - \omega_2^2 + 2i\delta_2\omega} \right)^{1/2}, \tag{5.38}$$

a combination of numerical and asymptotic approaches is necessary to obtain an accurate analysis and to gain a physical insight into the phenomenon of pulse propagation.

Current research efforts are concerned with the conversion of the entire asymptotic analysis into the $\alpha - \beta$ domain for a single-resonance medium (to be extended later to a double-resonance medium); the Sellmeier equation for the variation of the refractive index as a function of ω is currently being modified to include the effect of losses. Practical values for the damping constants are being calculated and asymptotic methods for evaluating the double integral over α and β are being devised. This effort will lead to the evaluation of LW solutions in lossy dispersive optical fibers. The analysis and results will be presented at a later date.

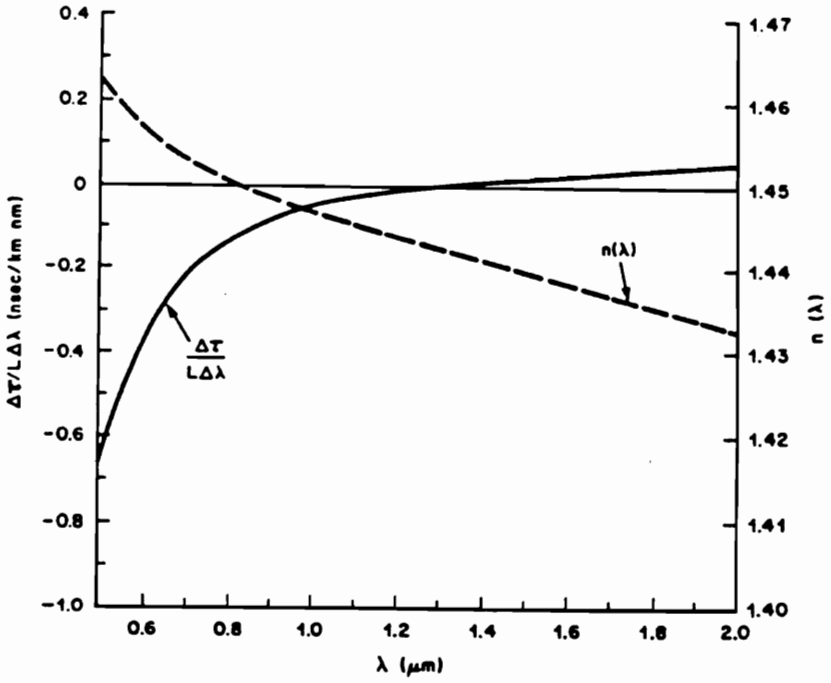

Figure 5.1. Refractive index and dispersion as a function of wavelength for a two-term Sellmeier expansion [36].

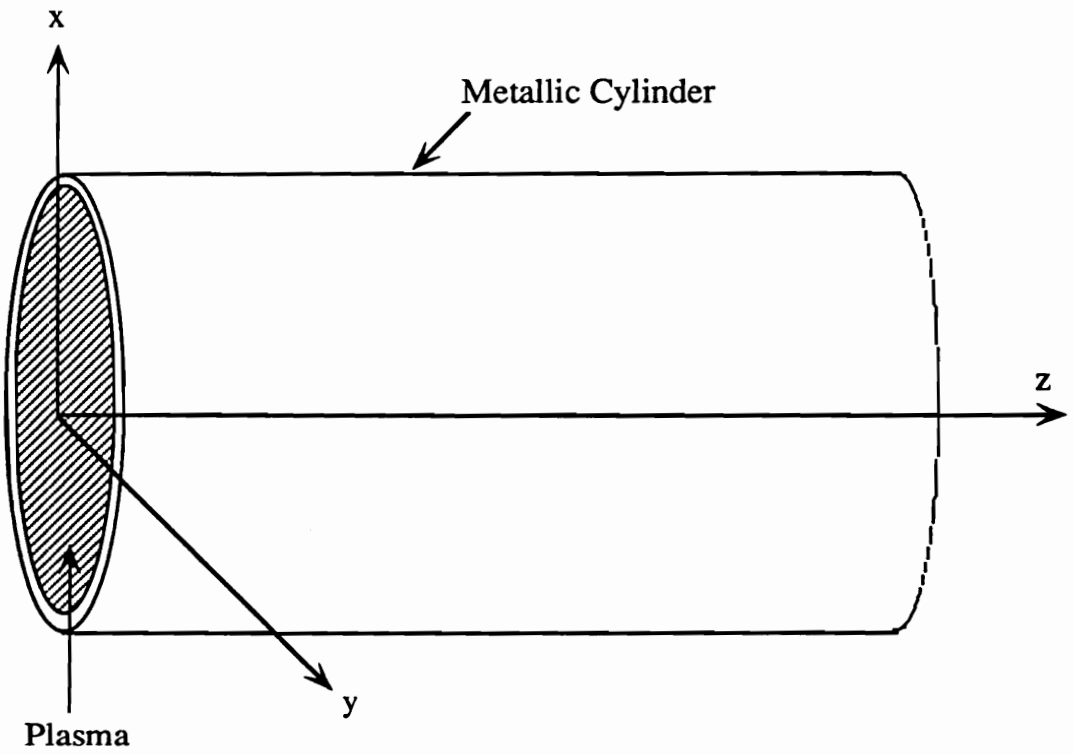

Figure 5.2. Schematic of metallic cylindrical waveguide filled with ionized, cold isotropic plasma.

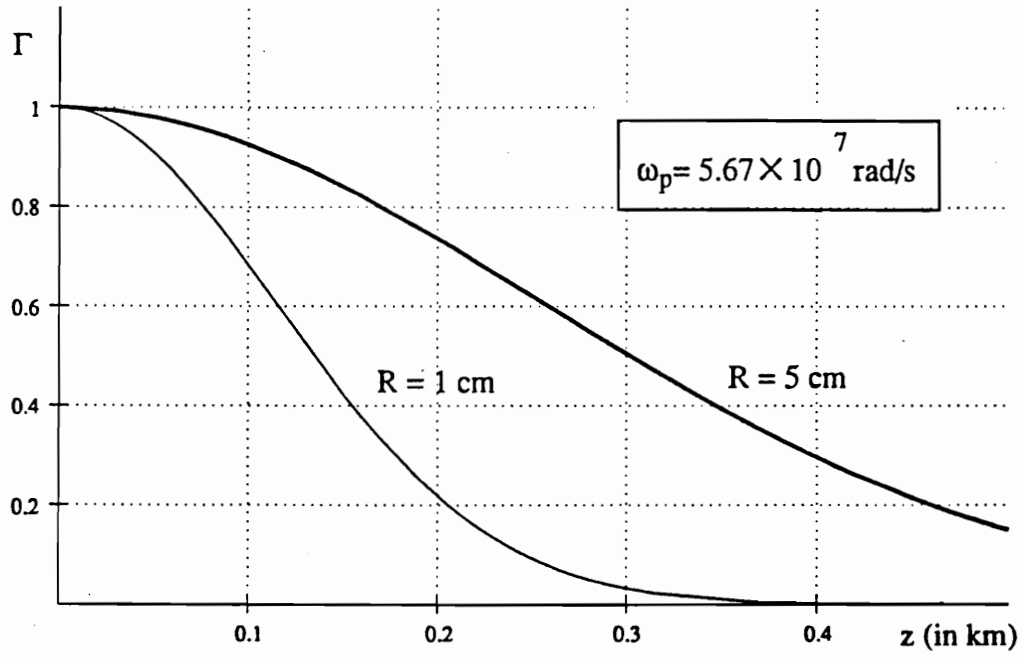

Figure 5.3. Variation of pulse decay factor with waveguide dimension for typical daytime ionosphere plasma frequency.

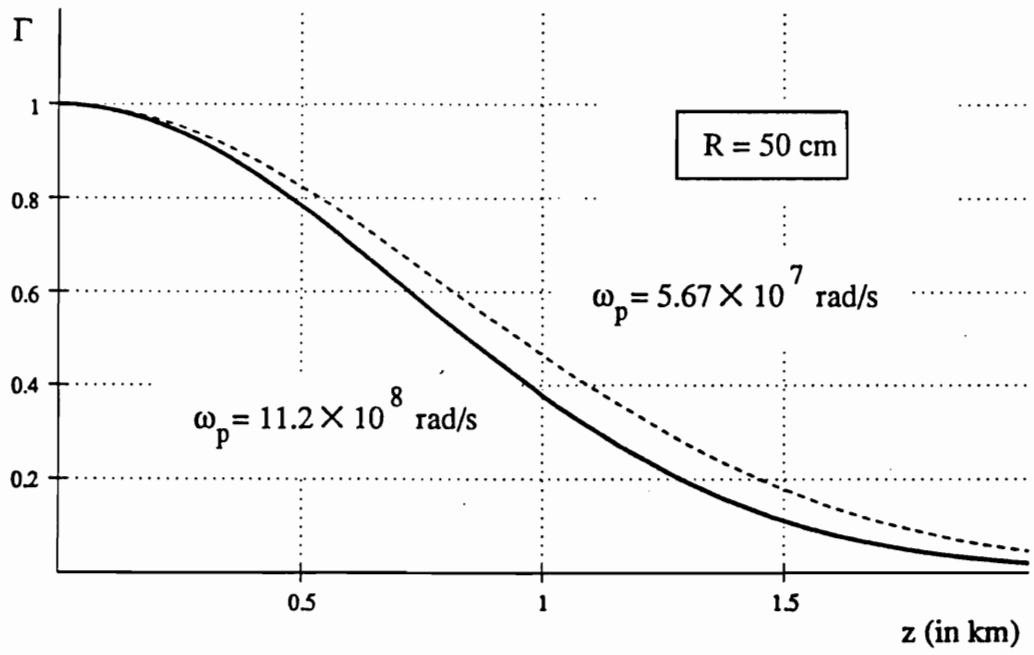

Figure 5.4. Variation of pulse decay factor with plasma frequency for a waveguide dimension, R = 50 cm.

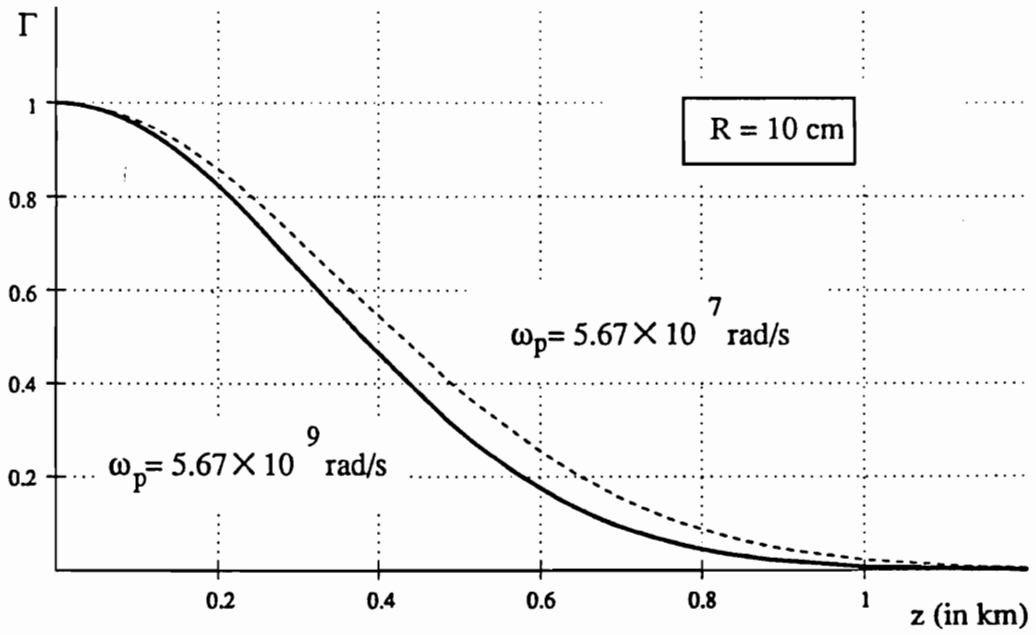

Figure 5.5. Variation of pulse decay factor with plasma frequency for a waveguide dimension, R = 10 cm.

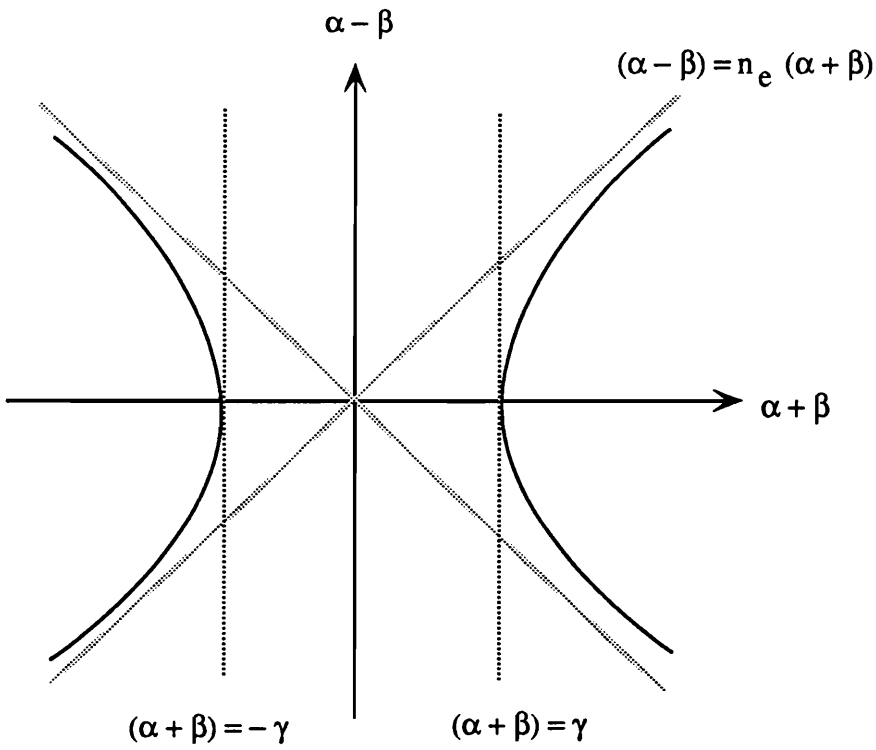

Figure 5. 6. Region of integration for a lossy waveguide.

5.2 The LP_{11} Mode

In this section we will consider the possibility of generating LW solutions of a higher order. Specifically, we will try the synthesis procedure using the Bessel function of the first order (which corresponds to the LP_{11} mode in the classical analysis) as a basis function in the radial direction. The analysis will be restricted to the unperturbed solution and we will not consider the effects introduced by the wall term. There are two ways of viewing the analysis. First, we may wish to investigate the possibility of higher order LW solutions that can function as carriers of information in a fiber optic system. Alternately, we would like to investigate whether the LP_{11} mode equivalent will act as a noise source in a system that uses LP_{01} modes as information signals. This viewpoint is fairly important since our analysis of the MPS pulse spectrum has shown that while 87% of the power will be contained below ω_{max} (or, above λ_{min}), 13% of the power in the spectrum is contained in a wavelength region where real solutions for the eigenvalue equation for the LP_{11} mode are available. [These approximate power spreads are based on the assumption that λ_{min} corresponds to the single-mode cut-off wavelength for the fiber.]

Fundamentally, one would not expect any difference in the analysis of this higher order mode except for the algebraic manipulations involved; hence, one would anticipate, *a priori*, that a nondecaying LW solution would result. A detailed analysis for the unperturbed MPS pulse is given below to check if this *a priori* conjecture is justified.

The fundamental solution for the LP_{11}^{even} mode is given by

$$\Phi(\rho) = \begin{cases} A\, J_1(\underline{\kappa}_1 \rho) \cos\varphi \\ \dfrac{A\, K_1(\underline{\kappa}_2 \rho)}{K_1(\underline{\kappa}_2 a)} J_1(\underline{\kappa}_1 a) \cos\varphi \end{cases}, \quad \begin{matrix} \rho < a \\ \rho > a \end{matrix} \tag{5.39}$$

where $\underline{\kappa}_1^2 = k_0^2 n_1^2 - \beta_{11}^2$ and $\underline{\kappa}_2^2 = \beta^2 - k_0^2 n_2^2$, β_{11} being the propagation constant of the LP_{11} mode. The synthesis procedure for the LW solution in the bidirectional representation ($\alpha - \beta$ domain) is similar to the one performed for the LP_{01} mode and we can substitute the MPS pulse spectrum given by (3.30) into the bidirectional superposition (3.31) and evaluate the unperturbed solution ψ_u as

$$\psi_u = \frac{p\cos\varphi}{8\pi} \int_{b/p}^{\infty} \frac{d\beta}{\beta} \exp\left[(-\beta p + b) a_2 + i\eta\right] \times \int_0^{\infty} d\underline{\kappa}_1\, \underline{\kappa}_1\, J_0(\underline{\kappa}_1 \rho) \exp\left(-\frac{\underline{\kappa}_1^2 (a_1 + i\zeta)}{4\beta}\right). \tag{5.40}$$

We use the identity (2.12.9.3) from Prudnikov *et al.* [24], viz.,

$$\int_0^{\infty} d\chi\, \chi^{\alpha-1} J_\nu(c\chi) \exp(-p\chi^2) = A_\nu^\alpha, \tag{5.41}$$

where

$$A_\nu^\alpha = c^\nu\, p^{-\frac{(\alpha+\nu)}{2}}\, 2^{-\nu-1}\, \Gamma\left[\begin{matrix} \dfrac{(\alpha+\nu)}{2} \\ \nu+1 \end{matrix}\right]\, {}_1F_1\left(\frac{(\alpha+\nu)}{2}; \nu+1; -\frac{c^2}{4p}\right). \tag{5.42}$$

In Eq.(5.42), ${}_1F_1$ is the confluent hypergeometric function defined by the series

$$ {}_1F_1(a; b; z) = \sum_{k=0}^{\infty} \frac{(a)_k}{(b)_k} \frac{z^k}{k!}, \tag{5.43} $$

where $(a)_k$ is defined by $(a)_k = a\,(a+1)\,.....\,(a+k-1)$. Using the identity (5.41) with $\nu = 1$, $\alpha = 2$, $c = \rho$ and $p = (a_1 + i\zeta)/4\beta$ and integrating over κ_1, we obtain

$$ \psi_u = \frac{p\,\rho \exp(ba_2)\cos\varphi}{8\sqrt{\pi}\,(a_1 + i\zeta)^{3/2}} \sum_{k=0}^{\infty} \frac{(3/2)_k}{(2)_k} \left(\frac{-\rho^2}{a_1 + i\zeta}\right)^k \tag{5.44} $$

$$ \times \int_{b/p}^{\infty} d\beta\, \beta^{k+1/2} \exp\left[-\beta\,(p\,a_2 - i\eta)\right]. $$

The integral in (5.44) is the incomplete Gamma function, $\Gamma(\alpha, \beta)$, and after some algebraic manipulations, one can rewrite the above equation as

$$ \psi_u = \frac{p\,\rho \exp(ba_2)\cos\varphi}{4\pi\left[(a_1 + i\zeta)(p\,a_2 - i\eta)\right]^{3/2}} \sum_{k=0}^{\infty} \frac{\Gamma(k+3/2)}{\Gamma(k+2)} \left[\frac{-\rho^2}{(a_1 + i\zeta)(p\,a_2 - i\eta)}\right]^k \tag{5.45} $$

$$ \times\ \Gamma(k+3/2,\ b/p)\,. $$

While a complete physical picture of the LP_{11} mode is still obscure from the above expression, one can see that the solution is inversely proportional to the term $(pa_2 - i\eta)$, thus implying that for localized non-decaying solutions, the product pa_2

should be much greater than the longitudinal distance, z, of interest. This condition is the same as that for the LP_{01} mode of the MPS pulse. Hence, one would expect that for the parametric values chosen for the localized propagation of the LP_{01} mode, an excitation of the higher order mode would similarly lead to a LW solution. In order to find the approximate behavior of the LP_{11} mode in the transverse direction, we take recourse to an approximate analysis which is best executed by carrying out the series evaluation prior to assessing the integral. Following this approach, we can manipulate the terms in the series to recast Eq. (5.44) as

$$\psi_u = \frac{p\,\rho\,\exp(ba_2)\cos\varphi}{8\sqrt{\pi}\,(a_1 + i\zeta)^{3/2}} \int_{b/p}^{\infty} d\beta\,\sqrt{\beta}\,\exp\left[-\beta\left(p\,a_2 - i\eta\right)\right] \times \left(\frac{-\rho^2\,\beta}{a_1 + i\zeta}\right)^{-1} \sum_{k=0}^{\infty} \frac{1}{k\,!\,(k+1)} \left[\frac{-\rho^2\,\beta}{2\left(a_1 + i\zeta\right)}\right]^{k+1}. \tag{5.46}$$

Using the series definition of the exponential function, (5.46) becomes

$$\psi_u = \frac{p\exp(ba_2)\cos\varphi}{8\sqrt{\pi}\,\rho\,(a_1 + i\zeta)^{1/2}} \int_{b/p}^{\infty} d\beta\,\frac{\exp\left[-\beta\left(p\,a_2 - i\eta\right)\right]}{\sqrt{\beta}} \times \left[\exp\left(\frac{-\rho^2\,\beta}{2\left(a_1 + i\zeta\right)}\right) - 1\right]. \tag{5.47}$$

Analytical, closed-form expressions for the integral in Eq. (5.46) can be obtained in

terms of a difference of complementary error functions by invoking the definition of the aforementioned functions. However, our motivation in this derivation is to take a closer look at the radial variation of the LP_{11} mode. This goal is easily achieved by using an endpoint evaluation of the integrals [given by (3.35)]. As a consequence, we obtain a final approximate expression for the LP_{11} mode, viz.,

$$\psi_u \approx \sqrt{\frac{p}{\pi b\ (a_1 + i\zeta)}}\ \frac{\cos\varphi}{8a_2\rho}\ \exp\left[i\frac{b}{p}\eta\right]\ \left[1 - \exp\left(\frac{-b\,\Omega}{p}\right)\right], \qquad (5.48)$$

where $\Omega = \rho^2/(a_1 + i\zeta)$, and we have assumed that $pa_2 >> \Omega$ and $pa_2 >> |\eta|$. The behavior of this function in the fiber core is shown in Figure 5.7. A typical first-order Bessel function, $J_1(\rho)$, is also plotted in Figure 5.8 for comparison. The plots show that the LP_{11} mode obtained from the MPS pulse spectrum is more focussed within the fiber core as compared to the Bessel function, as expected.

From the expression for the ideal, unperturbed pulse, one sees that the LP_{11} mode will remain localized for the choice of free parameters. A more detailed study of the noise introduced by this mode is currently in progress.

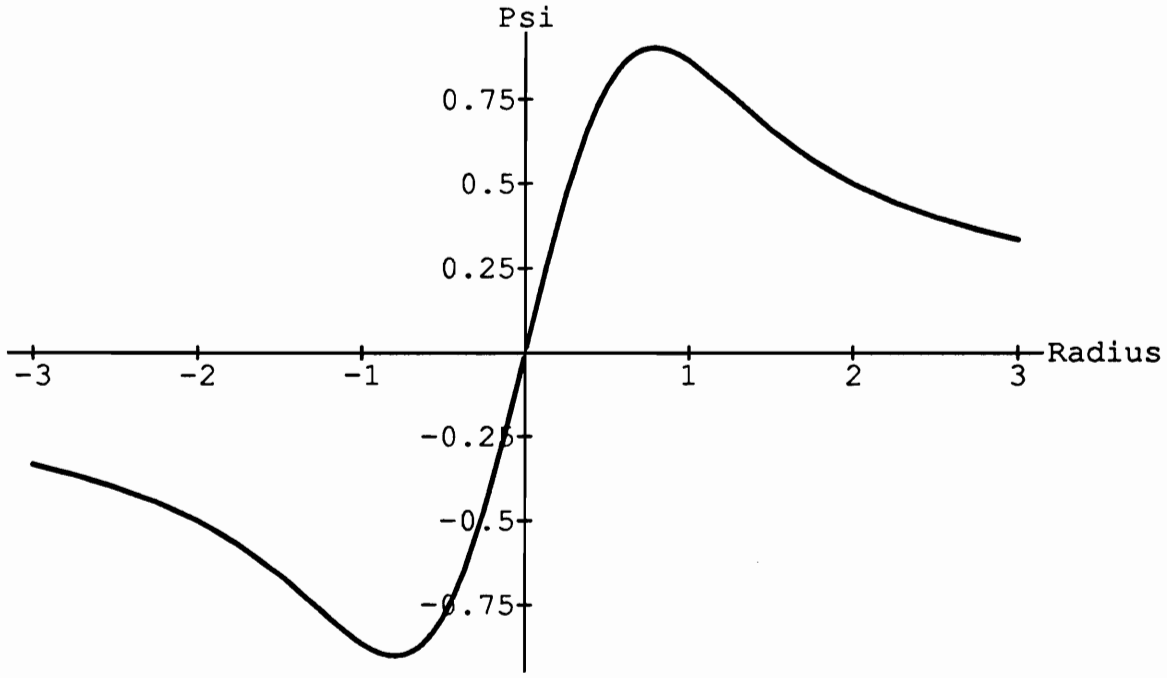

Figure 5.7. MPS pulse for the LP_{11} mode plotted in the fiber core.

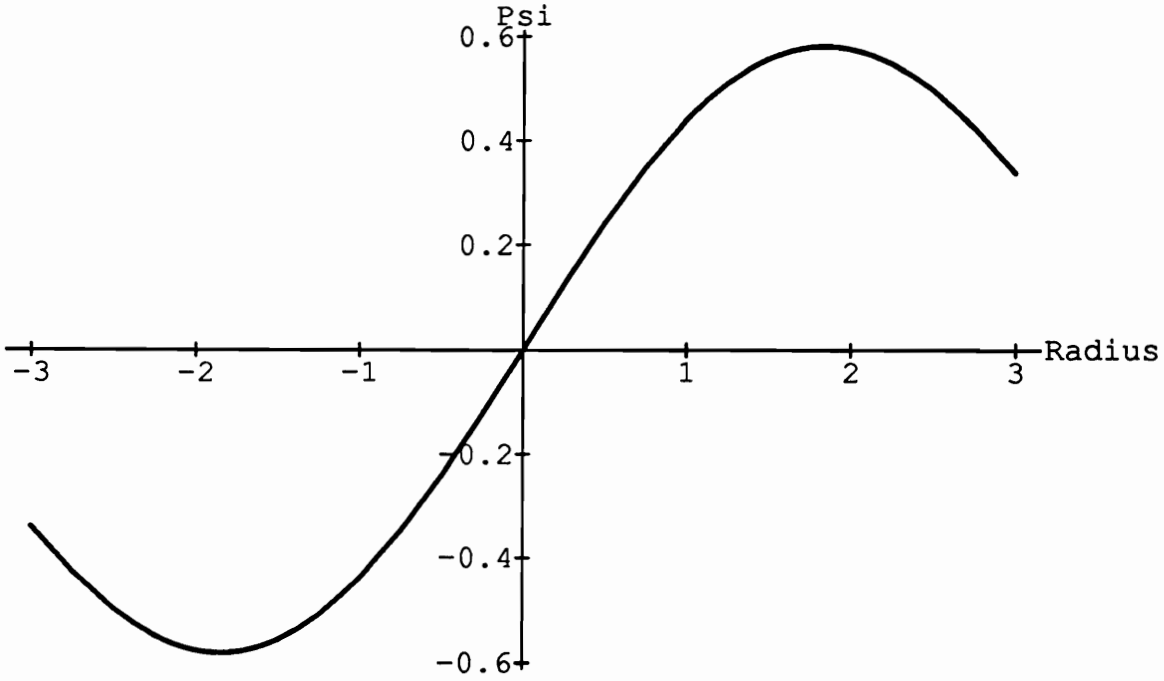

Figure 5.8. Bessel function of order one, $J_1(\underline{\kappa}_1\rho)$, plotted in the fiber core.

5.3 Source Considerations

In the past decade, the search for (electromagnetic) wave solutions that do not decay for extremely long distances has been an active area of interest in several inter-related disciplines. Wu's electromagnetic missiles, Durnin's Bessel beams, the search for super-gain/super-directive antennas and Ziolkowski's EDEPT's are examples of a seemingly disjoint, yet globally unified, effort that seeks to answer the question: "Is there a way of defeating the Rayleigh diffraction length for a radiating beam in free space?"

Despite extensive theoretical analyses that have been expounded to prove the plausible existence of such solutions, the question of practical feasibility still remains unanswered. Except for a handful of experiments that have demonstrated basic concepts, the immense theoretical promise held by LW solutions has not yet been fulfilled. Furthermore, some of the recent reviews [37 - 39] of diffraction-free beams have been hypercritical. Hafizi and Sprangle [39], for example, have questioned the basic methods used to compare the localization distances and have doubted original claims that these beams are "resistant to diffractive spreading commonly associated with all wave propagation [11] ".

We shall now review some of the practical methods that have been used to generate Ziolkowski's ADEPT's; specifically, a review of MPS pulse generation is instructional since it allows us to glean some of the pertinent implementation ideas and tune them for the optical regime. Ziolkowski's ADEPT's are closest in analogy to the

fiber optic LW solutions; also, they are free from objections raised about earlier attempts of generating directed pulses. For example, Wu's electromagnetic missiles require the use of pulses with extremely short rise times, whereas the supergain/super-directive antennas are impractical since any deviation from the exact theoretical solution results in mediocre array performance.

Consider the MPS pulse described by Candy, Lewis and Ziolkowski [40, 41], namely,

$$\psi(\rho, z, t) = \frac{1}{z_0 + i\,(z - ct)} \; \frac{\exp\left(-\,b\,s\,/\beta\right)}{\left[\left(s/\beta\right) + a\right]^{\alpha}}, \qquad (5.49)$$

where $s\,(\rho, z, t) = \rho^2 / [z_0 + i(z\text{-}ct)] - i\,(z + ct)$ and α, β, a, z_0 and b are free parameters that determine the source spectrum. A planar array comprising 101 independently addressable elements is chosen as the source for generating the MPS pulse described above. The first step in the array design involves a simulation of the solution (5.49) using well-chosen spatial-temporal sampling intervals. The simulation provides the designer with a complete spatiotemporal characterization which includes details of the time histories required at different spatial positions in order to generate a localized radiation. This trait, namely, the dependence of the time history (or, viewed in another way, the dependence of the frequency spectrum) on the spatial coordinate is peculiar and is a unique feature of the LW solutions described by Ziolkowski. Antenna array designers have used phased-array techniques in the past; however, their efforts have been limited to spatial phasing with individual elements being driven by monochromatic signals. In LW solutions described here, the driving function for each

element is a broad bandwidth waveshape determined by the solution (5.49) and its derivatives and is dependent on the position of the element in the array. A schematic description of an ADEPT/EDEPT array implementation is shown in Figure 5.9. Each individual element driven by its own time history radiates a pulse which combines with pulses emanating from other elements to form the resulting wave packet.

Instead of viewing the driving functions for the individual elements in the time domain, one can also consider the different pulses originating from different source points with a correlated frequency content. To quote Ziolkowski [10], ".. they (the pulses) arrive at the right place at the right time with the frequency components necessary to reconstruct the packet". An extension of this technique to fiber optic implementation now seems possible. For example, by slicing the Fourier spectrum of the MPS pulse at different spatial positions, one can envision the possibility of an array of point sources, each driven by a specific source spectrum defined by the slice. The focussing or the delivery of these different sources can be executed by a set of tapered fibers, as shown in Figure 5.10. Each source for the individual element needs to possess well shaped frequency spectra or be driven by ultrashort, appropriately shaped time functions. Current research in the generation of shaped pulses reflects the possibility of achieving LW source arrays in the future [42 - 44].

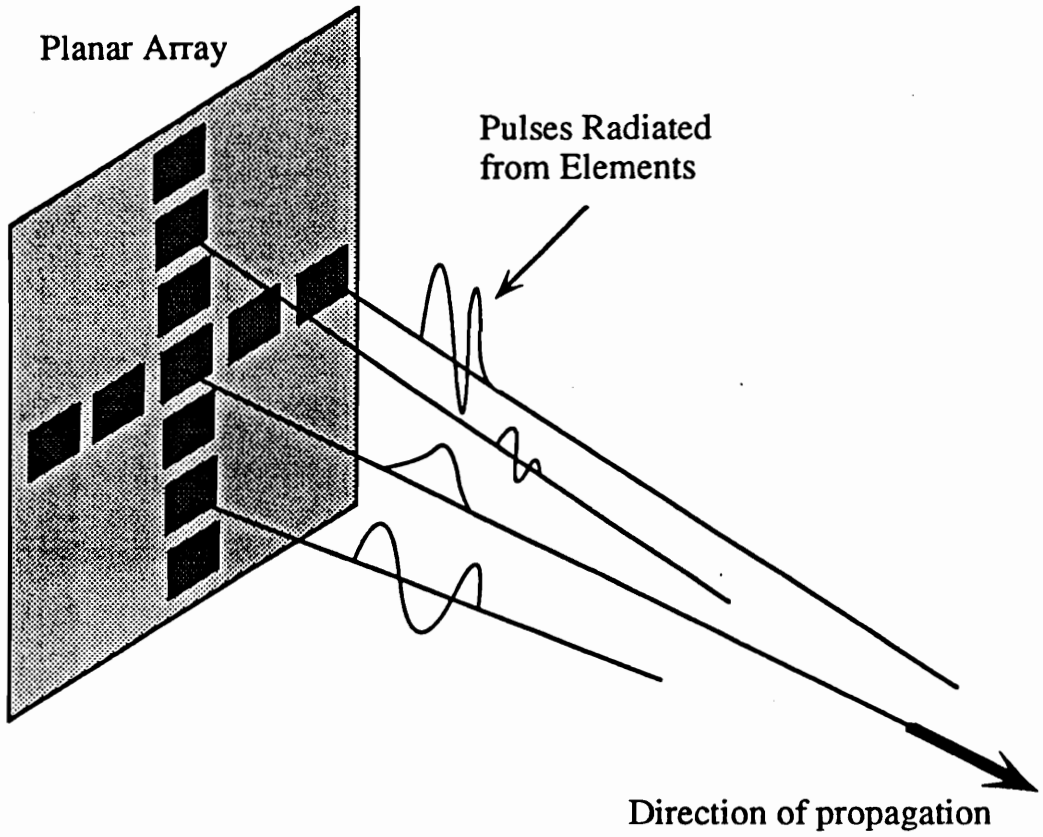

Figure 5.9. Generation of ADEPT-like pulse packets with the use of independently addressable point sources..

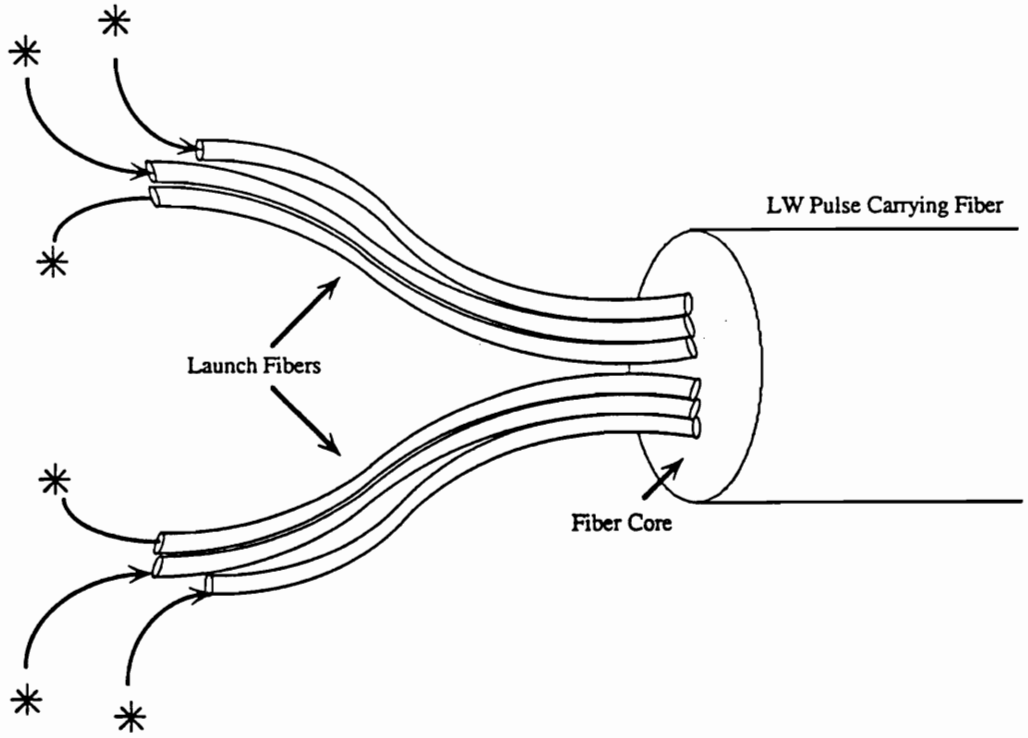

Figure 5.10. Fiber optic LW solution generation scheme: A possible implementation method.

5. 4 Material Issues

The preceding section addressed some of the issues on possible source requirements. The development of novel arrays of optical sources with the capability of possessing well-defined spectra or driving functions can, in the future, find applications in LW pulse propagation. While broadband sources may portend the feasibility of LW -based fiber-optic communication systems on the transmitting end, a major issue that remains unaddressed is the ability of the fiber material to propagate all wavelengths of interest without significant degradation. In this section, we will look at future technology trends, as related to material properties of fibers, that can lead us toward the development of a well-tailored LW communication system.

The detailed study of the MPS pulse in Chapter 3 has shown us that for the total solution to remain localized within the waveguide, the ratio of the maximum to minimum wavelengths should be at least in the range 5 - 10. This ratio requirement implies that the transmission medium should be capable of transmitting wavelengths in the range from 0.5 μm to 10 μm. While currently available fiber materials have specific windows of transmission, the burgeoning field of infrared fibers offer much encouragement for future feasibility. A spectral attenuation plot for silica based fibers used in present-day communication systems is shown in Figure 5.11. This plot, reproduced from Keiser [45], shows the movement of the operating wavelengths in the 1970's in the 800 nm band toward the 1300 and 1550 nm bands in present years. In the early 1980's, silica-based fibers reached the limit of their transparency and researchers turned their attention toward other materials that could result in lower losses at longer

wavelengths [46, 47]. This led to the emergence of the infrared fibers made from polycrystalline materials such as thallium and silver halides and non-oxide glasses composed of metal fluorides or chalcogenides. Chalcogenide fibers are composed of Ge, Se and Te and typical examples such as As_2S_3 and As_2Se_3 are capable of transmitting in the 1 to 10 μm range. Non-oxide fibers made from mixed fluorides such as ZrF_4, BaF_2, GdF_4, and AlF_3 have a transparency in the 1 to 6 μm range. Polycrystalline fibers, such as KRS-5 (thallium bromoiodide) and AgCl, are capable of transmitting wavelengths between 2 and 20 μm . The theoretical minimum losses for most such fibers have been predicted in the 0.001 dB/km range. Current fabrication techniques, however, have barely scratched the surface of the immense ultra-low-loss potential of IR fibers. Some of the data presented by P. W. France [48] in 1988 is reproduced in Figures 5.12 and 5.13. The samples had a minimum attenuation of 4.3 dB/km while the dotted graph in Figure 5.12 indicates the theoretical limit of 0.01 dB/km. The contaminants responsible for the high peaks are also mentioned in Figure 5.13. Recent results have reported lowest losses of < 0.1 dB / km at 2.55 μm [49, 50].

As soon as practical problems of impurities in raw materials, formation of microcrystallites (which induce scattering losses), water-solubility and toxicity are solved, these glasses will lead to the fabrication of novel transmission media that will be more suitable for the transmission of LW pulses. The associated problems of designing new sources and detectors will need to be addressed in parallel. While conquering dispersion seems to solve one of the problems, losses in the fiber will eventually set the limits for LW transmission; the question of regeneration and the possibility of having highly broadband optical amplifiers then comes into picture.

Only future technology trends and developments will disentangle this seemingly inextricable web of interrelated problems and shed light on the possibility of implementing LW transmission systems.

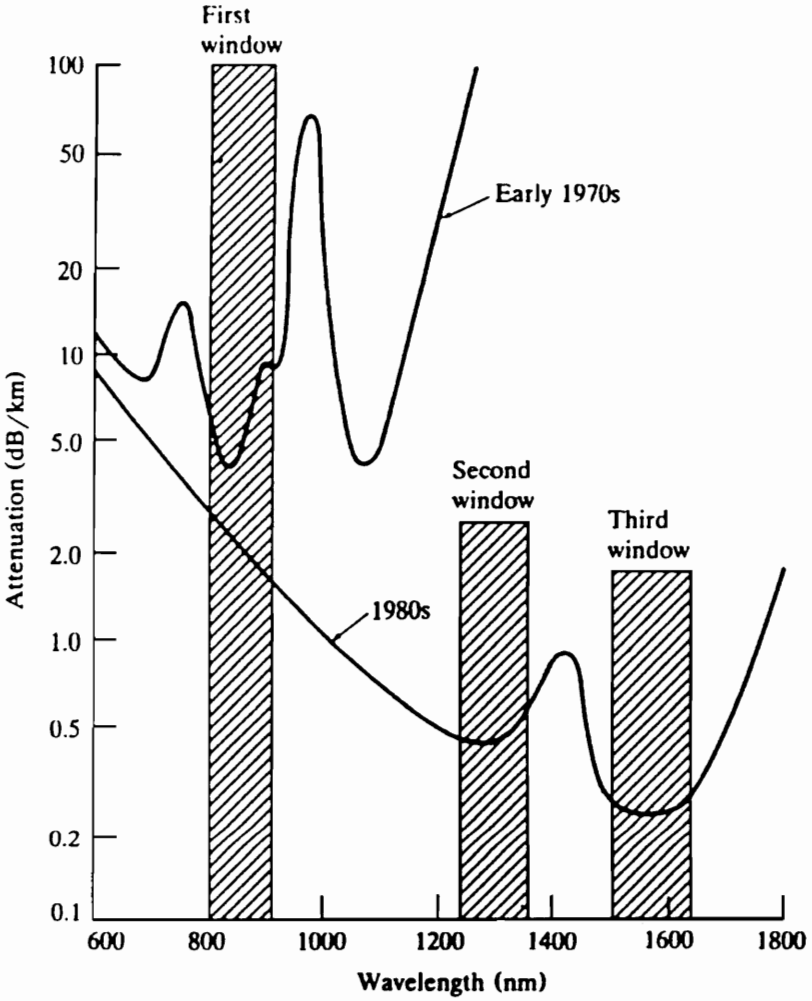

Figure 5.11. Spectral attenuation of typical silica based fibers.

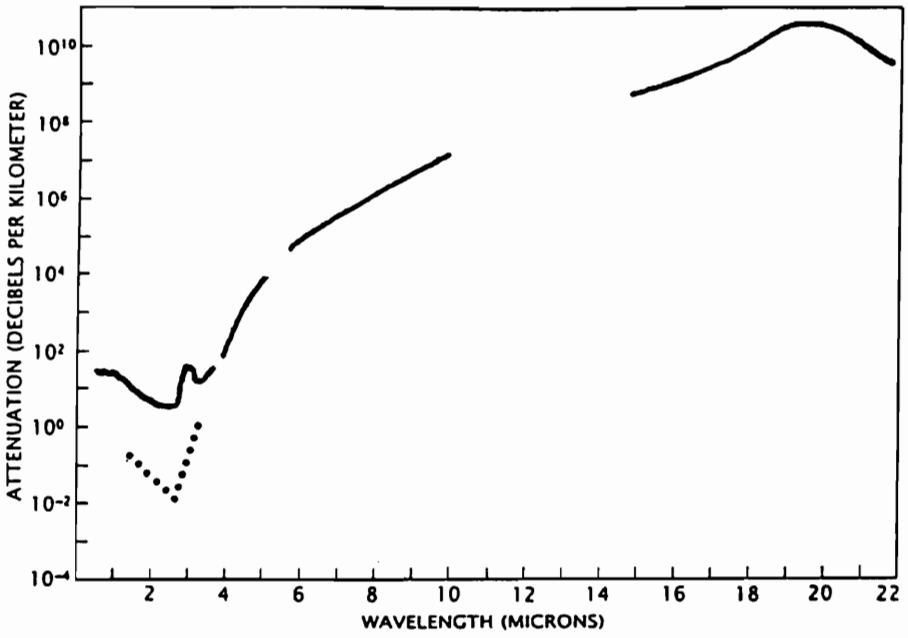

Figure 5.12. Attenuation measurements at four different wavelength regions for heavy-metal fluoride glasses [48].

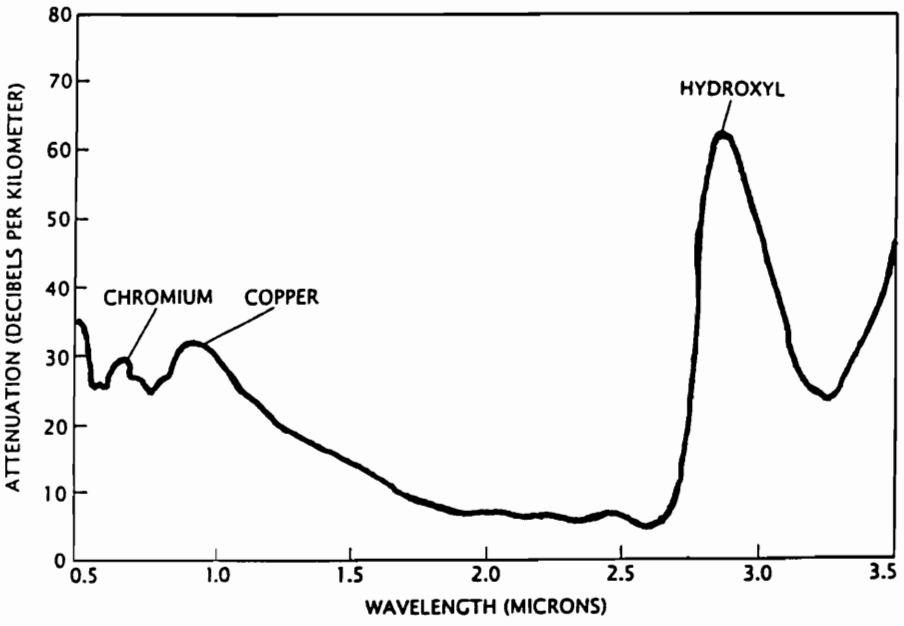

Figure 5.13. Exploded view of one wavelength region from Figure 5.12 for heavy-metal fluoride glasses [48].

6.0 SUMMARY AND CONCLUSION

A novel bidirectional decomposition of solutions to the scalar wave equation into multiplicatively backward and forward traveling plane waves was applied to an optical fiber operated in the linear region. The classical optical waveguide theory was adapted to accommodate the bidirectional representation and a weakly guiding theory was formulated in the (α, β) domain. Several source spectra were considered and closed-form solutions were obtained; in this work, we have presented results from four choices of spectra and evaluated distances for which the pulses would remain localized. In some cases, we have anticipated problems associated with the practical implementation of the spectra.

The MPS pulse proved that even though the solution deviated from the ideal free-space MPS pulse due to the waveguiding constraint, a proper choice of the free parameters could lead to large distances over which the pulse would maintain its original amplitude. The Fourier domain analysis of the MPS pulse spectrum led to the acquisition of practical parameters such as the minimum and maximum wavelengths in the spectrum as well as the waist of the initial pulse. Similar analyses are possible with all other source spectra. We also showed that the synthesis process leading to exact solutions needs to be performed with caution, and demonstrated this in the case of the splash pulse spectrum without the delta function where it was not possible to tweak the

free parameters to obtain nondecaying localized pulses confined to the fiber core. This example underscores the fact that all spectra that have given rise to LW solutions in free space need not be suitable for generating nondispersive solutions in waveguides.

In the practical realization of localized pulse-launching schemes, source spectra which are most easily implementable should be considered. It is not clear if the four spectra considered in this paper will prove to be the right candidates. However, a rich class of other related spectra $A(\alpha,\beta,\kappa)$ of the form $\delta(\beta-\beta')\exp(-\alpha a_1) I_0(a_2\kappa)$, $\delta(\beta-\beta')\exp(-\alpha a_1) J_0(a_2\kappa)$, $\delta(\beta-\beta')\exp(-\alpha a_1) J_0(a_2\kappa^2/4)$, or $\alpha \exp(-\alpha a_1)\exp(-\beta a_2)\exp(-a_3/\alpha)$, which are theoretically more cumbersome, may lend themselves to easier implementation because of the extra free parameters available for tweaking. Such spectra may also reduce the restriction on the highly broadband nature of the MPS pulse spectrum described in this paper. Utilizing the full potential of the bidirectional superposition may thus pave the way for future experimental systems.

In practical fiber optic systems, pulse dispersion is significantly affected by material properties, especially when a broadband spectrum is used as the source. In order to aid our analysis when material dispersion is present, we have looked at a much simpler system, namely, a plasma-filled cylindrical metallic waveguide. Our results indicate that despite the presence of material dispersion, localized propagation of pulses is feasible. Future theoretical efforts will include a more detailed analysis that incorporates material dispersion and losses in the fiber. Several numerical methods or asymptotic techniques available in literature can be used to perform this analysis. Despite the localization of the solutions derived from the fundamental LP_{01} modes at

the center of the fiber core, the possibility of generating higher order modes in the fiber cannot be ignored. Higher order modes will act as noise in the system and their effect on the localization of the fundamental solution needs to be further analyzed. In the practical arena, the availability of the optical equivalents of the arrays used for generating the acoustic LW's will finally determine the realizability of such schemes.

In summary, we have shown the existence of slowly-decaying, nondispersive solutions in an optical fiber waveguide operated in the linear region. It has been our attempt to lay the theoretical foundations for a more complex analysis that incorporates material dispersion and absorption. Several practical issues still remain unanswered and technology trends in the coming years will play a crucial role in the availability of answers to some of the questions posed in this thesis. Development of novel materials, availability of broadband sources, and the generation of more accurate models for the propagation of LW pulses in fibers will lead to a clearer understanding of this phenomenon. Hopefully, this is only the beginning of a new research area involving the merger of theoretical electromagnetics and practical optical fiber engineering.

REFERENCES

1. J. N. Brittingham, "Focus wave modes in homogeneous Maxwell's equations: Transverse Electric Mode", J. Appl. Phys. **54**, 1179 (1983).
2. T. T. Wu and R. W. P. King, "Comment on "Focus wave modes in homogeneous Maxwell's equations: Transverse electric mode"", J. Appl. Phys. **56**, 2587 (1984).
3. T. T. Wu and H. Lehmann, "Spreading of electromagnetic pulses", J. Appl. Phys. **58**, 2064 (1985).
4. P. A. Belanger, "Packetlike solutions of the homogeneous-wave equation", J. Opt. Soc. Am. A **1**, 723 (1984).
5. P. A. Belanger, "Lorentz transformation of the packetlike solutions of the homogeneous wave equation", J. Opt. Soc. Am. A **3**, 541 (1986).
6. A. Sezginer, "A general formulation of focus wave modes", J. Appl. Phys. **57**, 678 (1985).
7. R. W. Ziolkowski, "Exact solutions of the wave equation with complex source locations", J. Math. Phys. **26**, 861 (1985).
8. R. W. Ziolkowski, "Localized transmission of electromagnetic energy", Phys. Rev. A **39**, 2005 (1989).
9. R. W. Ziolkowski, D. K. Lewis and B. D. Cook, "Evidence of localized wave transmission", Phys. Rev. Lett. **62**, 147 (1989).
10. R. W. Ziolkowski and D. K. Lewis, "Verification of the localized wave transmission effect", J. Appl. Phys. Rev. **68**, 6083 (1990).

11. J. Durnin, "Exact solutions for nondiffracting beams. I. The scalar theory", J. Opt. Soc. Am. A **4**, 651 (1987).

12. J. Durnin, J. J. Miceli, Jr. and J. H. Eberly, "Diffraction-free beams", Phys. Rev. Lett. **58**, 1499 (1987).

13. I. M. Besieris, A. M. Shaarawi and R. W. Ziolkowski, "A bidirectional traveling plane wave representation of exact solutions of the scalar wave equation", J. Math. Phys. **30**, 1254 (1989).

14. P. Hillion, "Spinor focus wave modes", J. Math. Phys. **28**, 1743 (1987).

15. A. M. Shaarawi, I. M. Besieris and R. W. Ziolkowski, "Localized energy pulse trains launched from an open, semi-infinite, circular waveguide", J. Appl. Phys. **65**, 805 (1989).

16. A. Hasegawa and F. Tappert, "Transmission of stationary nonlinear optical pulses in dispersive dielectric fibers. I. Anomalous dispersion", Appl. Phys. Lett., **23**, 142 (1973).

17. L. F. Mollenauer, R. H. Stolen and J. P. Gordon, "Experimental observation of picosecond pulse narrowing and solitons in optical fibers", Phys. Rev. Lett., **45**, 1095 (1980).

18. E Snitzer, "Cylindrical dielectric waveguide modes", J. Opt. Soc. Am. **51**, 499 (1961).

19. E. Snitzer and H. Osterberg, "Experimental observation of the modes of a cylindrical dielectric waveguide at optical frequencies", J. Opt. Soc. Am. **51**, 499 (1961).

20. N. S. Kapany, *Fiber Optics Principles and Applications*, Academic Press, New York, 1967.

21. D. Gloge, "Weakly guiding fibers", Appl. Opt. **10**, 2442 (1971).

22. A. M. Shaarawi, *Nondispersive Wave Packets*, Ph. D. dissertation, Bradley Department of Electrical Engineering, Virginia Polytechnic Institute & State University, Blacksburg, VA 24061 (1989).

23. I. S. Gradshteyn and I. M. Ryzhik, *Tables of Integrals, Series and Products* (Academic, New York, 1965).

24. A. P. Prudnikov, Yu. A. Bruchkov and O. I. Marichev, *Integrals and Series Volume 2 : Special Functions* (Gordon and Breach, New York, 1986).

25. R. W. Ziolkowski, Personal Communication.

26. K. A. Connor and L. B. Felsen, "Complex space-time rays and their application to pulse propagation in lossy dispersive media", Proc. IEEE **62**, 1586 (1974)

27. L. B. Felsen and N. Marcuvitz, *Radiation and Scattering of Waves*, Prentice-Hall, Englewood Cliffs, NJ, 1973.

28. K. Suchy, "The velocity of a wave packet in an anisotropic absorbing medium", J. Plasma Phys. **8**, 33 (1972).

29. K. E. Oughstun and G. E. Sherman, "Propagation of electromagnetic pulses in linear dispersive medium with absorption (the Lorentz medium)", J. Opt. Soc. Am. B **5**, 817 (1988).

30. K. E. Oughstun and S. Shen, " Velocity of energy transport for a time-harmonic field in a multiple-resonance Lorentz medium", J. Opt. Soc. Am. B **5**, 2395 (1988).

31. P. Wyns, D. P. Foty, and K. E. Oughstun, "Numerical analysis of the precursor fields in linear dispersive pulse propagation", J. Opt. Soc. Am. A **6**, 1421 (1989).

32. S. Shen and K. E. Oughstun, "Dispersive pulse propagation in a double-resonance Lorentz medium", J. Opt. Soc. Am. B **6**, 948 (1989).

33. K. E. Oughstun, P. Wyns and D. Foty, "Numerical determination of the signal velocity in dispersive pulse propagation", J. Opt. Soc. Am. A **6**, 1430 (1989).

34. K. E. Oughstun and G. E. Sherman, "Uniform asymptotic description of electromagnetic pulse propagation in linear dispersive medium with absorption (the Lorentz medium)", J. Opt. Soc. Am. A **6**, 1394 (1989).

35. K. E. Oughstun and J. E. K. Laurens, "Asymptotic description of ultrashort electromagnetic pulse propagation in a linear, causally dispersive medium", Radio Sc. **26**, 245 (1991).

36. D. Marcuse, *Principles of Optical Fiber Measurements* (Academic Press, New York, 1981).

37. Yu. Yu. Ananev, "Nondiffracting light waves", Opt. Spectrosc. (USSR) **64**, 722 (1988).

38. B. B. Godfrey, "Diffraction-free microwave propagation", Sensor and Simulation Notes 320 (Weapons Laboratory, Kirtland Air Force Base, N. M., 1989).

39. B. Hafizi and P. Sprangle, "Diffraction effects in directed radiation beams", J. Opt. Soc. Am. A **8**, 705 (1991).

40. J. V. Candy, R. W. Ziolkowski and D. K. Lewis, "Transient wave estimation: A multichannel deconvolution application", J. Acoust. Soc. Am. **88**, 2235 (1990).

41. J. V. Candy, R. W. Ziolkowski and D. K. Lewis, "Transient waves: Reconstruction and processing", J. Acoust. Soc. Am. **88**, 2248 (1990).

42. T. Kobayashi, H. Ideno and T. Sueta, "Generation of arbitrarily shaped optical pulses in the subnanosecond to picosecond region using a fast electrooptic deflector", IEEE J. Quantum. Electron. **QE-16**, 132 (1980).

43. W. E. Martin and D. Milam, "Interpulse interference and passive laser pulse

shaper", Appl. Opt. **15**, 3054 (1976).

44. E. Yablonovitch, "Generation of a short optical pulse of arbitrary shape and phase variation", IEEE J. Quantum Electron. **QE-11**, 789 (1975).

45. G. Keiser, *Optical Fiber Communications* (McGraw Hill, New York, 1991).

46. J. Lucas, "Review: Fluoride glasses", J. Materials Sc. **24**, 1 (1989).

47. T. Katsuyama and H. Matsumura, *Infrared Optical Fibers* (Adam Hilger, Bristol, England, 1989).

48. M. G. Drexhage and C. T. Moynihan, "Infrared optical fibers", Scientific American, **11**, 110 (1988)

49. P. W. France, *Fluoride Glass Optical Fibres* (CRC Press, Boca Raton, FL, 1990).

50. L. E. Busse and I. D. Aggarwal, "Design parameters for fluoride multimode fibers", J. Lightwave Technol. **9**, 828 (1991).

Vita

Ashish Madhukar Vengsarkar was born in Bombay, India on October 2, 1963. He received the B. Tech. degree (1985) from the Indian Institute of Technology, Bombay and the M.S. degree (1988) from Virginia Polytechnic Institute and State University, both in Electrical Engineering.

He worked for one year (1985-1986) at the Indian Institute of Technology, Bombay as a consultant to the Naval Physical and Oceanic Laboratory, Cochin, India. While pursuing his doctoral degree (1988-1991), he worked at the Fiber & Electro-Optics Research Center as a Research Associate in the field of fiber optic sensors and components. In the summer of 1989, he was a Visiting Scholar under a NATO grant with the Optoelectronics Group at the University of Strathclyde, Glasgow, Scotland. His research interests concern the study of optical wave propagation in waveguides and the analysis of localized wave solutions. His other areas of specialization include theoretical and experimental analyses of optical fiber devices and components, multiparameter fiber sensors, elliptical-core few-mode fibers and the integration of fiber sensors in smart skins and materials.

Mr. Vengsarkar is a member of the Institution of Electrical and Electronic Engineers (IEEE), the Optical Society of America (OSA) and the Society of Photo-Optical Instrumentation Engineers (SPIE).

Ashish Vengsarkar